2008:03

LICENTIATE THESIS

L

# Rock Mass Behavior under Hydropower Embankment Dams

## *Results from Numerical Analyses*

Alexander Bondarchuk

Luleå University of Technology
Department of Civil, Mining and Environmental Engineering
Division of Mining and Geotechnical Engineering

2008:03 | ISSN: 1402-1757 | ISRN: LTU-LIC -- 08/03 -- SE

Licentiate Thesis

Division of Mining and Geotechnical Engineering

# Rock Mass Behavior under Hydropower Embankment Dams: Results from Numerical Analyses

Alexander Bondarchuk

Luleå University of Technology
Department of Civil and Environmental Engineering
Division of Mining and Geotechnical Engineering

## PREFACE

This work has been conducted under the research and development consortia "*väg-bro-tunnel*". The work has been funded by VINNOVA, NCC via SBUF, and Elforsk, and Luleå University of Technology. Their contribution is thankfully acknowledged.

I really want to thank my supervisors Associate Professor Maria Ask (LTU), Professor Lars-Olof Dahlström (LTU and NCC AB) and Professor Erling Nordlund (LTU), who help me to develop this project and have patience with me.

I would like to express my gratitude to my project reference group, for their support and good suggestions how to improve my work. This group consists of: T.D. Anders Isander (E.ON), T.D. Erik Nordström (Vattenfall), Licentiate Fredrik Johansson (KTH), T.D. Staffan Swedenborg (NCC AB).

I want to thank M.Sc. Mark Christianson from Itasca who helped me to implement my ideas into the numerical models.

I would like to thank my colleagues Lecturer Tomas Villegas, Licentiate David Saiang, who gave me hints how to solve the different problems, Assistant Professor Jenny Svanberg, who helped me with proofreading.

## ABSTRACT

There are about 1000 hydropower dams of varying size and age in Sweden. According to definitions by the International Commission of Large Dams (ICOLD), 190 of these dams are large (i.e., higher than 15 m) [e.g. *Bérburé*, 2004], and 117 of them are embankment dams. Dams in which the bulk of the construction comprises naturally occurring materials are considered as embankment dams.

The peak of dam construction in Sweden was between 1950 and 1980, hence, the majority of dams are between 30 and 60 years old. Ongoing concerns for the hydropower industry regard production and safety of the dams. Currently, the majority of ongoing research efforts on degradation of hydropower dams and dam safety regards the dam – system complex, whereas relatively little attention has been paid to the bedrock under the dam, which is a critical factor for construction integrity and functionality.

The objectives for the project are:

1. Reveal and increase the understanding of the rock mass response to the construction of a hydropower dam, i.e. the loads from the weight of the dam and the water in the reservoir; and
2. Investigate how static and cyclic loads of the hydropower dam affect the stability of the dam in term of foundation rock and the degradation process of the grout curtain.

Numerical analyses are well suited to study problems of high complexity; hence, the method is ideal for this study. The construction of a dam on rock foundation (with its water reservoir) cause redistribution of the stress field, and affect the state of mechanical- and hydrogeological properties of the rock mass beneath the dam. I have used Universal Distinct Element Code (UDEC) to achieve objectives of the project.This code was chosen because most deformation of the rock mass under a dam are believed to occur along discontinuities (e.g. joints and faults); UDEC is ideally suited to study potential modes of failure directly related to the presence of discontinuous features.

The analyses has been performed in two-dimensional plane strain conditions. A hydro-mechanical model has been developed which addresses mechanical properties of the intact rock and joints, together with their failure criteria, the presence of water, and the loading from the embankment dam and water reservoir. The model is a conceptual model, and typical parameters for Swedish conditions have been chosen. The individual influence on mechanical response, stability and degradation of each parameter is revealed by varying the individual parameters in the model. In the construction of the model, a number of sensitivity analyses have been conducted, comprising of the investigation of specifity of loading pattern of embankment dam on the foundation rock and layout / dimension of the model.

Numerical analyses has identified that construction of the dam generally induces limited shear- and normal displacements in the rock mass. These displacements are considered to be insignificant. At the same time impounding of the reservoir and varying of the water

table in the reservoir induces extensive shearing and opening of the discontinuities at certain conditions. The parameters, which cause these conditions are a) reduced friction angle of the discontinuity b) increased density of the discontinuities c) presence of high in-situ stress

# TABLE OF CONTENTS

# 1. INTRODUCTION

## 1.1. Project motivation

Globally, dams are built to store water for irrigation, municipal use, hydropower electricity generation, and/or flood prevention [e.g. *Wahlström,* 1974]. Size and complexity of dams range from small and structurally simple constructions in small streams to large and structurally more complex dams in large rivers [e.g. *Wahlström,* 1974]. The type and design of individual dams depends on factors such as amount of available water, topography, geology, and type and amount of local material available for constructing the dam [e.g. *Fell et al.,* 2005].

Embankment, concrete and masonry dams are used for hydropower electricity generation. Embankment dams are mainly composed of naturally occurring materials [e.g. *Fell et al.,* 2005]). The main construction component of concrete dams is concrete, and masonry dams comprise building of structures from individual units laid in and bound together.

There are 190 large dams in Sweden [e.g. *Bérburé*, 2004] that produce about 12% of the electricity in Sweden [e.g. *Swedish Energy Agency,* 2006]. Production of hydropower energy has the advantages of being flexible and instantaneous; therefore, it is often used to produce electricity at times of day or season when energy demand is higher than normal [e.g. *Ljunggren,* pers. comm., 2005], with low degree of energy waste [e.g. *Korsfeldt et al.*, 2007]. Energy production from hydropower is important for Sweden, and it is important that the dams are functioning with as few interruptions as possible.

In addition to a negative impact on the overall energy production, a dam accident, or a major failure, potentially would cause large damage to society (human life, infrastructure, etc) downstream of a hydropower dam. To predict and mitigate effects from dam accidents and failures, the International Commission on Large Dams, ICOLD has developed and established guidelines for dam safety [e.g. *ICOLD*, 1974; 1995; 2002]. ICOLD is a non-governmental international organization, and a forum for the exchange of knowledge and experience in dam engineering. In Sweden, dam owners have established guidelines for the safety of dams, the hydropower industry dam safety guidelines, RIDAS [e.g. *RIDAS,* 2002]. The behavior of the foundation rock under a hydropower embankment dam is investigated in this thesis project. Anticipated results of the thesis include improved knowledge on parameters of the foundation rock that lead to potential instability of the foundation, together with how these parameters influence the integrity of the grouting curtain. These results are important for predict and mitigate effects of dam accidents and failures.

Many studies have been addressing dam stability issues. However, most studies are focusing on the dam construction itself [e.g. *Johansson,* 1997*; Windelhed,* 2001], and/or causes of failure and accidents [e.g. *ICOLD*, 1974; 1983; 1995; *Foster*, 2000]. Geophysical studies may be useful for studying the internal structure of dams and their foundation [e.g. *Bérubé*, 2004]. Dam incidents are often caused by overtopping, embankment leakage or piping, foundation leakage or piping, flow erosion, slope

protection damage, and deformation. Other researches have attempted to predict the likelihood for dam failure based on statistical analysis of dam incidents [e.g. *Samad et al.*, 1987; *Cheng*, 1993]. The mechanical behavior of foundation rock under a hydropower dam, and the interaction between the construction and the foundation rock have been studied using experimental [e.g. *Reinius*, 1988] and numerical analyses [e.g. *Barla et al.*, 2004; *Dolezalova*, 2004].

This thesis is one of the few attempts to investigate the hydro-mechanical behavior of the foundation rock under hydropower embankment dams using 2D numerical analyses in UDEC, and it is the first to consider rock types typical for Swedish conditions. The foundation rock consists of a rock mass, which is intact rock intersected by discontinuities.

Numerical analyses may advance the knowledge on the response of the foundation rock, interaction, and stability of the foundation rock and the hydropower dam, which is important information for determining the status of a hydropower dam. This information may also be helpful for identifying the type of maintenance needed to ensure the functionality and safety of a hydropower dam.

Different aspects of the life time of a dam may be investigated using numerical analyses. Numerical analyses may be a part of the design procedure to help identifying possible scenarios of rock mass behavior in response to construction and future exploitation of dam. It may be implemented as an instrument, which would allow to identify the reasons of malfunctioning of the dam in term of foundation rock. It may be used as a tool to predict the effectiveness of remedial measures or reconstruction of the dam.

Variation in static and cyclic loading at different stages in the life of a hydropower embankment dam may induce deformation in the foundation rock. This deformation may lead to displacement of the soil material within the embankment dam, and of the grout curtain. Increased water flow through the grout curtain is one plausible effect that may change the pressure distribution in the foundation rock and result in higher water loss. Both an increase in water flow and a change in pressure distribution may have negative effects on dam stability, and, hence, increase the risk for dam failure.

## 1.2 Objectives and approach

This thesis project concerns an urgent problem for the hydropower industry: How to maintain good stability and functionality of aging hydropower dams. Several hydropower dams must be upgraded, and measures must be taken to improve their safety to address new calculation- and assessment models, as well as changed conditions (e.g. climate change to more precipitation). These actions all require large investments of time and money by the hydropower industry.

Potential responses of the foundation rock under an embankment dam are simulated along two Cross-sections striking parallel and perpendicular to the river valley. Simulations are made using the numerical code UDEC [e.g. *Itasca*, 2005].

The objectives for the project are :

1. Reveal and increase the understanding of the rock mass response to the construction of a hydropower dam, i.e. the loads from the weight of the dam and the water in the reservoir; and
2. Investigate how static and cyclic loads of the hydropower dam affect the stability of the dam in term of foundation rock and the degradation process of the grout curtain.

Anticipated results from this thesis include an improved understanding of degradation processes, which are of importance for development of appropriate maintenance actions, for example for reinforcement and grouting. The results may also important if new hydropower dams were to be developed in Sweden.

The new numerical model consists of seven parameters. The potential impact of individual parameters is investigated by varying one parameter a time. The response of the foundation rock has been studies along two cross-sections, with Cross-section A running parallel to the strike of the river valley, and Cross-section B running perpendicular to the strike of the river valley, in the reservoir up-stream of the dam. The behavior of the foundation rock in Cross-section A has been studied during three stages of the dam history, namely at the times of dam construction, of filling water into the reservoir, and of seasonal variation of water depth in the reservoir. The load cases during these three stages are static load from the dam construction, combined load from the dam construction and the water in the reservoir, and cyclic loading of water, respectively. Because the dam construction itself is not present in Cross-section B, only the two latter stages are analyzed for Cross-section B.

### 1.3 Outline of thesis

This thesis consists of five main parts:

The motivation and objectives are presented in Chapter 1, "*Introduction"*.

Chapter 2, "*Embankment dams and their foundations*" first briefly reviews different types of embankment dams and overview the incidents and their causes. The second part describes the foundation rock, or bedrock under embankment dams. Mechanical behavior and the movement of water in the rock mass, and aspects og grouting are also presented in Chapter 2.

Chapter 3, "*Properties of the foundation rock*" is a summary of important properties for the stability of foundation rock that are incorporated into the numerical model developed in this study.

Chapter 4, "*Conceptual numerical analyzes*" describes the numerical models used in this thesis. It covers the description of the model, the implemented assumptions used in analysis and verification models.

Chapters 5-7 presents, discusses, and concludes the results of my study. Chapter 8 contains recommendations for future research.

# 2. EMBANKMENT DAM AND THEIR FOUNDATION

## 2.1 Embankment dams

### 2.1.1 Definitions

Several definitions of embankment dams exist. A common feature for all definitions is that an embankment dam is a dam constructed of natural materials [e.g. *National Research Council,* 1983*; Goldin and Rasskazov*, 1992; *Varshney,* 1995]. Embankment dam may be characterized as a dam, in which the bulk of the construction consists of naturally occurring materials, e.g. soil, clay, sand, gravel, and natural boulder or quarried fragmented rock. Embankment dams may be subdivided into two major groups: (1) Earth-fill embankment dams; and (2) Rock-fill embankment dams.

Earthfill embankment dams are primarily constructed of compacted earth, either homogeneous or zoned, and contain more than 50% of earth. Rockfill dams contain more than 50% of compacted and dumped permeable rock fill. The latter dams must have an impermeable (water right) upstream blanket, or an impermeable core [e.g. *National Research Council,* 1983].

*National Research Council* [1983] proposed three criteria to base the classification of embankment dams:

(1) The predominant material of the dam (it could consist of either rock or earth);
(2) The method used to place material in the embankment; and
(3) The geometric configuration, or layout of the zones of the dam.

*Goldin and Rasskazov* [1992] suggested a larger number of criteria to classify embankment dams than, for example, the *National Research Council* [1983]. His criteria include type of material, design, construction technology, height, and seepage preventions measures. However current work is concentrated on the behavior of the foundation rock under the embankment dams than the embankment dams itself, so only simplified classification based on structure is introduced.

*Homogeneous embankment dams*

Homogeneous embankment consists almost entirely of one type of the material (Figure 2.1). This type of dam has evolved to reduce the construction costs in areas where only one main type of material is available near the dam site. Usually homogeneous embankment dams consist of low permeability material and require flatter slopes than zoned embankment dams.

Figure 2.1 Homogeneous embankment dam [*Goldin and Rasskazov,* 1992]

*Zoned embankment dams*
Zoned embankment dams are made up of two or more different types of material (Figure 2.2). This type of dam includes different sections, including a 'core', which is an impermeable zone inside the dam, and a 'shell', which is the outer zone on both sides of dam. The 'shells' are usually made from permeable material, and if several different types of material are available, those with higher permeability is placed on the outer faces. Separation of different zones in the dam is performed with the help of filters.

Figure 2.2 Zoned embankment dam with thin central core [*Goldin and Rasskazov,* 1992]

A standard Swedish embankment dam with a central impermeable core is presented in Figure. 2.3 [*RIDAS*, 2002].

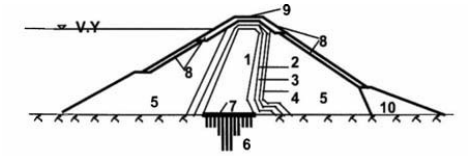


Figure 2.3 Standard Swedish embankment dam with a central impervious core [*RIDAS*, 2002]

### 2.1.2 Safety guidelines

Dam failures are rated as one of the major low-probability, high-loss events [e.g. *National Research Council,* 1983]. Studies of past dam failures show three major causes: seepage and internal erosion in the embankment, seepage and erosion of the foundation, and overtopping [e.g. *ICOLD*, 1995].

Realizing importance of historic performance of dams in assessing dam safety, ICOLD carried out extensive review of incidents of large dams, i.e. more than 15 m high. The most common causes of accidents and failures were investigated [e.g. *ICOLD*, 1974; 1983; 1995; *Foster,* 2000]. Other researches have attempted to predict the likehood of

dam failure based on the statistical analysis of dam incidents, for example *Samad et al.* [1987] and *Cheng* [1993]. Although piping through the foundation of the embankment dam is not the biggest threat to the integrity of the dam, nearly 15% of all known failures are caused by piping. This shows that hydrological properties of the rock are important for the stability of embankment dams, and that closer attention should be paid to these properties during numerical analyses.

According to Swedish law, the dam owners have the responsibility for dam safety.[*Mcgrath*, 2000]Although the Swedish government gives permission for the construction of a dam, the dam owners normally operates and maintains their dams. Therefore, owners are working in non-regulatory environment. Individual towns are responsible for emergency planning for accidents whilst Country Councils have responsibility for major events such as dam failures.

In 1997, the first guidelines for Swedish dam owners were finalized, the Hydropower Industry Dam Safety Guidelines, RIDAS. These guidelines were review in 2002. There are three main objectives for the RIDAS guidelines, namely to: (1) Define requirements and establish guidelines for adequate and uniform dam safety; (2) Constitute a basis for a uniform evaluation of dam safety and identify measures needed to improve dam safety; and (3) Support authorities in their supervision of dam safety.

## 2.2 Foundation rock

### 2.2.1 General characteristics

The foundation rock, or rock mass under an embankment dam has two main purposes [e.g. *National Research Council*, 1983]: To provide stable support with little deformation and settlement under all conditions of saturation and loading; and, for economic purposes, to provide resistance to leakage of water. Homogeneous and zoned embankment dams require different types of the foundation rock [e.g. *Singh,* 1995]. Homogeneous embankment dams may have uniform quality of the rock across the entire foundation, while zoned embankment dams generally have different quality of the foundation rock for the outer shells and the impermeable core.

The foundation rock of the outer shells should be resistant against sliding and major settlements, whereas minor foundation settlements may be tolerated without any damage to the construction of the dam. The physical properties of this foundation rock is equal or better than the properties of the dam shell [e.g. *Singh*, 1995].

For the zoned embankment dam, the contact area between the impermeable core and the foundation rock is the most critical in terms of integrity of the core [e.g. *Singh*, 1995]. To guarantee the integrity of that contact area, the foundation rock should consist of hard rock with few joins and fault plains [e.g. *Goldin and Rasskazov*, 1992; *Singh*, 1995]. These conditions are usually obtained by removing weak, weathered rock until rock with required quality is reached, and by using consolidated grouting to reduce the permeability of the foundation rock [e.g. *Singh*, 1995; *Goldin and Rasskazov*, 1992].

The interface between embankment dam and foundation rock is a critical contact for all types of embankment dams. Poor bonding between the two may lead to piping along the contact area, which later may develop into seepage paths and internal erosion [e.g. *National Research Council*, 1983]. Improper treatment of foundation discontinuities, and/or together with inadequate filters between the embankment dam and joints in the foundation rock, may also lead to piping in the embankment dam, and subsequently to collapse due to internal erosion [e.g. *National Research Council* 1983].

To reduce a risk of incidents there have been proposed methodology of preparation of foundation rocks before construction reservoir [e.g. *RIDAS,* 2002; *USACOE,* 2004].

### 2.2.2 Mechanic behavior

*Reinius* [1988] investigated stresses and deformation of the foundation rock before and after filling up water in the reservoir. He designed a simple analogue experimental model of an embankment dam to obtain an approximate idea what forces and stresses act on the foundation rock of the embankment dam due to load (Figure 2.4). The model consists of a homogeneous, symmetrical, triangular, prismatic sand embankment dam, lying on a homogeneous, elastic foundation rock with a horizontal surface in front of the reservoir impoundment. *Reinius* [1988] found that horizontal tension stresses occur in the foundation rock when the dam load is placed on the rock surface (Figure 2.5), and that they further increase when the water level of the reservoir is raised to the full storage level (Figure 2.6). Tensional stresses may lead to an increase in the width of the discontinuities. *He* suggest two causes for the tension stresses and opening cracks: The first one is related to differential settlement, due to sloping foundation in the direction of the longitudinal dam axis (Figure 2.7) and rapid changes of the rock quality. The second cause is that the soil and water pressures are acting in a direction perpendicular to the long axis of the dam. Cracks with widths of several millimeters may cause considerable water leakage, and they may be a way for transportation of the material from the core.

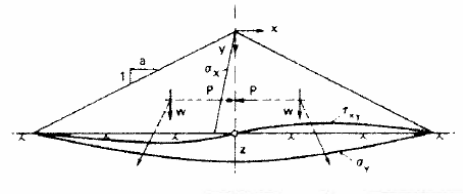


Figure 2.4 Forces and stresses in a triangular, prismatic earth fill dam [*Reinius*, 1988]

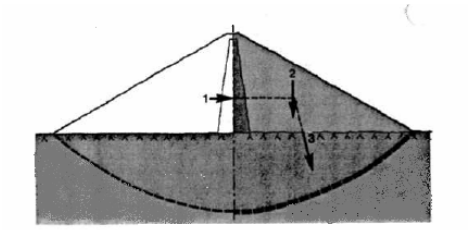


Figure 2.5 Embankment dam with central core. Stresses redistribution in foundation rock after construction of embankment dam. [*Reinius*, 1988]

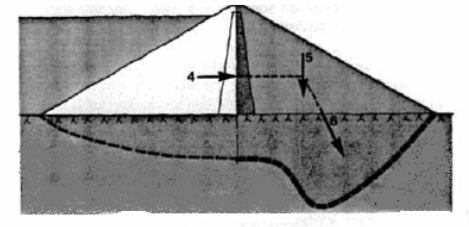


Figure 2.6 Embankment dam with central core. Stresses redistribution in foundation rock after impounding the reservoir. [*Reinius*, 1988]

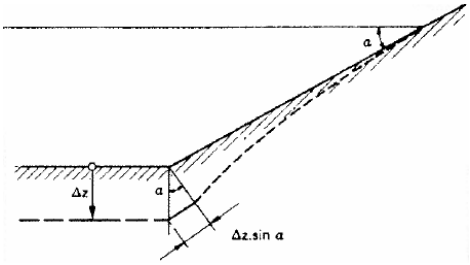


Figure 2.7 Elongation along a rock slope caused by settlement of the rock surface $\Delta z$ by the weight of the dam [*Reinius*, 1988]

### 2.2.3 Influence of water

Dams are constructed to store large volumes of water on foundation rocks that are never homogenous, but rather consist of many discontinuities. Some discontinuities may form a connection between the storage area and the downstream side of the dam, where the water loss due to seepage is high. Detailed characterization and good understanding of the hydrogeological model are important to the design of grouting the foundation rock, as well as to assess a likely magnitude of the water seepage and erodibility of the foundation rock [e.g. *Idel*, 1980; *Fell et al.,* 2005].

When water is filled into the dam, the different elevation of the water on both sides of the dam result in a hydraulic gradient. In addition, the cross sectional area through which water flow can take place decreases, because the low permeability of the dam body increase the velocity of seeping water [e.g. *Bandara and Imbulana*, 1996]. Increase in

velocity may lead to erosion of material in the foundation rock, which may lead to piping. *Fell et al.* [2005] formulated required conditions that contribute to the development of piping: (1) There must be a seepage flow path and a source of water; (2) There must be erodable material within the flow path and this material must be carried by the seepage flow; (3) There must be unprotected exit, from which the eroded material may escape; and (4) For a pipe to form, the material being piped, or the material directly above, must be able to form and support "roof" for the pipe.

Several authors [e.g. *Bandara and Imbulana*, 1996; *Hwang and Houghtalen*, 1996] argue that the best way to estimate the amount of seepage is to implement a flow net technique. In this technique, flow patterns are presented graphically via streamlines and their corresponding equipotent lines.

### 2.2.4 Grouting

Blanket- and curtain grouting are the two main grouting programs that normally are used for embankment dam construction (Figure 2.8). Near-surface rocks are often weathered and highly fractured because of natural causes as well as activities related to the preparation and construction of the dam. Blanket grouting is used to reduce seepage looses, seepage velocities through a relatively permeable near-surface zone, and the possibility of transporting embankment material in to foundation. Blanket grouting is introduced by drilled shallow holes with different patterns, depending on the type of the dam and the geological conditions and it is usually restricted to the upper 5m to 20 m [e.g. *Duncan*, 1999; *Fell et al.,* 2005; *RIDAS,* 2007; *Weaver and Bruce*, 2007]. Grout curtain is designed to create a narrow barrier through an area of high permeability. It usually consists of a single row of grout holes that are drilled and grouted to the base of the permeable rock, or to such depths that acceptable hydraulic gradients are achieved. For large dams on foundation rocks, and dams on very permeable rock, three, five or even more lines of grout holes may be grouted [e.g. *Fell et al.*, 2005]. Sometimes the vertical depth of the grout curtain is accepted as two thirds of the height of the dam [e.g. *Vattenfall*, 1988; *RIDAS* 2007; *Weaver and Bruce*, 2007].

Normally, two basic types of grouts are used, Portland cement-base slurry and chemical grouting solution. Portland cement slurries are far most widely used in grouting and by addition of various substances such as clay, sand, and bentonite or addition of chemicals to increase or reduce setting time, are used in wide range of applications [Weaver and Bruce, 2007]. Chemical grouting solutions are commonly used if the aperture of openings and cracks are smaller than the particle suspensions, or if the grouting conditions are hard, e.g., because of high water pressure or chemical composition of in situ water. However, chemical grouts are rather expensive compared to cement based grout. Information of grouting technique can be found in *USACOE* [1984] and *Fell et al.* [2005]. The recent book by *Weaver and Bruce* [2007] discusses dam foundation grouting.

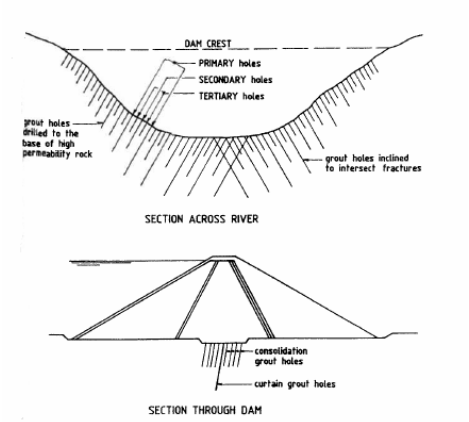


Figure 2.8 Consolidation (blanket) and grout curtain under an embankment dam with central core [*Fell et al.*, 2005]

The introduction of cement grout into discontinuity void space affects its mechanical as well as hydrological properties. *Swedenborg* [2001] carried out laboratory tests on a cement grouted crystalline rock samples and implemented numerical analyze to estimate mechanical effects of grouting.

Filling the discontinuities of the rock mass with cement substance reduces their hydraulic conductivity hence reducing seepage rate and seepage exit gradient [e.g. *Fellet al.*, 2005; *Hwang and Houghtalen,*1996; *Swedenborg*, 2001]. (Figure 2.9) Effectiveness of rock mass sealing against water movement depends on the quality of performed grouting work.

The leakage control in foundation rock under embankment dams is implemented through grout curtain. *RIDAS* [2007] specified hydraulic properties and deep of grout curtain depending on the height of the dam (Table 2.1).

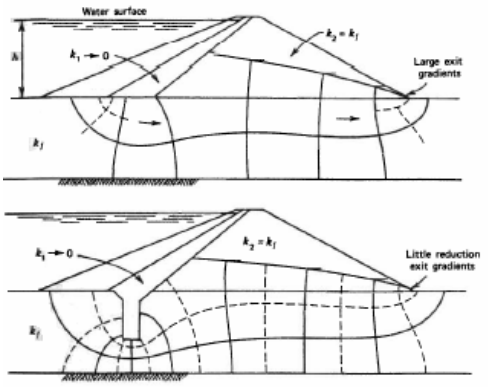


Figure 2.9 Effect of partial cutoff on position of line of seepage [*Fell et al.*, 2005]

Table 2.1 Required tightness or rock under central core [*RIDAS*, 2007]

| **Height of dam, m (*h*)** | **Deep of rock, m** | **Required tightness of rock, depending on deep of rock, L = Lugeon** |
|---|---|---|
| $h < 30$ m | Blanket grouting: min 6 m | 0 – 6 m: 2L |
| | Curtain grouting: min 10 m | 6 – 10 m: 3L |
| | max 20 m | 10 – 20 m: 4L |
| $h > 30$ m | Blanket grouting: min 6 m | 0 – 6 m: 1L |
| | Curtain grouting: min 1/3 *h* | 6 – 1/3 *h*: 2L |
| | max 2/3 *h* | (1/3 – 2/3) *h*: 3L |

# 3. PROPERTIES OF THE FOUNDATION ROCK

The conceptual model is described in full in Chapter 4. It consists of a dam body and a foundation rock. The embankment dam body is represented by a solid block discretized into deformable triangular finite-different zones. The foundation rock consists of blocks of intact rock and discontinuities. In this chapter, I describe the theory, the test methods and empirical correlations for parameters that are incorporated directly or indirectly into the numerical analyses.

## 3.1 Intact rock

Intact rock consists of unfractured blocks, which occur between structural discontinuities in a typical rock mass. The size of these pieces of blocks may range from a few millimeters to several meters [e.g. *Hoek et al*., 1997]. The strength of the rock is much higher than for the discontinuities, therefore, the rock mass strength is governed by the properties of the discontinuities included in it.

The Mohr-Coulomb failure criterion expresses the strength of intact rock through cohesion, *c* and friction angle, $\phi$ [e.g. *Brown and Brady*, 1985]:

$$\sigma_1 = \sigma_3 \cdot \frac{(1+\sin\phi)}{(1-\sin\phi)} + \frac{2 \cdot c \cdot \cos\phi}{(1-\sin\phi)} \qquad \text{(Eq. 3.1)}$$

where $\sigma_1$ is the major principal stress at failure, and $\sigma_3$ is the minor principal effective stress at failure.

The Hoek-Brown failure criterion expresses strength of intact rock through uniaxial compression strength, $\sigma_{ci}$ and the constant, $m_i$ [e.g. *Hoek et al*., 1997]:

$$\sigma_1^{'} = \sigma_3^{'} + \sigma_c \cdot \left( m_i \cdot \frac{\sigma_3^{'}}{\sigma_c} + 1 \right)^{\frac{1}{2}} \qquad \text{(Eq. 3.2)}$$

where $\sigma_1^{'}$ is the major principal effective stress at failure, $\sigma_3^{'}$ is the minor principal effective stress at failure, $\sigma_c$ is the uniaxial compressive strength of the intact rock, $m_i$ is the material constant for the intact rock. Table 3.1 shows some examples of uniaxial compressive strength and the constant $m_i$ for different types of rock. The constant $s = 1$ for intact rock.

Estimation of the uniaxial compression strength of intact rock may be identified using simple field measurements [e.g. *Brown and Brady*, 1985]. However, the most reliable values of both the uniaxial compressive strength, $\sigma_{ci}$ and the material constant. $m_i$ are obtained from the result of the triaxial tests [e.g. *Hoek et al*., 1997]. Uniaxial compression test is also very common for estimation of the strength of intact rock. The procedures for these tests are described in ISRM suggested methods [e.g. *ISRM*, 1978]

Two important parameters for describing the strength of intact rock are uniaxial compression strength, $\sigma_{ci}$ and the tensile strength, $\sigma_{ti}$ [e.g. *Brady and Brown*, 1985].

Table 3.1 Some examples of the constant $m_i$ and the uniaxial compressive strength, $\sigma_{ci}$ [*Hoek and Brown*, 1980]

| **Rock type** | $m_i$ | $\sigma_{ci}$ **[MPa]** |
|---|---|---|
| Gabbro | 17.3 – 22.9 | 205 - 351 |
| Gneiss | 21.2 – 29.8 | 235 – 254 |
| Granite | 20.8 – 32.8 | 116 – 344 |
| Limestone | 3.2 – 14.1 | 47 – 201 |
| Marble | 5.9 – 11.7 | 50 – 133 |
| Quartzite | 14.1 – 23.3 | 227 – 327 |
| Sandstone | 6.4 – 27.3 | 40 – 398 |

The uniaxial compressive strength may be estimated from triaxial test [e.g. *Brady and Brown*, 1985], according:

$$\sigma_{ci} = \frac{2 \cdot c \cdot \cos\phi}{1 - \sin\phi} \qquad \text{(Eq. 3.3)}$$

The value of tensile strength of intact rock is difficult to determine. The tensile strength may be estimated indirectly using brazilian test or applying tensile load on specimen [e.g. *ISRM*, 1978]. Another way to estimate tensile strength of intact rock is using Hoek-Brown failure criteria [e.g. *Hoek and Brown*, 1980]

$$\sigma_{ti} = \frac{1}{2} \cdot \sigma_{ci} \cdot \left( m_i - \sqrt{m_i^2 + 4s} \right) \qquad \text{(Eq. 3.4)}$$

Intact rock is normally modeled as a continuum material with assumed linear elastic behavior. To estimate the stress-strain response of the intact rock, it is necessary to determine the Young's modulus, *E* and Poisson's ratio, $\nu$. Young's modulus and Poisson's ratio can be derived from the slope of the stress-strain curve during uniaxial unconfined compression tests.

## 3.2 Discontinuities

A discontinuity is any mechanical discontinuity in a rock mass having different strength properties. In this study, the term discontinuitiy is used interchangeable with the term joint, which is a discontinuity in which there has been no observable relative movement. There are several other types of discontinuities, form example fault, bedding, cleavage, and foliation [e.g. *Wyllie and Mah* 2004].

At shallow depth gravity driving sliding on the discontinuities and rotation of the individual rock block plays a dominant role [e.g. *Hoek et al*., 1997]. Since discontinuity governs the stability of the rock system, therefore it is very essential to asses the shear strength of the discontinuities. However, determination of shear strength is associated with some uncertainty. Several factors must be considered, such as aperture, the wall

strength, the roughness, the scale effect, the presence of filling material and presence of water. To model stress-strain response, shear and normal stiffness are required parameters, together with dilation angle [e.g. *Johansson*, 2005].

Estimation of shear strength may be done under laboratory conditions, although the results should be taken with precaution due to scale effect reasons. In-situ measurements will also consider the scale effect, however, these test are associated with high cost and requires much time [e.g. *Johansson*, 2005]. There are also two empirical methods: Barton's empirical failure criteria and back analysis of failures, which is based on calculation shear strength parameters using experience or from other sites with similar characteristics.

A fundamental quantity for shear strength of discontinuities is the basic friction angle, $\phi_b$. This is approximately equal to the residual friction angle, $\phi_r$ [e.g. *Hoek et al*., 1997]. The basic friction angle is related to the size and shape of the grains, exposed on the discontinuity surface. It may be measured by testing sawn or ground rock surfaces [e.g. *Wyllie and Mah*, 2004]. The basic friction angle normally varies within 25 to 40° for common rock types (Table 3.2).

Table 3.2 Approximate values for the basic friction angle for different rocks [*Hoek and Bray*, 1981].

| **Rock** | **Friction angle [°]** |
|---|---|
| Amphibolite | 32 |
| Basalt | 31 – 38 |
| Conglomerate | 35 |
| Chalk | 30 |
| Dolomite | 27 – 31 |
| Gneiss (schistose) | 23 – 29 |
| Granite (fine grain) | 29 – 35 |
| Granite (coarse grain) | 31 – 35 |
| Limestone | 33 – 40 |
| Porphyry | 31 |
| Sandstone | 25 – 35 |
| Shale | 27 |
| Silstone | 27 – 31 |
| Slate | 25 - 30 |

Note: Lower values is generally given by tests on wet rock surfaces.

A natural discontinuity surface in hard rock is never as smooth as sawn specimens which are used in laboratory tests for estimation of basic friction angle. The undulation and asperities on a natural joint have a significant influence on its shear resistance. Generally the surface roughness of the joint increase its shear strength [e.g. *Hoek et al*., 1997]. Patton [1966] demonstrated the importance of roughness in terms of shear resistance in shear test using "saw-tooth" specimens (Figure 3.1).

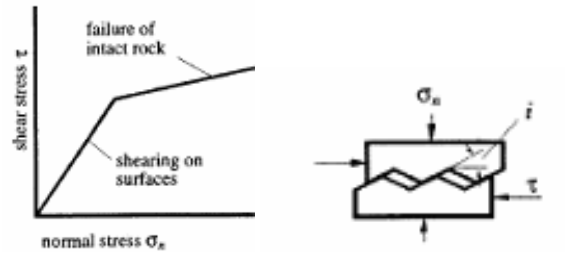

Figure 3.1 Influence of roughness of joints on shear resistance [*Hoek et al*., 1997].

Based on detailed studies of natural joints, Barton [*1973*] proposed that the peak shear strength could be expressed as:

$$\tau = \sigma_n \cdot \tan\left[\phi_b + JRC \cdot \log_{10}\left(\frac{JCS}{\sigma_n}\right)\right] \quad \text{(Eq. 3.5)}$$

where $\sigma_n$ is the normal stress acting on the discontinuity, $\phi_b$ is the basic friction angle, JRC is the joint roughness coefficient, and JCS is the wall compressive strength. ISRM has published suggested methods for the estimation of JRC [e.g. *ISRM*, 1978]. They recommend tilt- and shear tests to estimate JRC, which is obtained from:

$$JRC = \frac{\alpha - \phi_b}{\log_{10}\left[\frac{JCS}{\sigma_n}\right]} \quad \text{(Eq. 3.6)}$$

where $\alpha$ is the tilt angle, and $\sigma_n$ is the normal stress acting on the discontinuity when sliding occurs. If no laboratory tests are available, they propose to estimate JRC by comparing the roughness of the surface of the discontinuity with standard profiles [e.g. *Barton and Choubey*, 1977].

The scale effect is an important factor for estimating the shear strength. Smaller sized sample have higher peak shear strength than larger ones [e.g. *Hoek et al.*, 1997]. They suggest that JRC decreases with increasing scale, which lead to a reduction of shear strength of the discontinuity. An increase in scale also lead to a reduction of the average JCS, because the possibility for weakness in the sample increases with an increasing sample size [e.g. *Hoek et al*., 1997]. Figure 3.2 represents the influence of scale effect on the shear strength of the discontinuity. It may be observed that peak shear strength gradually decrease with increasing sample size.

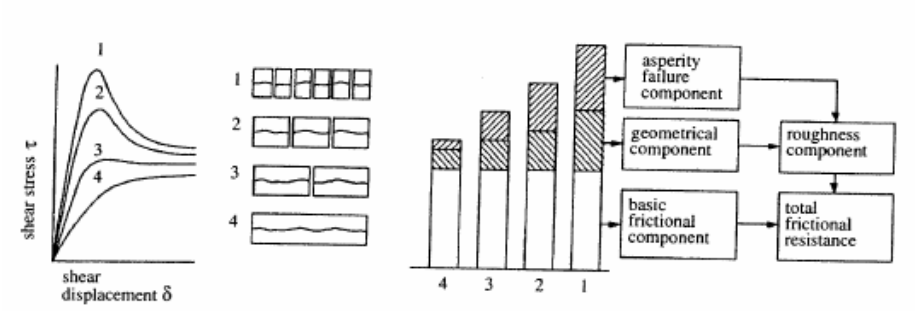


Figure 3.2 Influence of scale on the three components of the shear strength of a rough discontinuity [*Hoek et al*., 1997]

The influence of the infilling on the shear strength properties of a discontinuity depends on the thickness and strength properties of the infilling material [e.g. *Hoek and Bray*, 1981, *Swedenborg*, 2001]. If the thickness of the asperity is more than 25-50% of the amplitude of the asperities, there will be little or no rock-to-rock contact and shear strength properties of discontinuity will be dictated by properties of the infilling material [e.g. *Goodman*, 1980]. When water is present in discontinuities, the shear strength is reduced even more, as the result of a decrease in effective normal stress [e.g. *Hoek and Bray*, 1981]

*Barton* [1974] performed a series of direct shear test to determine peak friction angle and cohesion for filled discontinuities, and proposed that the infilling can be subdivided in two groups: The first group comprises of clays, with friction angles from about 8-20°, and cohesion values up to about 200 kPa. The second group comprises of faults, shear zones, and breccias, with friction angles from about 25-45° and cohesion values up to about 100 kPa. *Barton* [1974] also found that the residual friction angle only is about 2-4° lower than the peak friction angle, while the residual cohesion is zero.

A second criterion by *Barton* [1974] regards whether there has been previous displacement along the discontinuity. He proposed two general categories: Recently displaced discontinuities, and undisplaced discontinuities, respectively (Figure 3.3). Recently displaced discontinuities include faults, shear zones, clay mylonites, and bedding-surface shears. Their shear strength is assumed to be close to the residual strength, and there will be a small reduction in strength when further displacement takes place. Undisplaced discontinuities include igneous and metamorphic rocks that have weathered along discontinuity surfaces to form clay layers. Further subdivisions of these two categories have been made to include normal- and over-consolidated materials [e.g. *Wyllie and Mah*, 2004], and these discontinuities have significantly different peak strength values.

Today there is no theoretical model or empirical correlation which would allow accurately determine the shear strength of filled discontinuities. The best test method available today is in situ shear tests [e.g. ISRM, 1975; *Matsuoka et al.*, 2001].

Parameters for describing the relation between stress and strain for discontinuities include normal- and shear stiffness, $K_n$ and $K_s$, respectively, maximum closure, $\delta_0$, and the dilation angle, $\psi_{dis}$ [e.g. *Johansson*, 2005]. Normal stiffness is measured while the sample is subjected to normal deformation, and the normal deformation is measured with sensitive gauges. The shear stiffness and dilation angle are determined in shear tests, where the constant normal load is applied to the sample, and rate of shear loading is kept on same level.

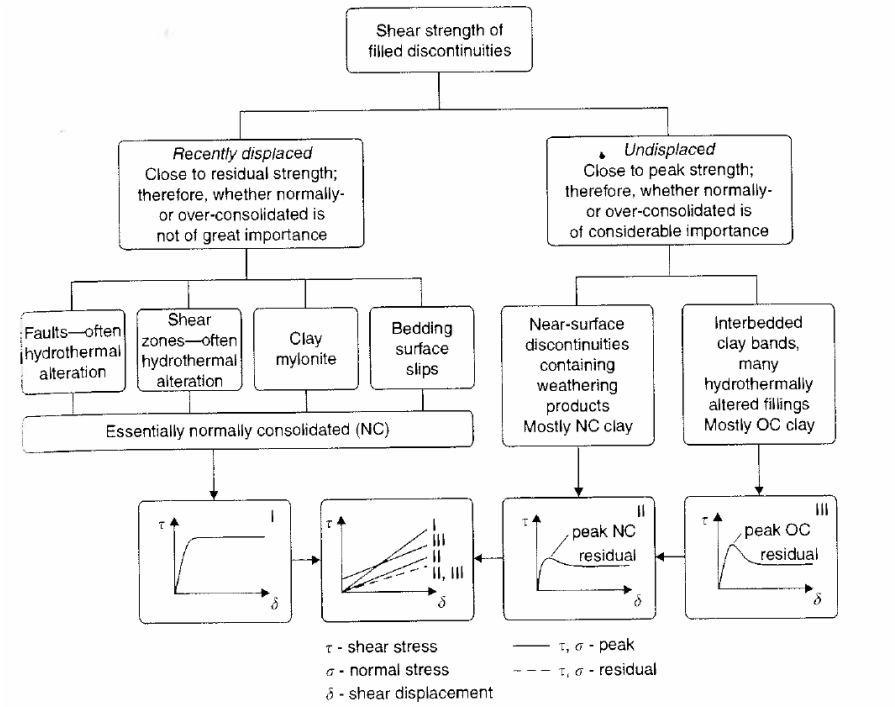


Figure 3.3 Simplified division of filled sicontinuities into discplaced and undisplaced, and normal consolidated and over-consolidated categories [*Wyllie and Mah*, 2004]

## 3.3 Rock mass

The term rock mass may be presented as a system consisting of intact rock intersected by numerous sets of discontinuities with different length and direction. Therefore the shear strength and stress-strain response of the rock mass are dictated by properties of the intact rock and discontinuities.

Large scale laboratory triaxial tests on rock masses to determine the shear strength are rather unusual [e.g. *Thorpe et al.*, 1980], because it is difficult to obtain undisturbed samples of sufficient size. In situ testing may also be performed, but they are associated with high costs. Another method to estimate rock mass strength is to use empirical failure

criterion such as the Hoek-Brown failure criteria or rock mass classification system [*e.g. Edelbro*, 2004].

Figure 3.4 shows conditions when the Hoek-Brown failure criteria may be used. As stated above, this criterion can be applied to heavily jointed rock masses that are considered homogeneous and/or isotropic. For systems consisting only of two joint sets, the criterion should only be used if neither of the joint sets have a dominant influence on the rock mass behavior [e.g. *Hoek et al*., 1997].

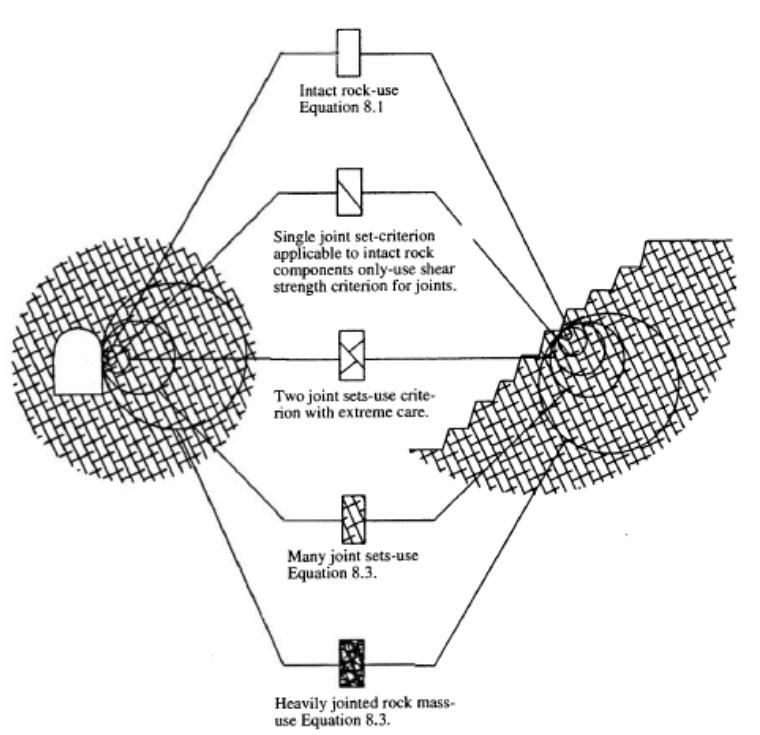


Figure 3.4 Rock mass conditions under which the Hoek-Brown failure criterion can be applied [*Hoek et al*., 1997]

Very often in numerical models and limit equilibrium analyzes the strength of rock mass is expressed through Mohr-Coulomb failure criteria. In that case it is necessary to estimate an equivalent set of cohesion and friction parameters for given Hoek-Brawn failures. This can be done with the following equations [e.g. *Hoek et al*., 1997]:

$$\sigma_n = \sigma_3 + \frac{\sigma_1 - \sigma_3}{\partial\sigma_1 / \partial\sigma_3 + 1} \quad \text{(Eq. 3.7)}$$

$$\tau = (\sigma_n - \sigma_3) \cdot \sqrt{\partial\sigma_1 / \partial\sigma_3} \quad \text{(Eq. 3.8)}$$

For the $GSI > 25$, when $a = 0.5$:

$$\frac{\partial \sigma_1}{\partial \sigma_3} = 1 + \frac{m_b \cdot \sigma_c}{2 \cdot (\sigma_1 - \sigma_3)} \quad \text{(Eq. 3.9)}$$

For the $GSI > 25$, when $s = 0$:

$$\frac{\partial \sigma_1}{\partial \sigma_3} = 1 + a m_b^a \cdot \left( \frac{\sigma_3}{\sigma_c} \right)^{a-1} \quad \text{(Eq. 3.10)}$$

where $m_b$ is the value of the constant $m$ for the rock mass, $a$ and $s$ are constants which depend upon the characteristics of the rock mass, $\sigma_{ci}$ is the uniaxial compressive strength of the intact rock pieces, $\sigma_1$ and $\sigma_3$ are the axial and confining principal stresses respectively. When a set of ( $\sigma_n$ , $\tau$ ) have been calculated average cohesion and friction angles can be estimated by linear regression analyzes.

Several methods exist for characterizing jointed rock masses and to estimate deformability and strength properties [e.g. ISRM, 1981; *Edelbro,* 2004]. Methods of interest for my study are Rock mass rating, RMS [e.g. *Bieniawski*, 1976], the rock mass quality (Q)-system [e.g. *Barton et al*., 1974] and Geological strength index, GSI [e.g. *Hoek, et al.,* 1998; *Cai et al.,* 2004]. In practical engineering cases, this can for example be done by using the program RocLab [e.g. Hoek, 2002].

The deformation modulus of the rock mass is in this study, as in the design of rock constructions in Sweden today, calculated using rock mass classifications. The most commonly used relations are summarized in Table 3.3

In this thesis, I have used properties of granite, i.e. high strength and good quality, and that this rock type is representative for Swedish conditions. A quick comparison with a geologic map of Sweden supports this assumption, because the bedrock of Sweden is dominated by felsic to intermediate intrusive rock, which granite is a subgroup of.

Table 3.3 Most used relations for calculating deformation modulus of a rock mass.

| **Purpose** | **Equation** | **Reference** | **Eq. No** |
|---|---|---|---|
| Estimate $E_m$ from GSI | $E_m = \left( \frac{\sigma_{ci}}{100} \right)^{0.5} \cdot 10^{(GSI-10)/40}$ (GPa) | *Hoek and Brown* [1997]. | 3.11 |
| Modified estimate $E_m$ from GSI, to consider effect from blast damage and stress relaxation (factor D). | $E_m = \left(1 - \frac{D}{2}\right) \cdot \left( \frac{\sigma_{ci}}{100} \right)^{0.5} \cdot 10^{(GSI-10)/40}$ | *Hoek et al.* [2002] | 3.12 |

### 3.4 State of stress

The knowledge of rock stress in Earth's crust is important to the problems dealing with rocks mass in civil and mining engineering, because stresses have much influence on other properties of rock mass. For instance, stress field changes the permeability of rock mass because compressive stresses tend to close discontinuities while tensile stresses trend to open them, or rock mass strength might be increased due to confinement effect of stress [e.g. *Amadei and Stephansson*, 1997].

Stress may be defined as a tensor with six independent components: three normal stress components and three shear stress components (Figure 3.5a). With reference to an arbitrary set of Cartesian co-ordinate axes, the stress at a point is expressed in matrix form [e.g. *Brady and Brown*, 1985]:

$$[\sigma] = \begin{bmatrix} \sigma_{xx} & \tau_{xy} & \tau_{xz} \\ \tau_{xy} & \sigma_{yy} & \tau_{yz} \\ \tau_{xz} & \tau_{yz} & \sigma_{zz} \end{bmatrix} \quad \text{(Eq. 3.13)}$$

where $\sigma_{xx}$, $\sigma_{yy}$, and $\sigma_{zz}$ are normal stresses, and $\tau_{xy}$, $\tau_{xz}$, and $\tau_{yz}$ are shear stresses.

A change in the orientation of the planes on which the stress components are applied will change the values of the six stress components. At a particular orientation of the planes, the shear stresses become zero, and only normal stress components are acting on the planes; these normal stresses ($\sigma_1$, $\sigma_2$, $\sigma_3$) are termed principal stresses (Figure 3.5b):

$$\begin{bmatrix} \sigma_1 & 0 & 0 \\ 0 & \sigma_2 & 0 \\ 0 & 0 & \sigma_3 \end{bmatrix} \quad \text{(Eq. 3.14)}$$

It is common to describe the *in situ* state of stress by the magnitude and direction of the three principal stresses [e.g. *Hudson and Cooling*, 1988] or the in situ stresses can be described by vertical stress $\sigma_v$ and two horizontal stresses, minor $\sigma_h$ and major $\sigma_H$ [e.g. *Nordlund et al*., 1997].

Rock stress is often subdvided into two groups [e.g. *Amadei and Stephansson*, 1997]: (1) *In situ* (or natural, primary, and virgin) stresses that exist in the rock mass prior to any man-made disturbance; and (2) Induced (or man-made and secondary) stressed that refers to stresses induced by artificial disturbance from, for example, excavation, drilling, or pumping. Figure 3.6 shows sources of in situ stresses [e.g. *Amadei and Stephansson,* 1997]. Gravitational stresses are generated from the weight of overburden. Tectonic stresses are formed by plate tectonic processes, and they are usually very uniform over a large areas. Residual stresses are usually related to inhomogeneous physic or chemical processes in a certain volume of rock material.

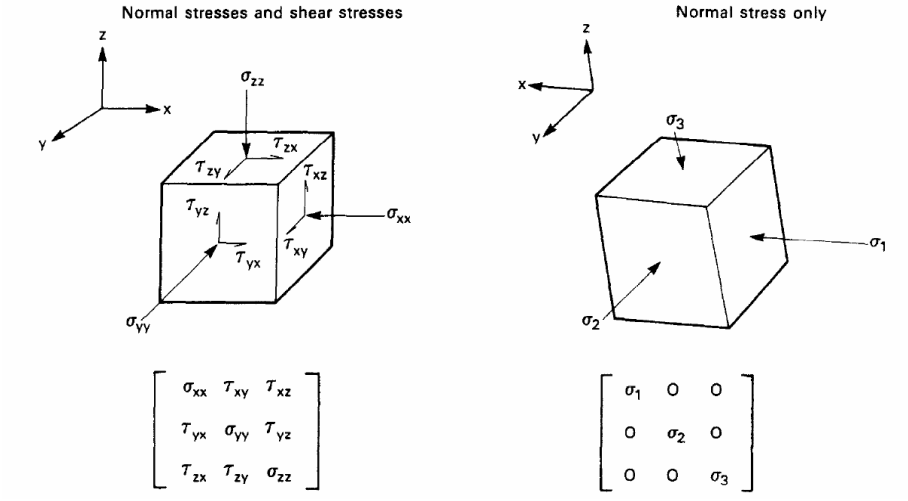

Figure 3.5 The general stress state and principal stress state at a point in a solid [*Hudson and Cooling*, 1988]

The state of stress at shallow depths is hard to determine, and seldom measured [e.g. *Perman and Sjöberg*, 2007]. Most stress measurements are made at depths below 50 m, whereas stresses at the shallow depths have been estimated mostly through extrapolation [e.g. *Töyrä*, 2006]. Such extrapolations may produce results of questionable quality, because the stress state at shallow depths is different than that at great depths [e.g. *Amadei and Stephansson*, 1997]. For example, rock mass properties at shallow depths are highly variable, even over short distances. In addition, because rock stress measurements generally only present part of the solution, and are associated with uncertainties, they must be conducted carefully and skillfully. For example, *Hoek and Brown* [1978] collected stress data world-wide that revealed huge variation in stresses at shallow depths. Furthermore, Leijon [1989] showed that overcoring is associated with a random measuring error in the average normal stress corresponding to a standard deviation of $\pm 2$ MPa, and that the value of standard deviation is in the same order of magnitude as the average stress value [e.g. *Töyrä*, 2006].

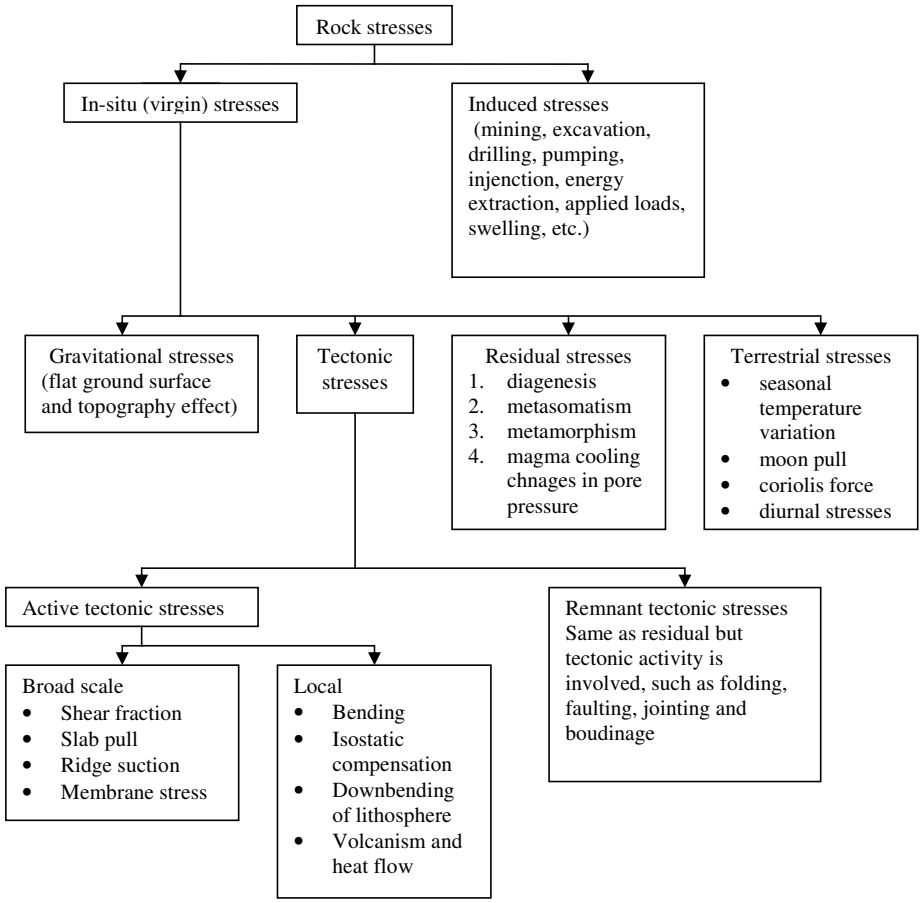


Figure 3.6 Terminology of rock stresses (*Amadei and Stephansson*, 1997)

The stress field in Sweden is generally characterized by higher horizontal than vertical stresses, with a mean orientation of the major horizontal stress of about NW-SE [e.g. *Reinecker et al*. 2005] (Figure 3.7 *and* Table 3.4). Domination of horizontal stresses over vertical is mainly thought to be caused by tectonic stresses and, possible, by glacial rebound effects [e.g. *Müller et al.*, 1993].

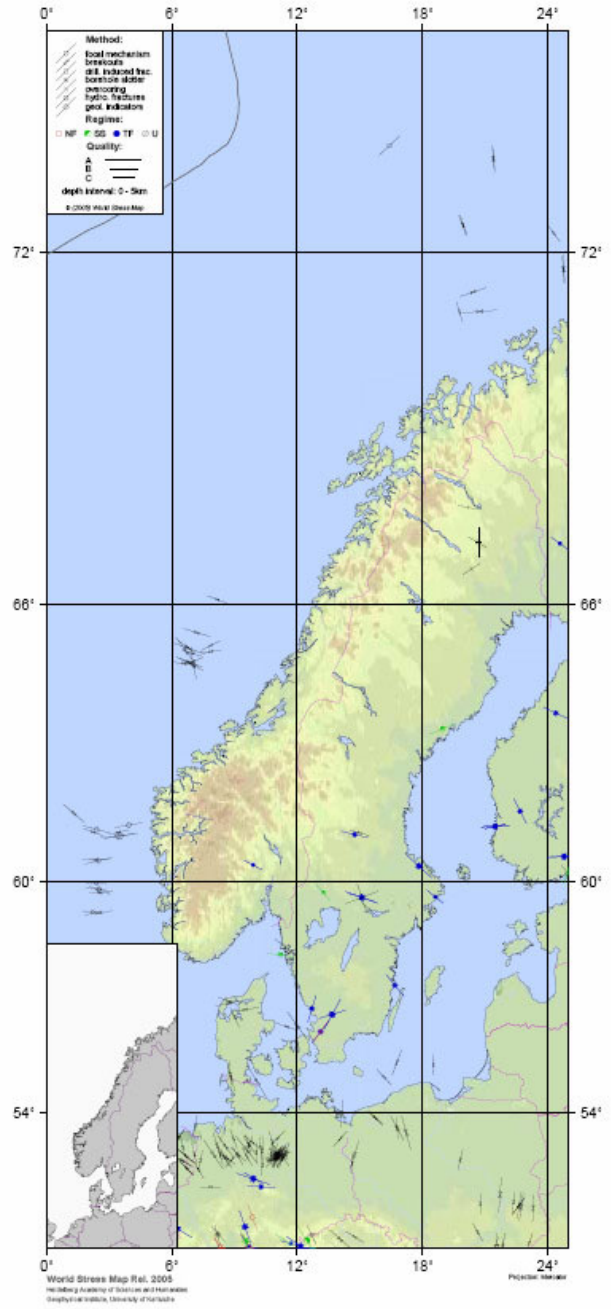


Figure 3.7 Summary of stresses in Fennoscandian shield (*Reinecker et al*. 2005)

Table 3.4. Stress uncertainty range in different parts of Sweden

| **Place** | **Vertical depth [m]** | **Type of relationship** | $\sigma_H$ **[MPa]** | $\sigma_h$ **[MPa]** | $\sigma_v$ **[MPa]** | **Method** | **Reference** |
|---|---|---|---|---|---|---|---|
| Sweden | 0-1000 | | *2.8+0.0399z* | *2.2+0.0240z* | $\rho gz$ | HF | *Stephansson*, 1993 |
| | | | *6.7+0.0444z* | *0.8+0.0329z* | $\rho gz$ | OC | |
| Stockholm | 0-40 | | *0.0676z* | *4-5* | $\rho gz$ | OC | *Klasson*, 1993 |
| Forsmark | 230-450 | | *0.085z* | *0.022z* | $\rho gz$ | OC | *Sjöberg et al.*, 2005 |
| Arlandabanan | | | *z/5.27* | *z/10* | $\rho gz$ | NA | *Töyrä*. 2006 |
| Äspö HRL | | | *4.3+0.0373z* | *3.3+0.0174z* | *0.027z* | | *Mas Ivars et al*,2004 |
| T-Blå (Stockholm) | 0-60 | | *4.0+0.0677z* | *2.1+0.0284z* | $\rho gz$ | | *Chang*, 2007 |
| Norrmalm (Stockholm) | 0-80 | Min | *3.0+0.075z* | *0.5+0.0275z* | *0.021z* | OC | *Perman and Sjöberg,* 2007 |
| | | Typ | *4.7+0.075z* | *2.3+0.0275* | *0.0265z* | | |
| | | Max | *5.8+0.075z* | *3.5+0.0275* | *0.032z* | | |
| Södermalm (Stockholm) | 0-80 | Min | *2.0+0.075z* | *0.0265z* | *0.021z* | | |
| | | Typ | *2.0+0.125z* | *1.0+0.100z* | *0.0265z* | | |
| | | Max | *5.8+0.125z* | *2.0+0.100z* | *0.032z* | | |

1. Keys: $\sigma_H$ , maximum horizontal stress; $\sigma_h$ , minimum horizontal stress, $\sigma_v$ , vertical stress; OC, overcoring; HF, hydraulic fracturing NA, numerical analyses.

### 3.5 Flow of water

The movement of water in foundation rock occurs predominantly along discontinuities, because the hydraulic conductivity of intact crystalline rock is much lower than the discontinuities. Consequently, the conductivity of foundation rock is strongly by the characteristics of the discontinuities [e.g. *Wyllie and Mah*, 2004]. The flow of water in a jointed rock mass may be carried out either assuming that rock mass is a continuum or that the rock is a non-continuum [e.g. *Thiel*, 1989; *Wyllie and Mah*, 2004]. The continuum approach is used for the rock mass where discontinuities spacing is sufficiently close that the fractured rock acts hydraulically as a granular porous media and is considered as a permeable homogeneous material with a coefficient of permeability, *k* (Figure 3.8).

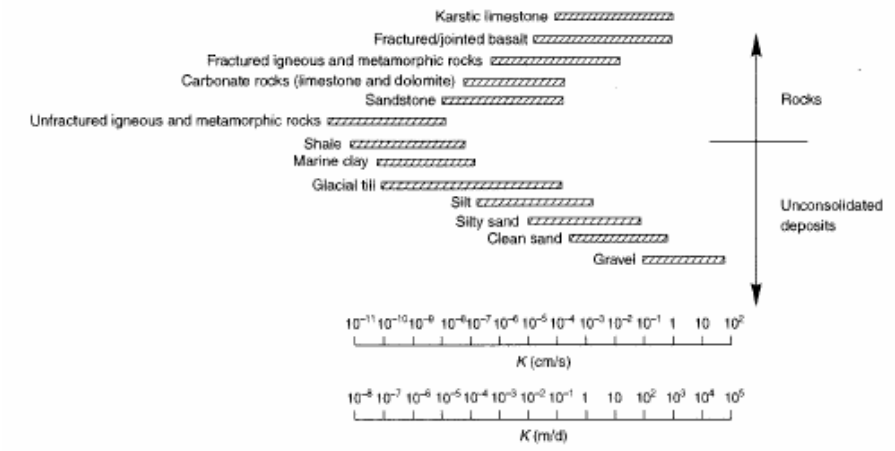


Figure 3.8 Hydraulic conductivity of various geologic materials [*Wyllie and Mah*, 2004]

According to Darcy law, water flow through a material proportionally to the hydraulic gradient [e.g. *Darcy*, 1856]:

$$Q = k \cdot I \cdot A \qquad \text{(Eq. 3.15)}$$

where *Q* is rate of flow, *I* is the gradient or head loss between two points and *A* is the cross-section area. Darcy's law is only applicable to the laminar flow, and can not be used for turbulent flow [e.g. *Wyllie and Mah*, 2004]. If boundary conditions and permeability of the material is known, the pore pressure, *u* may be calculated at different points in the material using Darcy's law:

$$u = \gamma_w \cdot h \qquad \text{(Eq. 3.16)}$$

where $\gamma_w$ is the unit weight of the water, and *h* is the pressure height. *Terzaghi* [1943] used Eq. 3.16 to develop the principle of effective stresses:

$$\sigma' = \sigma - u \qquad \text{(Eq. 3.17)}$$

where $\sigma'$ is effective stress, $u$ is pore pressure, and $\sigma$ is total stress.

The equivalent hydraulic conductivity (Figure 3.9) of an array of parallel, smooth, clean discontinuities may be expressed as [e.g. *Wyllie and Mah*, 2004]:

$$K \approx \frac{g \cdot e^3}{12 \cdot \upsilon \cdot b} \qquad \text{(Eq. 3.18)}$$

where $g$ is the gravitational acceleration, $e$ and $b$ are the discontinuity aperture and spacing, respectively, and $\upsilon$ is the coefficient of kinematic viscosity.

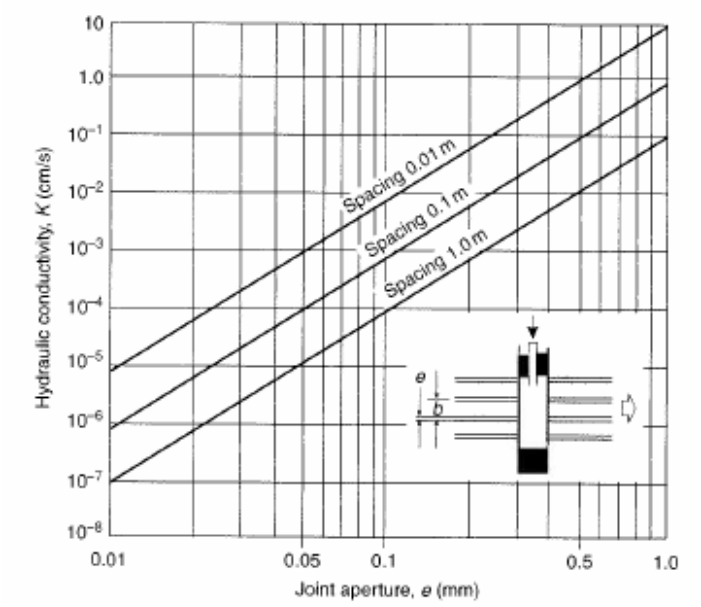


Figure 3.9 influence of joint aperture and spacing on hydraulic conductivity in the direction of a set of smooth parallel joints in a rock mass [*Wyllie and Mah*, 2004]

The hydraulic conductivity is very sensitive the aperture, hence, small changes in the aperture significantly reduce the conductivity. Eq. 3.18 can be applied only to laminar flow in planar, smooth, parallel discontinuities and represents the highest equivalent hydraulic conductivity for fracture system. However, presence of filling material in the discontinuities reduces their hydraulic conductivity, so Eq. 3.18 modifies into:

$$K = \frac{e \cdot K_f}{b} + K_r \qquad \text{(Eq. 3.19)}$$

where $K_f$ is the hydraulic conductivity of the filling, and $K_r$ is that of intact rock.

Based on Darcy's law, an expression on hydraulic conductivity and the area expressed in width, $w$ and aperture, $e$, the flow between two parallel planar plates may be expressed with the cubic law:

$$Q = -\frac{\rho_w \cdot g \cdot w \cdot a^3}{12 \cdot \upsilon_w} \qquad \text{(Eq. 3.20)}$$

where $\rho_w$ is the density of water, $\upsilon_w$ is the kinematic viscosity of water. *g* is gravitational acceleration, *w* is discontinuity spacing, and *a* is aperture.

It is difficult to model movement of water in the rock mass using discontinuous approach, because the flow is influenced by a number of parameters (Figure 3.10). As stated above, a reduction in aperture result in a substantial reduction of the hydraulic conductivity, and it also result in ejection of infilling material (e.g. water). *Thiel* [1989] discuss the issue of modeling based on the spacing between the discontinuities and the size of rock mass or structure in question.

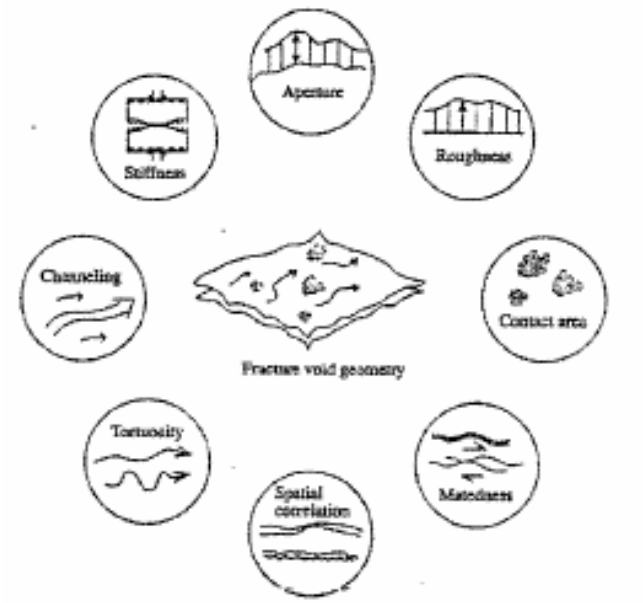


Figure 3.10 Properties of discontinuities that affect the flow [*Hakami*, 1995]

# 4. CONCEPTUAL NUMERICAL ANALYSES

## 4.1 General

The Universal Distinct Elements Code (UDEC) of *Itasca* [2005] is a two-dimensional program based on the distinct element method for discontinuum analyses. It simulates the response of discontinuous media (such as a jointed rock mass) subjected to static or dynamic loading. UDEC is most suitable code for fulfilling the objectives of this thesis, based on the assumption that the behavior of the rock mass is primarily controlled by the major discontinuities in the foundation rock. *Itasca* [2005] states that UDEC is ideally suited to study potential modes of failure directly related to the presence of discontinuities features.

I have conducted the conceptual numerical analyze in three steps. The first step comprises selection of the layout and parameters for a Base Case (BC) Model. The selected layout of the BC Model and its input data has been chosen to resemble Swedish conditions as much as possible. Furthermore, the dam type resembles a homogeneous embankment dam, i.e. the dam body has uniform properties and low density. The second step consists of verification models. Those models have been implemented with the purpose to clarify uncertainties related to stress caused by the weight of the embankment dam on the foundation rock, and magnitude of distribution of the discontinuities in the model (see below). The third and final step includes evaluation of how individual parameter influences the behavior of the rock mass during three stages of the life time of the dam. The three stages are summarized in Table 4.1, i.e. static loading from constructing the dam, impounding the reservoir, and cyclic loading of water in the reservoir**.** Sensitivity analyses have been performed by varying one parameter at a time. Note that the model yet has to be calibrated to a real case; therefore, the preliminary results presented here should be viewed as potential scenarios for rock mass behavior.

Table 4.1 Stages of the life time of the dam.

| Stage | Activity |
|---|---|
| 1 | Constructing the dam on the rock foundation |
| 2 | Filling the reservoir with water (35 m water depth) |
| 3 | Varying the water table in the reservoir |

## 4.2 Limitations and assumptions

The following limitations and assumptions have been made:

1. Potential failure mechanisms within the dam itself are not considered;
2. Damage of the dam is assumed to occur when the grout curtain is broken, and this occurs after the aperture of a joint reaches a maximum value, and/or when there are large opening/shear displacements along discontinuities close to the foundation;
3. The model does no separate between zoned and homogeneous embankment dams, rather, it assumes that the two dam types produce identical loads on the underlying rock mass;

4. The interface between the dam and the foundation rock is considered to have the same properties as those of rock discontinuities in the model;
5. The study is focused on Swedish conditions. The rock mass properties presents a good quality (GSI around 80) rock mass, intersected by sub-vertically and sub-horizontally (banking planes) oriented discontinuities;
6. It is assumed that the *in situ* stress field has not been influenced by the construction sequence of the dam, for example by diverting the river from the former valley;
7. Only static and cyclic loading conditions from the dam and the water in the reservoir are considered, whereas dynamic loading (e.g. seismicity) is not included in the model;
8. The model includes movement of water in the rock mass, but it is assumed that the water does not erode the rock mass, mechanical properties of rock mass are constant in time; and
9. Presence of water in the dam body causes hydraulic pressure on the dam-foundation interface. The pattern of load is considered to be as in homogeneous embankment dams.
10. Total flow is assumed to be represented by amount of water moving from the rock mass downstream side of the dam into free space. To be able to calculate this amount the FISH function has been implemented
11. Usually grout curtain in numerical analyses is introduced as impermeable barrier for water, which propagates into foundation rock at certain depth. However this project considers it is as permeable, to make the model as realistic as possible. This feature is based on the fact that discontinuities smaller than 0.1 to 0.2 mm are not capable of taking any of the cement suspension [*Idel*, 1980; per.com. Håkan Stille].

### 4.3 Input data

The constitutive model used in the analyses were linear elastic-perfectly plastic for the blocks and Mohr-Coulomb for the discontinuities. The simulation of the construction of the foundation rock has been performed in two steps. The construction of the dam is first performed using high discontinuity strength values (to inhibit any shear displacements) and elastic block properties. The joint strength properties and the block properties are then returned to their correct values and the model is allowed to reach a final equilibrium state. This approach has been used to prevent any extensive deformations due to dynamic loading caused by placement of the heavy structure on the ground surface. The same reasons are behind the approach selected for the simulation of filling the reservoir. Therefore, the dam is impounded into two steps.

Only gravitation load and pore pressure from the ground water table, established at the level of ground surface, are included in the model. The direction of the major horizontal stress has been set along the river valley. Most of the rivers in the Sweden are directed NW-SE, and according to available stress data [e.g. *Sjöberg* et al., 2005; 2007] and the World Stress Map [e.g. *Reinecker et al.*, 2005], the average orientation of the major horizontal stress in Scandinavia coincides with this trend. The vertical stress is taken to be equal to the weight of the overburden [e.g. *Sjöberg*, 2007]. The estimation of

uncertainty ranges for magnitudes of horizontal stresses is based on *Sjöberg et al.* [2005; 2007]. The initial stress field is set according to assumption that it might represent the mean stress field [e.g. *Amadei and Stephansson*, 1997]:

$$\sigma_H = 2.8 + 0.0399 \cdot z$$

$$\sigma_h = 2.2 + 0.0240 \cdot z$$

$$\sigma_v = \rho g z$$

where z is the depth in meters.

It should be noted that stresses used in basic case has been obtained through hydraulic fracturing method. Stresses, used to analyze the influence, have been received implementing the overcoring method. Figure 4.1 shows the change of different stress state used in analyze with depth.

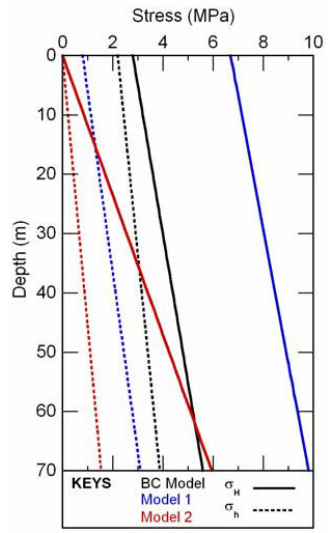


Figure 4.1 Variation of the stress with depth for the BC Model, and Models 1 and 2. The BC Model stress relationship is proposed by Stephansson [1993]. The stress relationships in Models 1 and 2 are obtained from OC method, and proposed by Stephansson [1993] and Sjöberg *et. al* [2005]

All models were first run to an equilibrium pre-construction state (with all stresses, loads and boundary conditions applied). The construction of the dam was then carried out, followed by the simulation of impounding. Finally, the variation of the water level in the reservoir is simulated. Each step in the simulation is finalized by brining the model to the equilibrium state. Steady state flow logic [e.g. *Itasca*, 2005] is applied to simulate water movement in the rock mass foundation.

The selection of the parameters has been done to resemble typical Swedish rock mass conditions. However, the term “typical condition” is highly variable. Rock mass properties are site specific, and highly variable, especially close to the ground surface.

The rock mass consists of intact rock intersected by discontinuities; hence, its properties can be described as a combination of properties of intact rock and properties of discontinuities.

Tables 4.2 lists the mechanical properties of the rock blocks which have been determined using the generalized Hoek and Brown failure criteria coupled with the rock mass characterization system GSI [e.g. *Hoek et al*., 2002, *Rocscience*, 2007].

Table 4.3 shows the input values for the RocLab [e.g. *Rocscience*, 2007]. A GSI value of 80 seems to be a representative value for typical Swedish rock at shallow depths [e.g. *Töyrä*, 2006; *Sjöberg and Perman*, 2007]. This value corresponds to interlocked, partially disturbed rock mass with multifaceted angular blocks formed by four or more discontinuity sets [e.g. *Hoek*, 1997] with good/fair surface condition. The uniaxial compressive strength of the rock has a wide uncertainty range. Assuming that gabbro and gneiss resemble the rock mass type in Sweden, the value is in the 100-250MPa [e.g. *Hoek*, 1997]. A mean value 180 MPa has been chosen for the numerical analysis. The disturbance factor has been set to 0. The value has been chosen on the assumption that during preparation work for the foundation overburden (weathered) rock have been removed and the dam has been built on fresh, un-weathered rock. The factor $m_j$ has been set to 33 based on the data from RocLab [e.g. *Rocscience*, 2007)] for the gabbro/ gneiss rock type. The value of $\sigma_{3\max}$ has been determined based on two-dimensional linear-elastic stress analysis of the base model.

Table 4.2 Rock blocks properties for the base case.

| **Parameter** | **Value** | **Reference** |
|---|---|---|
| Density, $\rho$ [kg/m$^3$] | 2700 | *Knutsson*, pers. comm |
| Young's modulus, $E$ [GPa] | 61 | *Rocscience*, 2007 |
| Poisson's ratio, $\nu$ [-] | 0.25 | *RG* |
| Friction angle, $\theta$ [$^o$] | 69 | *Rocscience*, 2007 |
| Cohesion, $c$ [MPa] | 5.142 | *Rocscience*, 2007 |
| Tensile strength, $T$ [MPa] | 1.21 | *Rocscience*, 2007 |

KEYS: RG, my reference group and advisers

Table 4.3 Input data for RocLab.

| **Parameter** | **Value** |
|---|---|
| Geological Strength Index, *GSI* [-] | 80 |
| Unconfined compressive strength of intact rock, $\sigma_{ci}$ [MPa] | 180 |
| Intact rock parameter, $m_i$ [-] | 33 |
| Disturbance factor, $D$ [-] | 0 |
| Minor effective principal stress at failure, $\sigma_{3max}$ [MPa] | 1 |

Table 4.4 summarizes the properties used for discontinuities. The elastic-perfectly plastic Mohr-Coulomb model is used for the behavior of the discontinuities. In this constitutive model the discontinuity normal displacement (opening/closure) due to an increase/decrease in normal effective stress is controlled by the discontinuity normal stiffness. The Mohr-Coulomb model also reproduces the mechanism of dilation/contraction induced during shearing in the discontinuity. The shear stiffness controls the elastic shear response while the plastic response is controlled by the shear strength of the discontinuity. The shear strength is dependent on the friction angle, the effective normal stress acting on the discontinuity and the cohesion. As sliding occurs in the discontinuity , dilation/contraction occurs with the associated changes in aperture and flow rate [e.g. *Ivars*, 2004].

Table 4.5 presents values used for simulation of the grouted area under the dam. Treating of the rock mass with cement based substances in the case of grout curtain have a positive affect on the strength properties of discontinuities and prevents movement of water through the opening between the surfaces of the discontinuity. The effect of grouting on the rock mass have extensively been covered in several works, e.g., *Swedenborg* [2001] and *Eriksson* [2002].

Table 4.4 Properties of discontinuities.

| **Name** | **Value** | **References** |
|---|---|---|
| Joint normal stiffness [GPa/m] | 10 | *Mören*, 2005 |
| Joint shear stiffness [GPa/m] | 10 | *Mören*, 2005 |
| Aperture for zero normal stress [m] | $0.25 \cdot 10^{-3}$ | *Barla et al.*, 2004 |
| Residual aperture [m] | $0.125 \cdot 10^{-3}$ | *Barla et al.*, 2004 |
| Joint cohesion [MPa] | 0 | *RG* |
| Joint residual cohesion [MPa] | 0 | *RG* |
| Joint friction angle[$^o$] | 35 | *RG* |
| Joint residual friction angle [$^o$] | 30 | *RG* |
| Joint dilation angle [$^o$] | 9 | *Swedenborg*, 2001 |
| Joint permeability constant$^*$ [1/Pa s] | 300 | *Barla et al., 2004*; *Itasca*, 2004 |
| Joint tensile strength [MPa] | 0 | *RG* |
| Joint residual tensile strength [MPa] | 0 | *RG* |
| Distance between joints$^{**}$ [m] | 2 and 3 | *RG* |

KEYS: $^*$, Joint permeability constant may also be termed joint permeability factor, $k_j$ ; $^{**}$, Distance between joints are 2 and 3 m in the base case, RG, my reference group and advisers

Table 4.5 Properties of grouted discontinuities

| Parameter | Value | References |
|---|---|---|
| Permeabilitet, $k_j$ [1/Pa s] | 300 | *Itasca*, 2004 |
| Height ( $H$ ) of the grouting | 2/3 H | *Vattenfall* , 1988 |
| Joint normal stiffness [GPa/m] | 12 | *RG*, pers. comm |
| Joint shear stiffness [GPa/m] | 12 | *RG*, pers. comm |
| Joint dilation angle [$^o$] | 9 | *Swedenborg*, 2001 |
| Joint friction angle [$^o$] | 35 | *Swedenborg*, 2001 |
| Joint residual friction angle [$^o$] | 25 | *Swedenborg*, 2001 |
| Aperture for zero normal stress [m] | $0.12 \cdot 10^{-3}$ | *Stille*, 2007 |
| Residual aperture at high stress [m] | $0.06 \cdot 10^{-3}$ | *Stille*, 2007 |
| Joint cohesion [MPa] | 0.6 | *Swedenborg*, 2001 |
| Joint residual cohesion [MPa] | 0 | *RG*, pers. comm |
| Joint tensile strength [MPa] | 0 | *RG*, pers. comm |

KEYS: RG, my reference group and advisers

The fictitious joints have been assigned high strength properties according to the recommendation from Itasca to prevent any shear/normal displacements along [e.g. *Christianson*, pers. comm.].

Table 4.6 presents values used for simulation of the embankment dam. The embankment dam body is shown by a solid block discretized into deformable triangular finite-different zones. The model assumed linearly elastic and isotropic conditions.

Table 4.6 Properties of the embankment dam, which is a soft body.

| Parameter | Value | References |
|---|---|---|
| Density, $\rho$ [kg/m$^3$] | 2100 | *Knutson*, pers. comm. |
| Young's modulus, $E$ [MPa]* | 6 | *Knutson*, pers. comm. |
| Poisson's ratio, $\nu$ [-] | 0.4 | *Knutson*, pers. comm. |

***KEYS:*** $^*$, $E$ of soft material normally ranges from 4 to 8 MPa.

## 4.4 Verification models

Two verification models have been set up to select the most suitable set of parameters in terms of load on the foundation rocks, the cut- and dam body models. The cut model was conducted to determine which of two joint layouts gave most reliable results. In the first approach, joint sets transected the entire model, whereas they only were defined within a specific area close to the dam in the second approach. The second approach is preferred, because it represents more realistic conditions regarding the length of discontinuities, and it is much more time efficient. In addition, the first approach resulted in atypical behavior of discontinuities close to their lateral boundaries.

The dam body model was made to find realistic values for the mechanical properties of the dam body that could be used without numerical problems (contact overlap). An embankment dam is soft that generates a specific loading pattern, with higher stresses under the dam center than at the heel and toe. The results were satisfying, and Table 4.6 shows the values used in simulation of the dam construction.

## 4.5 Cross sections

### 4.5.1 Cross-section A, parallel to the river valley

Cross-section A was selected to investigate potential shear- and normal displacements of the discontinuities during the three stages of the life time of the dam (Figure 4.2; Table 4.1). Displacements in the rock mass may threat the integrity of the dam construction. Additional attention have been given to the amount of seepage water coming through the foundation rock. Seepage may lead to piping through the foundation rock, as well as to reducing the amount of water in the reservoir, hence an economic loss for the dam owner.

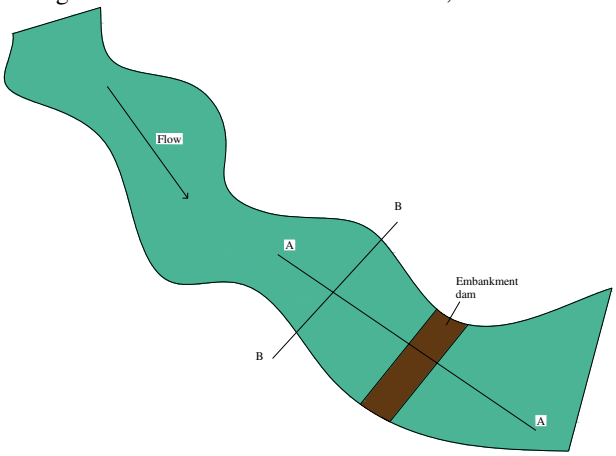


Figure 4.2 Cross-section A and Cross-Section B

The model size has been chosen based on the information received from other works [e.g. *Dolezalova, 2004; Barla et al., 2004*], hints received from Itasca, and from trial-and-error, in order to reduce possible boundary effects. The dimension of the model is 1000 x 500 m (width · height). Roller boundary conditions has been used on the vertical and bottom boundary of the model, whereas the top boundary (ground surface) has been simulated as a free surface. During Stages 2 and 3 of the dam life time (Table 4.1), the permeability of the lateral boundaries is set to zero (impermeable).

The rock mass has been discretized into deformable triangular finite-different zones (deformable material). To achieve good resolution in the areas of interest while keeping the calculation time within reasonable limits, the model has been divided into four areas with different zones size. The minimum size of the finite-difference zones have been chosen to be 2 m, less than the joint space (3 m). The zone size has been gradually increased towards the model boundaries by multiplying former zone size with factor between 2 and 3. The factor values have been chosen according to the recommendations by Itasca to guarantee smooth transition of displacements between areas with different zoning (Figure 4.3). The subdivision of the model into areas with different discretization has been done with help of fictitious discontinuities, which have been assigned high

strength parameters to inhibit any slip/separation failure. This approach has been advised by *Christianson* [e.g. pers. comm., 2007].

The discontinuity characteristics of the rock mass have been introduced only into the areas of interest, i.e. close to the dam construction (Figure 4.3). To exclude the possible disturbance of this approach (joints only allocated into certain areas) on the results, verification models have been run. (Section 4.4 *"Verification models"*). Discontinuities are represented by subvertical and banking joints with normal spacing from 3 to 5 m.

The location of the embankment dam has been selected to be in the middle of the free surface (ground surface). It allows observations of the behavior of foundation rock on the upstream and downstream sides due to construction of dam and impounding the reservoir as well as the variation of the water table in the pool. The dimensions of the dam construction (height, width of the crest and inclination of the upstream/downstream sides) has been chosen based on experience from Swedish hydropower dams (Figure 4.4).

The location of the grout curtain, under the middle part of the dam, has been chosen based on the construction recommendations and the most common design of Swedish dams [e.g. *Fell et al.*, 2005]. The height of the grouted zone is selected from *Vattenfalls handbok* [1988], and equals 2/3 of the height of the dam. The width of the grout curtain is site specific, and depends on the local structural geology. A width of 8 m is used in the model.

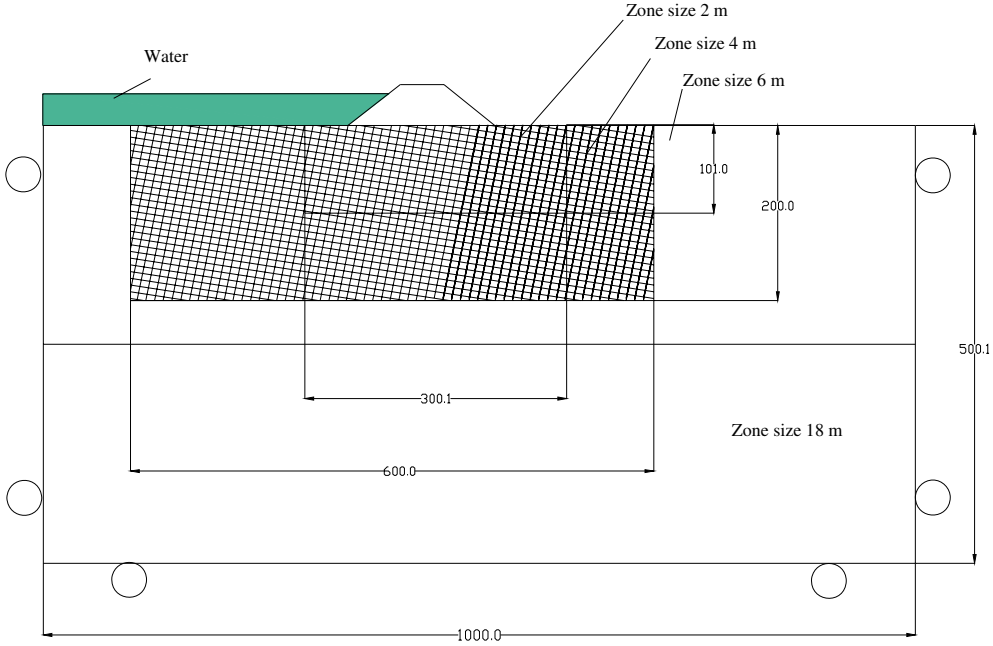


Figure 4.3 Layout of the Cross-Section A

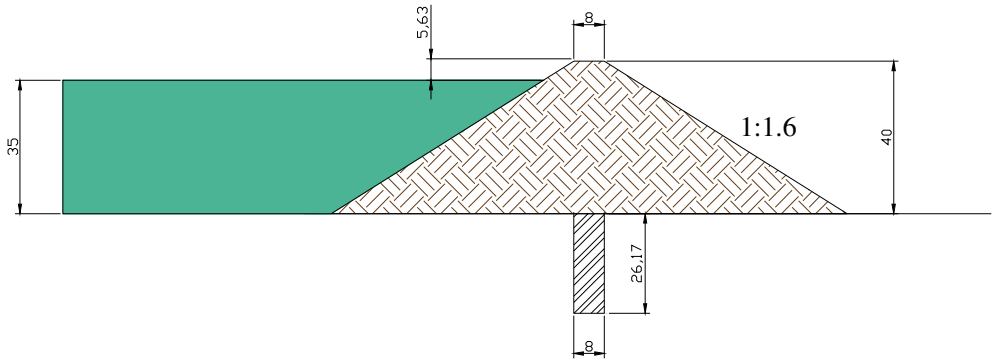


Figure 4.3 Dimension of the embankment dam and grout curtain.

### 4.5.2 Cross-section B, perpendicular to the river valley

Cross-section B (Figure 4.2) was chosen to study the normal displacements (opening) of discontinuities due to applied hydrostatic pressure caused by filling the reservoir and due to the variation of the water level. Cross-section B was especially important because joints that were striking (sub-) parallel to the river valley could be studied. The process of opening joints on the upstream side of the dam under the reservoir may be a start point of development of seepage under the dam.

The set-up of the model has been kept almost the same as for Cross-section A, except for some modifications (Figure 4.4). The dimension of the Cross-section B across the river valley are: Height of the banks are 40 m, and equal the height of the dam. The inclination of the banks is 45°, and the width of the dam is 500 m [e.g. *Lindfors*, pers. comm.2005]. The dimension of the areas of interest has been expanded to meet the requirements of new layout, whereas the ratio of zone sizes of adjacent areas is kept the same as in the longitudinal case. The stress field is oriented as follows: the major horizontal stress is the out-of-plane stress and the minor horizontal stress is directed parallel to Cross-section B.

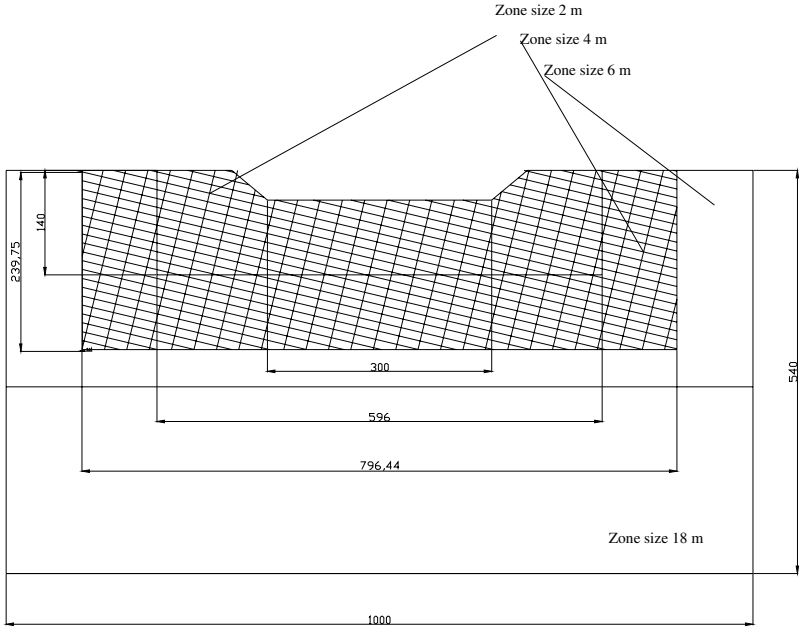


Figure 4.4 Lay-out of Cross-Section B

The calculation sequence of all models involved first running them to an equilibrium pre-excavation state (with all stresses, loads and boundary conditions applied). In the first model the ground surface was flat. The river valley was then excavated and the model was again run to equilibrium. In these two calculation sequences the block material was linear elastic and the strength values of the discontinuities were set to high values, to prevent plastic flow and inelastic movements along the discontinuities as an effect of dynamic phenomena arising from the change of conditions. After this the impounding of water in the reservoir was simulated. Finally the variation of the water level in the reservoir is simulated. Each step in the simulation is finalized by brining the model to the equilibrium state first using high strength values and then the real ones.

# 5. RESULTS

## 5.1 Sensitivity analyses

The amount and location of maximum normal- and shear displacements along discontinuities, and the total water flow through the rock mass have been studied in a total number of 61 sensitivity analyses. The analyses consider three stages in the life time of an embankment dam (Table 4.1). These three stages are thought to be critical with respect to dam stability and functionality of the grouting curtain. To account for discontinuities oriented perpendicular and parallel to the river valley, analyses have been made along two cross sections. Cross-section A runs parallel to the strike of the river valley, and Cross-section B is oriented perpendicular to the strike of the river valley.

As described in Chapter 4, "*Conceptual Numerical Analyses",* a base case (BC) model has been constructed using parameters with typical average values for Swedish crystalline rocks. One parameter at a time has then been altered to investigate the influence on rock mass and total water flow. Figure 5.1 illustrates three of the factors included in the sensitivity analyses, state of stress, dip of joints, and spacing of subvertical joints. In addition to these three parameters, the models also investigate three other parameters, namely properties of the discontinuities (i.e. joints) regarding their dilation- and friction angle, and hydraulic aperture. Furthermore, two and three parameters are kept constant during modeling along Cross-sections A and B, respectively (Table 5.3). The individual influence of these six parameters is investigated using a BC model and 14 additional models for Cross-section A, and 11 additional models for Cross-section B. Tables 5.1 and 5.2 show the configuration of parameters in all models and their values of the sensitivity analyses.

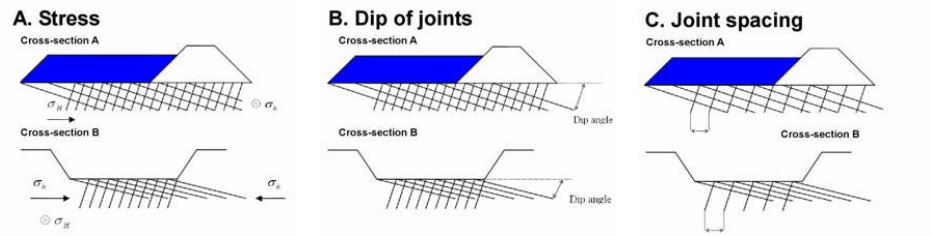


Figure 5.1. Three factors included in the sensitivity analyses. A, State of stress; B, Joint dips; C, Joint spacing.

Each model is run to equilibrium. The values of the model parameters have been obtained from literature [e.g. *Swedenborg*, 2001; *Mören*, 2005; *Sjöberg et al*., 2005; *Töyrä*, 2006; *Sjöberg*, 2007], and from discussions within my reference group [e.g. *RG*, pers. comm. 2006; 2007].

Table 5.1 Model parameters and values for sensitivity analyses along Cross-section A

| Model No. | Maximum horizontal stress, $\sigma_H$ [MPa] | Minimum horizontal stress, $\sigma_h$ [MPa] | Joint Friction Angle [°] | Joint Dilation Angle [°] | Dip of banking joints [°] | Dip of subvertical joints [°] | Normal subvertical joint distance [m] | Hydraulic aperture [m] |
|---|---|---|---|---|---|---|---|---|
| Base Case (BC) | $2.8+0.0399z$ | $2.2+0.0240z$ | 35 | 9 | -5 | 85 | 5 | $0.25\cdot10^{-3}$ |
| 1 | $6.7+0.0444z$ | $0.8+0.0329z$ | 35 | 9 | -5 | 85 | 5 | $0.25\cdot10^{-3}$ |
| 2 | $0.085z$ | $0.022z$ | 35 | 9 | -5 | 85 | B: 3<br>SV: 5 | $0.25\cdot10^{-3}$ |
| 3 | $2.8+0.0399z$ | $2.2+0.0240z$ | 25 | 9 | -5 | 85 | 5 | $0.25\cdot10^{-3}$ |
| 4 | $2.8+0.0399z$ | $2.2+0.0240z$ | 30 | 9 | -5 | 85 | 5 | $0.25\cdot10^{-3}$ |
| 5 | $2.8+0.0399z$ | $2.2+0.0240z$ | 40 | 9 | -5 | 85 | 5 | $0.25\cdot10^{-3}$ |
| 6 | $2.8+0.0399z$ | $2.2+0.0240z$ | 35 | 0 | -5 | 85 | 5 | $0.25\cdot10^{-3}$ |
| 7 | $2.8+0.0399z$ | $2.2+0.0240z$ | 35 | 9 | -5 | 70 | 5 | $0.25\cdot10^{-3}$ |
| 8 | $2.8+0.0399z$ | $2.2+0.0240z$ | 35 | 9 | -5 | 100 | 5 | $0.25\cdot10^{-3}$ |
| 9 | $2.8+0.0399z$ | $2.2+0.0240z$ | 35 | 9 | -10 | 85 | 5 | $0.25\cdot10^{-3}$ |
| 10 | $2.8+0.0399z$ | $2.2+0.0240z$ | 35 | 9 | -5 | 85 | 1 | $0.25\cdot10^{-3}$ |
| 11 | $2.8+0.0399z$ | $2.2+0.0240z$ | 35 | 9 | -5 | 85 | 9 | $0.25\cdot10^{-3}$ |
| 12 | $2.8+0.0399z$ | $2.2+0.0240z$ | 35 | 9 | -5 | 85 | 5 | $0.5\cdot10^{-3}$ |
| 13 | $2.8+0.0399z$ | $2.2+0.0240z$ | 35 | 9 | -5 | 85 | 5 | $1\cdot10^{-3}$ |
| 14 | $2.8+0.0399z$ | $2.2+0.0240z$ | 35 | 9 | -5 | 85 | 5 | $2.5\cdot10^{-3}$ |

KEYS: $\sigma_H$ is oriented parallel to the river valley; $\sigma_h$ is oriented out of plane.

Table 5.2 Model parameters and values for sensitivity analyses along Cross-section B

| Model No. | Maximum horizontal stress, $\sigma_H$ [MPa] | Minimum horizontal stress, $\sigma_h$ [MPa] | Joint Friction Angle [°] | Joint Dilation Angle [°] | Dip of banking joints [°] | Dip of subvertical joints [°] | Normal subvertical joint distance [m] | Hydraulic aperture [m] |
|---|---|---|---|---|---|---|---|---|
| Base Case (BC) | $2.2+0.0240z$ | $2.8+0.0399z$ | 35 | 9 | -5 | 85 | 5 | $0.25\cdot10^{-3}$ |
| 1 | $0.8+0.0329z$ | $6.7+0.0444z$ | 35 | 9 | -5 | 85 | 5 | $0.25\cdot10^{-3}$ |
| 2 | $0.022z$ | $0.085z$ | 35 | 9 | -5 | 85 | B: 3<br>SV: 5 | $0.25\cdot10^{-3}$ |
| 3 | $2.2+0.0240z$ | $2.8+0.0399z$ | 25 | 9 | -5 | 85 | 5 | $0.25\cdot10^{-3}$ |
| 4 | $2.2+0.0240z$ | $2.8+0.0399z$ | 30 | 9 | -5 | 85 | 5 | $0.25\cdot10^{-3}$ |
| 5 | $2.2+0.0240z$ | $2.8+0.0399z$ | 40 | 9 | -5 | 85 | 5 | $0.25\cdot10^{-3}$ |
| 6 | $2.2+0.0240z$ | $2.8+0.0399z$ | 35 | 0 | -5 | 85 | 5 | $0.25\cdot10^{-3}$ |
| 7 | $2.2+0.0240z$ | $2.8+0.0399z$ | 35 | 9 | -5 | 70 | 5 | $0.25\cdot10^{-3}$ |
| 8 | $2.2+0.0240z$ | $2.8+0.0399z$ | 35 | 9 | -5 | 100 | 5 | $0.25\cdot10^{-3}$ |
| 9 | $2.2+0.0240z$ | $2.8+0.0399z$ | 35 | 9 | -10 | 85 | 5 | $0.25\cdot10^{-3}$ |
| 10 | $2.2+0.0240z$ | $2.8+0.0399z$ | 35 | 9 | -5 | 85 | 1 | $0.25\cdot10^{-3}$ |
| 11 | $2.2+0.0240z$ | $2.8+0.0399z$ | 35 | 9 | -5 | 85 | 9 | $0.25\cdot10^{-3}$ |

KEYS: $\sigma_H$ is oriented out of plane; $\sigma_h$ is oriented perpendicular to river valley.

Table 5.3 Parameters that were kept constant throughout testing, and their values

| Parameters | Value / Relationships |
|---|---|
| ***Models along Cross-section A*** | |
| Vertical stress, $\sigma_v$ [MPa] | $\rho gz$ |
| Spacing of normal banking joints [m] | 3 |
| ***Models along Cross-section B*** | |
| Vertical stress, $\sigma_v$ [MPa] | $\rho gz$ |
| Spacing of normal banking joints [m] | 3 |
| Hydraulic aperture [mm] | 0.25 |

Below, results are presented for the behavior of the rock mass during Stages 1-3, along Cross-sections A and B, with respect to maximum normal- and shear displacements in rock mass and grout curtain, and total flow. The results are presented in three ways. First, the variation in maximum magnitude of shear- and normal displacements for the models are presented for the three stages of dam life along the two cross sections to give an impression of the individual influence of the parameters in the models. Second, the location of shear- and normal displacements for the models are presented to allow identification of potential areas of unwanted deformation. Third, the total flow is calculated and presented to give the understanding how much water is lost from the reservoir under the model conditions.

## 5.2 Maximum magnitude of displacement

The term maximum magnitude of displacement identifies the largest deformation which can be observed in the model. To specify the location of the largest deformation in the model I have used term “a point”.

### 5.2.1 False displacement caused by UDEC simulation

Two cases of false displacements have been found during the sensitivity analyses. The first case results from the fact that the dam is simulated as a solid block by UDEC along Cross-section A. The addition of water during Stage 2 result in extensive normal motion along the interface between dam and rock mass at the heel of the dam, along Cross-section A (Figure 5.2). This behavior is unrealistic and related to the specific of the model. This kind of normal deformation is not observed in soft-bodied embankment dams; therefore, all maximum normal- and shear displacements near this area are considered with caution. The second case is found in the points of intersection between the banks and the bottom of the reservoir along Cross-section B. The lay-out of the model, with sharp inflection points between banks and bottom of the reservoir result in high stress concentrations in these points. Because natural reservoirs do not have such sharp inflection points, the extensive displacements in those points are related to specifics of the numerical code. The effects from these false displacements are removed from the models by hand. The upper limit of maximum deformation is gradually reduced until the

extensive displacements disappears. Figure 5.3 shows two examples of gradually reduced values of along Cross-sections A and B.

Note that normal- and shear displacements often occur along the interface between the dam and the foundation rock. However, the behavior of this interface is outside the scope of this study; hence, this data have been disregarded.

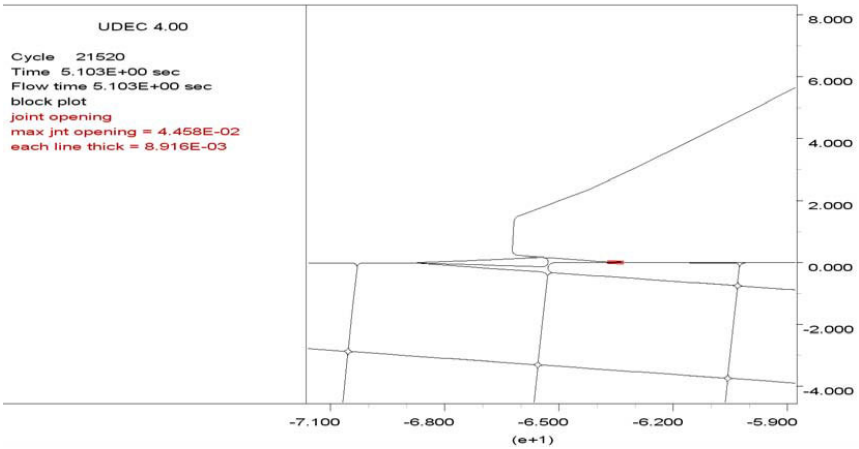


Figure 5.2 Lifting of the dam heel with extensive normal deformation of discontinuities. The figure shows results from the BC Model (cf. Table 5.1). This phenomenon is considered to be related to the numerical code, and not something that occur in-situ.

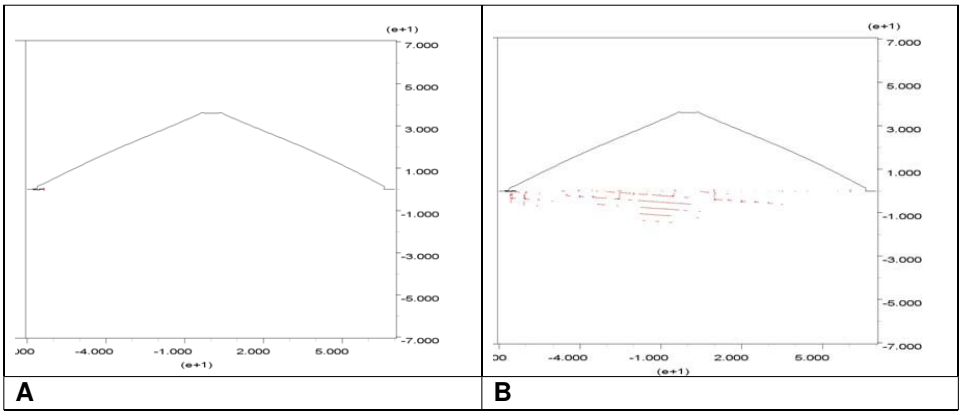


Figure 5.3 False displacements are removed by hand in the BC Model. A, View before false displacements are removed. Extensive normal deformation is found in the interface between the dam and the foundation. B, View after false displacements are removed.

### 5.2.2 Maximum displacement along Cross-section A

Results from Stage 1, dam construction

No water is present during Stage 1, consequently, the sensitivity analyses only consider normal- and shear deformation along discontinuities (i.e. Models 1-11 of Table 5.1).

The magnitudes of maximum displacement in rock mass and grout curtain vary from 0 to 1370 µm (Table 5.4). The displacements in the rock mass are many times greater and vary more than those of the grout curtain (Table 5.4). The average magnitudes of shear- and normal displacements in the rock mass for the different models and their standard deviation are 204±375 µm and 90±197 µm, respectively. Corresponding values for the grout curtain are 3±4 µm and 2±3 µm, respectively.

Table 5.4 Maximum displacements in a point from Cross-section A, during Stage 1

| Model No | Rock mass | | Grout Curtain | |
|---|---|---|---|---|
| | Shear displacement [µm] | Normal displacement [µm] | Shear displacement [µm] | Normal displacement [µm] |
| BC | 45 | 27 | 1 | 0 |
| 1 | 119 | 72 | 4 | 4 |
| 2 | 59 | 9 | 0 | 2 |
| 3 | 230 | 54 | 1 | 1 |
| 4 | 41 | 27 | 1 | 1 |
| 5 | 27 | 24 | 2 | 3 |
| 6 | 100 | 18 | 0 | 1 |
| 7 | 20 | 6 | 0 | 1 |
| 8 | 222 | 35 | 2 | 2 |
| 9 | 185 | 88 | 3 | 2 |
| 10 | 1370 | 710 | 16 | 11 |
| 11 | 34 | 13 | 0 | 1 |
| ***Av. ±s.d.*** | ***204±375*** | ***90±197*** | ***3±4*** | ***2±3*** |

KEYS: ***Av.***, average value; ***s.d.***, standard deviation

### Results from Stage 2, filling the reservoir with water

The magnitudes of maximum displacement in rock mass and grout curtain vary from 10 to 3000 µm (Table 5.5). In general, the shear displacements are higher than the normal displacements. Furthermore, the displacements in rock mass tend to be greater than those in the grout curtain. The average magnitudes of shear- and normal displacements for the different models and their standard deviation are 1209±812 µm and 390±638 µm, respectively. Corresponding values for the grout curtain are 194±545 µm and 38±11 µm, respectively.

The calculation of total flow from the hydraulic aperture is described in Chapter 4, *Conceptual Numerical Analyses*. The total flow in the drill curtain varies from 0.02 to 61.5 l/s, with an average value of 4.71±15.74 l/s (Table 5.5).

Table 5.5 Maximum displacements in a point from Cross-section A, during Stage 2.

| **Model No.** | **Foundation rock** | | **Grout Curtain** | | **Total Flow (l/s)** |
|---|---|---|---|---|---|
| | **Shear displacement (µm)** | **Normal displacement (µm)** | **Shear displacement (µm)** | **Normal displacement (µm)** | |
| ***BC*** | 1800 | 96 | 20 | 33 | 0.28 |
| ***1*** | 3000 | 310 | 300 | 42 | 1.05 |
| ***2*** | 232 | 26 | 10 | 28 | 0.03 |
| ***3*** | 2100 | 2170 | 2140 | 32 | 0.12 |
| ***4*** | 1750 | 1030 | 90 | 57 | 0.19 |
| ***5*** | 459 | 156 | 12 | 37 | 0.25 |
| ***6*** | 90 | 22 | 10 | 24 | 0.02 |
| ***7*** | 1340 | 110 | 17 | 46 | 0.3 |
| ***8*** | 2100 | 160 | 25 | 29 | 0.33 |
| ***9*** | 641 | 162 | 183 | 36 | 0.15 |
| ***10*** | 1230 | 1420 | 27 | 64 | 1.77 |
| ***11*** | 710 | 40 | 10 | 36 | 0.16 |
| ***12*** | 1210 | 66 | 20 | 36 | 0.78 |
| ***13*** | 728 | 50 | 20 | 41 | 3.79 |
| ***14*** | 746 | 41 | 20 | 29 | 61.5 |
| ***Av. ±s.d.*** | ***1209±812*** | ***390±638*** | ***194±545*** | ***38±11*** | ***4.71±15.74*** |

KEYS: ***Av.***, average value; ***s.d.***, standard deviation

Results from Stage 3, varying water level (cyclic loading)

The magnitudes of maximum displacement in rock mass and grout curtain vary from 20 to 6010 µm (Table 5.6). The shear displacements are greater and have higher variability than the normal displacement. Furthermore, the displacements in rock mass tend to be greater than those in the grout curtain. The average magnitudes of shear displacements for the different models and their standard deviation are 2260±1382 µm for the rock mass, and 486±923 µm for the grout curtain. Corresponding normal displacement values are 186±253 µm for the rock mass and 45±17 µm for the grout curtain. The total flow varies from 0.03 to 117.0 l/s, with an average value of 8.55±30.03 l/s (Table 5.6).

Table 5.6 Maximum displacements in a point from Cross-section A, during Stage 3

| **Model No.** | **Foundation rock** | | **Grout Curtain** | | |
|---|---|---|---|---|---|
| | **Shear displacement (µm)** | **Normal displacement (µm)** | **Shear displacement (µm)** | **Normal displacement (µm)** | **Total Flow (l/s)** |
| ***BC*** | 2570 | 100 | 65 | 57 | 0.22 |
| ***1*** | 6010 | 1000 | 965 | 40 | 1.16 |
| ***2*** | 510 | 63 | 21 | 26 | 0.03 |
| ***3*** | 3720 | 71 | 2800 | 41 | 0.07 |
| ***4*** | 2720 | 85 | 2550 | 35 | 0.18 |
| ***5*** | 872 | 27 | 38 | 35 | 0.24 |
| ***6*** | 300 | 30 | 20 | 20 | 0.03 |
| ***7*** | 2260 | 100 | 43 | 34 | 0.3 |
| ***8*** | 2820 | 110 | 73 | 36 | 0.31 |
| ***9*** | 1580 | 292 | 400 | 36 | 0.13 |
| ***10*** | 2730 | 485 | 85 | 75 | 2.45 |
| ***11*** | 1970 | 92 | 39 | 33 | 0.18 |
| ***12*** | 2100 | 110 | 67 | 64 | 0.82 |
| ***13*** | 1840 | 117 | 64 | 71 | 5.10 |
| ***14*** | 1900 | 112 | 61 | 66 | 117.00 |
| ***Av. ±s.d.*** | ***2260±1382*** | ***186±253*** | ***486±923*** | ***45±17*** | ***8.55±30.03*** |

KEYS: ***Av.***, average value; ***s.d.***, standard deviation

### Comparison of results from the three stages

Figures 5.4 to 5.7 show the variation of normalized maximum displacement of individual parameters with respect to shear- and normal deformation in the rock mass and grout curtain during the three stages of the dam life. The magnitudes of displacements for the three stages and for normal- and shear displacements in the rock mass and grout curtain vary from 0 to 6010 µm. In general, the smallest displacements are obtained as normal deformation in the grout curtain, and the largest displacements are obtained as shear deformation in the rock mass. By normalizing the values within each group with respect to the maximum value within that group allows comparison of individual parameters and groups at the same scale.

Figure 5.4 shows the normalized shear displacements in the rock mass for Stages 1 to 3. In general, Stage 3 (varying the water level in the reservoir) results in larger shear displacement than Stages 2 and 1. The high stress state of Model 1 resulted in the largest shear displacement of 6010 µm during Stage 3. Several models result in a normalized shear displacement from 0.3-0.6, i.e displacement values from about 2000 to 3600 µm.

A different result is obtained from the normalized normal displacements in the rock mass (Figure 5.5). The maximum amount of normal deformation (2170 µm) is obtained for Model 3 (joint friction angle is 25°) during Stage 2. Normalized normal displacement greater than 0.4 is obtained only for three other models: Models 4 and 10 during Stage 2, and Model 1 during Stage 3. Remaining normalized normal displacement generally are less than 0.2 for the other models.

Almost the reversed trends are observed for the normalized shear- and normal displacements in the grout curtain (Figures 5.6 and 5.7). Three models during Stages 2 and 3 indicate higher normalized shear displacements than 0.3; whereas the majority of all models from Stages 2 and 3 have a higher normalized normal displacement than 0.4. The maximum amount of shear deformation (2800 µm) is obtained for Model 3 (joint friction angle = 25°) during Stage 3. The corresponding value for maximum normalized normal displacement is 75 µm, which is obtained for Model 10 during Stage 3 with 1 m joint spacing.

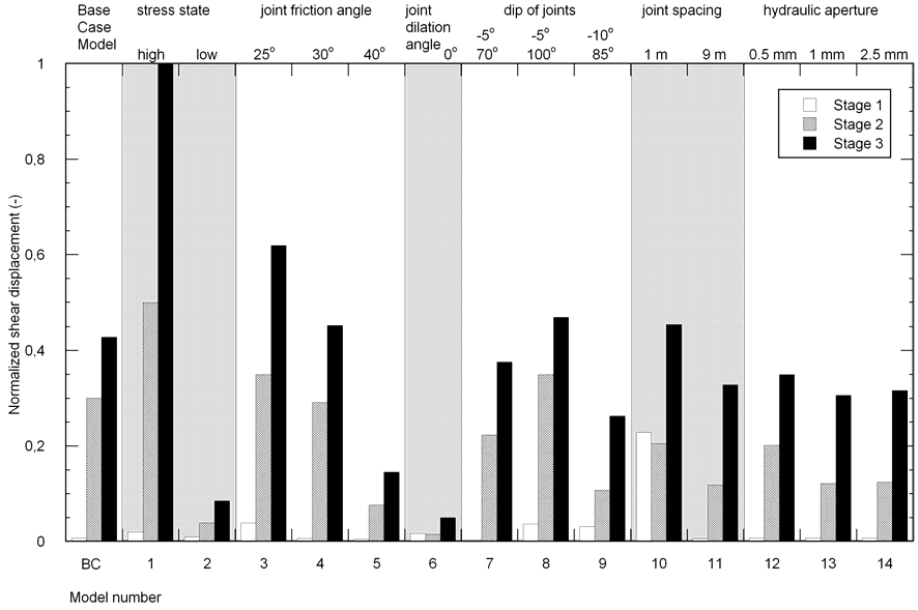


Figure 5.4 Cross-section A, Stage 1-3 shear displacements in the rock mass

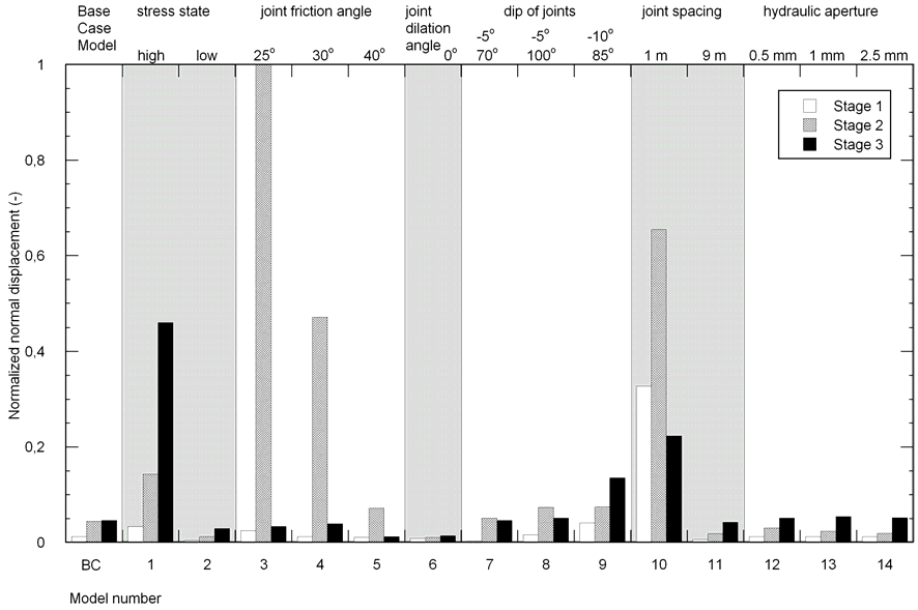


Figure 5.5 Cross-section A, Stage 1-3 normal displacements in the rock mass

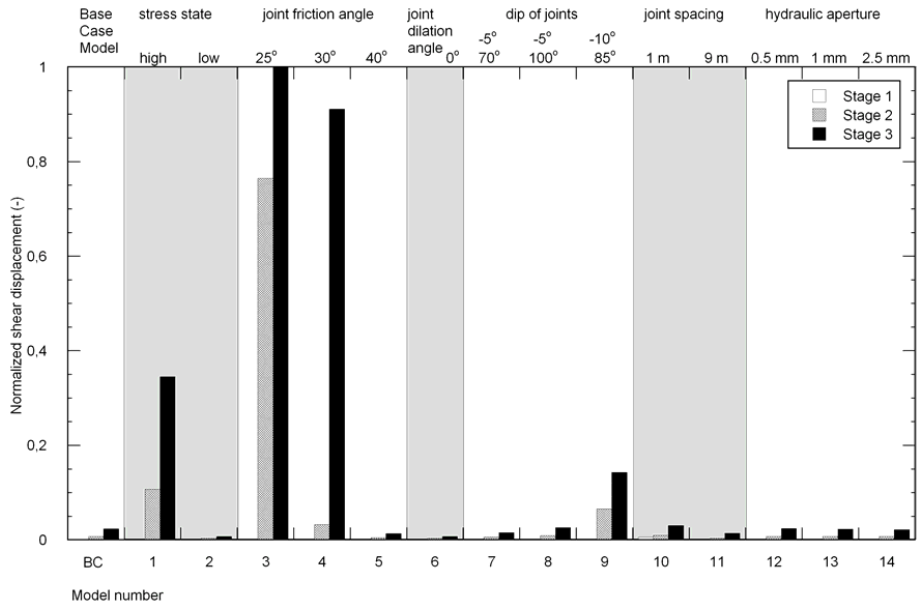


Figure 5.6 Cross-section A, Stage 1-3 shear displacements in the grout curtain

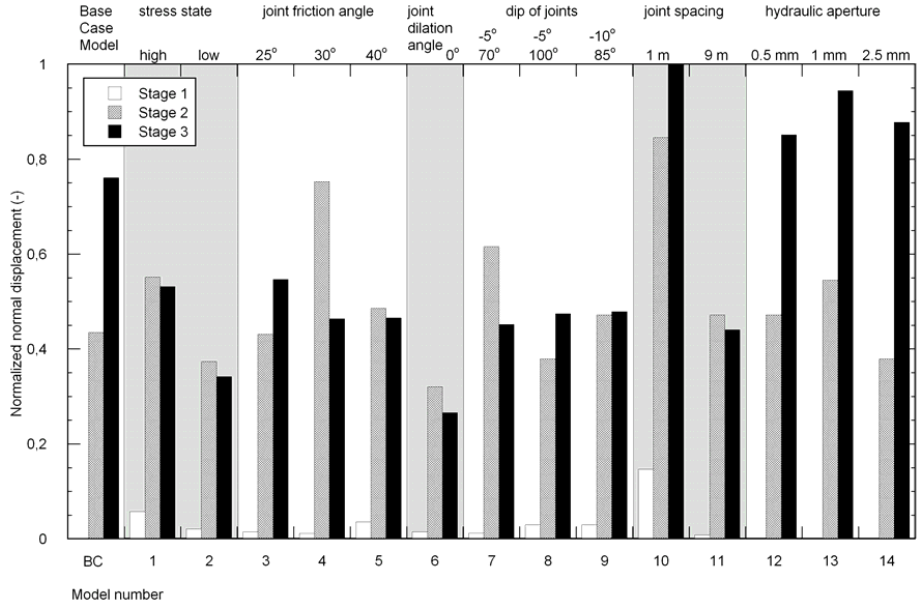


Figure 5.7 Cross-section A, Stage 1-3 normal displacements in the grout curtain.

### 5.2.3 Maximum displacement along Cross-section B

Results from Stage 2, filling the reservoir with water

The magnitudes of maximum displacement in the rock mass vary from 100 to 2000 µm (Table 5.7), with the shear displacements being about ten times higher than the corresponding normal displacements. The average magnitude of shear displacements for the different models and its standard deviation is 1289±574 µm. The corresponding value for the normal displacements is 375±302 µm.

Results from Stage 3, varying water level (cyclic loading)

The magnitudes of maximum displacement in rock mass and grout curtain vary from 100 to 4730 µm (Table 5.8). In general, the shear displacements are higher and more variable than the normal displacements. The average magnitude and the standard deviation for shear- and normal displacements for the different models of Stage 3 are 2111±1236 µm and 408±516 µm, respectively.

Comparison of results from the three stages

Figures 5.8 to 5.9 show the variation of normalized maximum displacement of individual parameters with respect to shear- and normal deformation in the rock mass during the two later stages of the dam life. Stage 1 is not included in the analyses, because it is assumed that the reservoir bottom and its banks are not affected by the dam construction.

Table 5.7 Maximum displacements in a point from Cross-section B, during Stage 2

| **Model No.** | **Shear displacement (µm)** | **Normal displacement (µm)** |
|---|---|---|
| ***BC*** | 2000 | 300 |
| ***1*** | 900 | 200 |
| ***2*** | 1000 | 900 |
| ***3*** | 1000 | 200 |
| ***4*** | 2000 | 300 |
| ***5*** | 2000 | 800 |
| ***6*** | 1000 | 200 |
| ***7*** | 761 | 100 |
| ***8*** | 1000 | 200 |
| ***9*** | 385 | 200 |
| ***10*** | 2000 | 900 |
| ***11*** | 1420 | 200 |
| ***Av ±s.d*** | ***1289±574*** | ***375±302*** |

KEYS: ***Av.***, average value; ***s.d.***, standard deviation

Table 5.8 Maximum displacements in a point from Cross-section B, during Stage 3

| Model No. | Shear displacement (μm) | Normal displacement (μm) |
|---|---|---|
| ***BC*** | 1400 | 200 |
| ***1*** | 962 | 200 |
| ***2*** | 4000 | 100 |
| ***3*** | 3130 | 200 |
| ***4*** | 1960 | 300 |
| ***5*** | 1290 | 300 |
| ***6*** | 2000 | 300 |
| ***7*** | 945 | 300 |
| ***8*** | 2340 | 600 |
| ***9*** | 1150 | 200 |
| ***10*** | 4730 | 2000 |
| ***11*** | 1430 | 200 |
| ***Av ±s.d*** | **2111±1236** | **408±516** |

KEYS: ***Av.***, average value; ***s.d.***, standard deviation

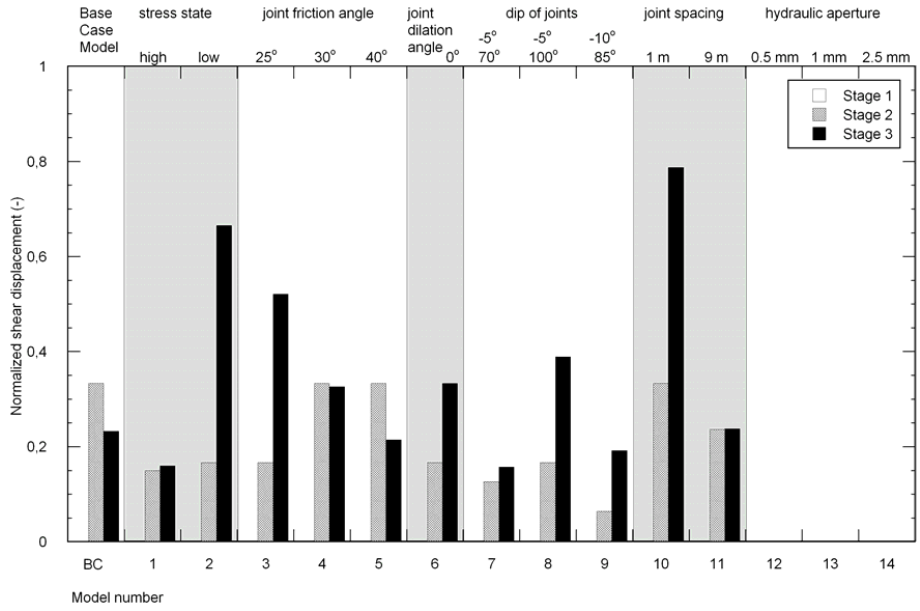


Figure 5.8 Cross-section B, Stage 2-3 shear displacements in the rock mass.

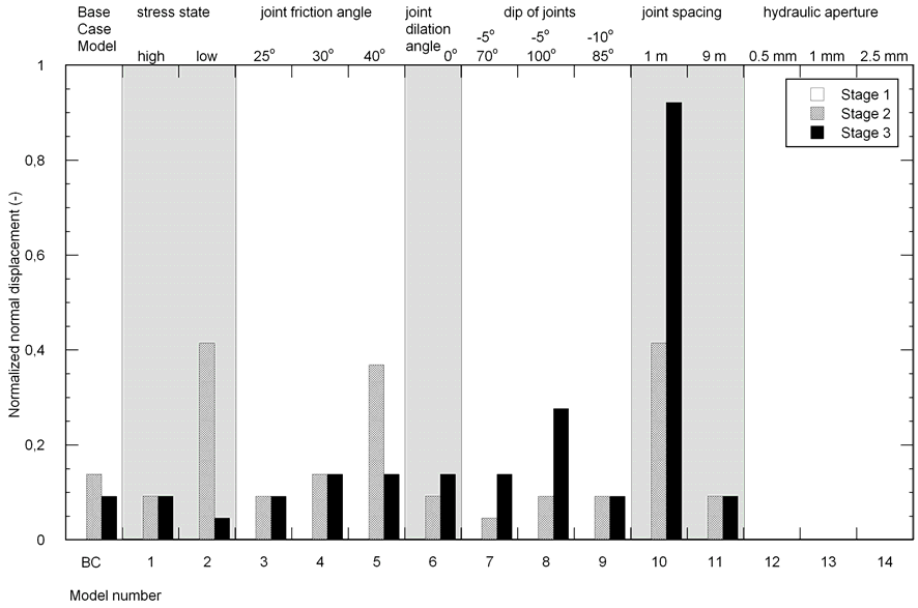


Figure 5.9 Cross-section B, Stage 2-3 normal displacements in the rock mass.

Figure 5.8 shows the normalized shear displacements in the rock mass for Stages 2 to 3. In general, Stage 3 (varying the water level in the reservoir) results in larger shear displacement than Stage 2. The BC Model and Model 5 (joint friction angle = 40°) are the only two clear exceptions from this trend, and have largest displacements during Stage 2. The values are normalized against the maximum shear displacement in the rock mass, 6010 µm, which is obtained during Stage 3 for Model 1 along Cross-section A. Three higher values of normalized shear displacement between 0.4 and 0.8 is obtained for Models 10, 2 and 3, respectively.

The results from the normalized normal displacements in the rock mass along Cross-section B (Figure 5.9) show that the 1 m joint spacing of Model 10 during Stage 3 results in highest normalized normal displacement, ~0.95, along this cross-section. The data are normalized against 2800 µm, the highest value, obtained for Model 3 (joint friction angle (25°) during Stage 2, along Cross-section A. Most other models propose a normalized normal displacement less than 0.2 (<560 µm).

## 5.3 Location of displacements

The curtain commands of UDEC have been used to identify the maximum shear- and normal displacements in each model. This group of commands plot a certain range of values of displacements. The upper limit of the plotted range is the maximum displacement found in the model. The lower limit is calculated by dividing the maximum values by 5. The result is that the scale of each plot varies, and depends on the maximum amount of shear- and normal displacement: If the magnitude of maximum displacement is high, lower values ( $< (\text{maximum displacement})/5$ ) of displacements are cut off from the

plot. Because small values of displacement are cut off in, most plots with relatively high amount of maximum displacement are characterized by localized deformation. On the other hand, if the magnitude of displacement is low, only a restricted interval of small displacements is plotted. The tendency is that the deformation in these plots are widespread. Hence, a first comparison between two plots with high and low magnitudes of maximum displacement, respectively, gives the impression that deformation is more significant in the model with low magnitude of maximum deformation. However, this impression if false, because the small values of displacement have been cut off in plots with high maximum magnitudes of displacement. To remind the reader on the different scales, the scale of the plot window is included in all cross sections.

### 5.3.1 Occurrence of displacement along Cross-section A

Stage 1, Shear displacements in the rock mass

Figure 5.10 shows a summary of results for the BC Model and remaining 11 models of Stage 1. The locations of shear displacement are shown in red in the Figure 5.10. The thickest line represents the location of the maximum shear displacements. The results reveal that the construction of the dam may result in shear displacement close to top of the rock foundation on the upstream side of the dam and close to the middle part, in the BC Model.

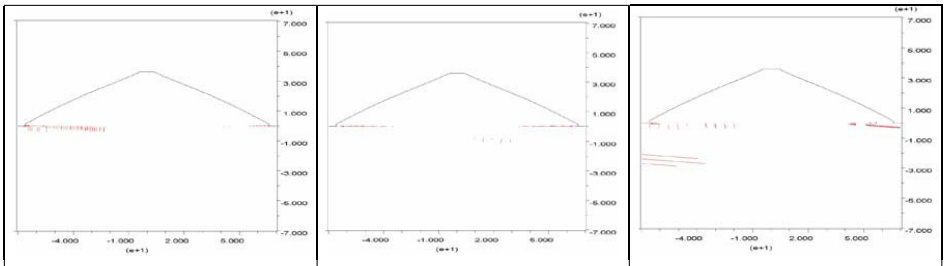

| Model 10 (joint spacing, 1 m)<br>PW: 1370-274 µm | Model 3 (joint friction angle, 25°);<br>PW: 230-46 µm | Model 8 (joint dips, -5°, 100°)<br>PW: 222-44 µm |
|---|---|---|

Figure 5.10 Shear displacements for the BC Model and Models 1-11 during Stage 1 along Cross-Section A. The scale on both axes is in tens of meters; hence, the width of all models is about 120 m and the height is about 140 m. The red dots show location of shear displacements, with thicker lines indicating higher magnitudes of displacements. Note that the range of displacements varies for each plot window (PW)

| | | |
|---|---|---|
| 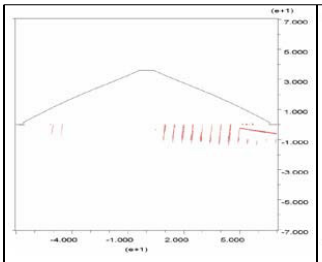 Model 9 (joint dips, -10°, 85°) PW: 185-37 µm | 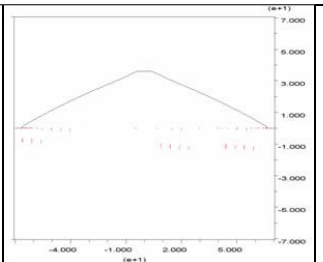 Model 1 (high stress state) PW: 119-24 µm | 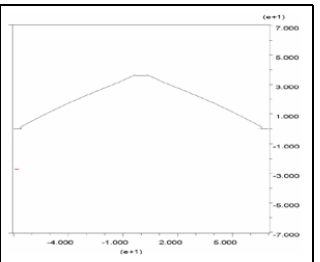 Model 6 (joint dilation angle, 0°) PW: 100-20 µm |
| 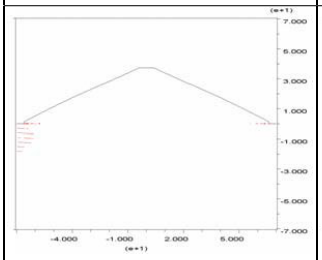 Model 2 (low stress state) PW: 60-12 µm | 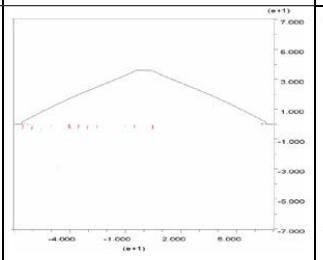 Model 5 (joint friction angle, 40°); PW: 57-5 µm | 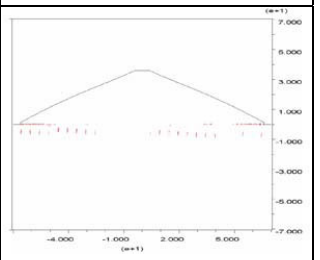 Model 4 (joint friction angle, 30°); PW: 41-8 µm |
| 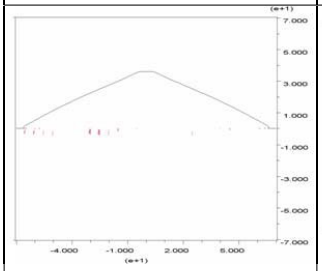 **BC Model** PW: 45-9 µm | 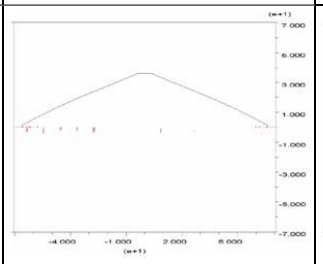 Model 11 (joint spacing, 9 m) PW: 37-7 µm | 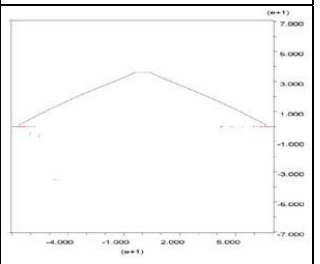 Model 7 (joint dips,, -5°, 70°) PW: 20-4 µm |

Figure 5.10 (continued)

Largest size of shear deformation is obtained for a joint spacing of 1 m (Model 10 of Figure 5.10). A shear zone along the banking plane below the outer shell on the heel side of the dam is obtained. In comparison, smaller joint spacing (i.e., BC Model and Model 11) have much smaller amount of displacements; however, the deformations in these latter two models occur in a similar area as that of Model 19.

Low friction angle (25°, Model 3) and steeply dipping subvertical joints (Models 8 and 9) have about 10% of the deformation obtained for Model 10. While Model 8 result in shearing along banking planes at about 30 m depth under the heel of the dam, steeper

dips of banking and subvertical joints result in shearing along subvertical joints under the downstream side of the dam (Figure 5.10).

Remaining models show sporadic and separate small areas of shear displacements, mostly at shallow depths along subvertical joints.

### Stage 1, Normal displacements in the rock mass

Construction of the dam result in only small, detached sections with normal displacements. Figure 5.11 shows that coherent motion generally is less than 5 m long.

The model with joint spacing of 1 m (Model 10) reveal most amount of normal displacement. Motion is mainly restricted to a small section along a subvertical joint near horizontal and vertical coordinates 0 and -15 m, respectively. Models 9 and 1 are about 10% of that of Model 10. Normal motion is restricted to subvertical- and banking joints under the downstream side of the dam (Figure 5.11).

Detached patches of normal displacements along banking joints is also observed in many other models (Models 3, 8, 4, 11), but the magnitude of displacement is very limited (Table 5.1)

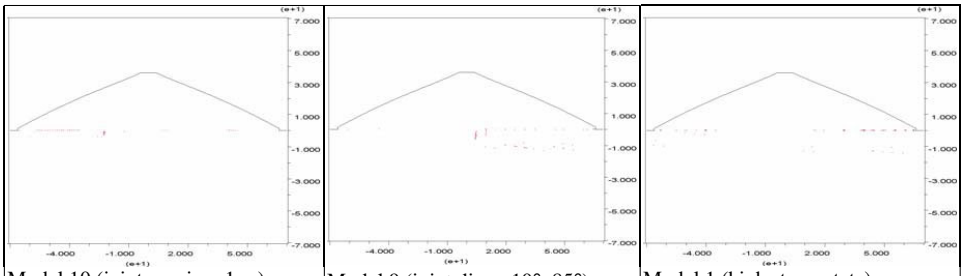

Model 10 (joint spacing, 1 m)
PW: 710-142 μm

Model 9 (joint dips, -10°, 85°)
PW: 88-18 μm

Model 1 (high stress state)
PW: 72-14 μm

Figure 5.11 Normal displacements for the BC Model and Models 1-11 during Stage 1 along Cross-Section A. The scale on both axes is in tens of meters; hence, the width of all models is about 120 m and the height is about 140 m. The red dots show location of shear displacements, with thicker lines indicating higher magnitudes of displacements. Note that the range of displacements varies for each plot window (PW).

| | | |
|---|---|---|
| 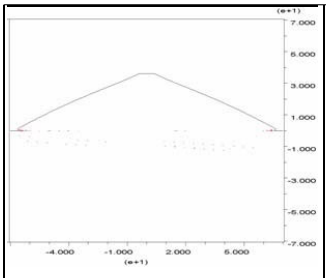 Model 3 (joint friction angle, 25°) PW: 54-11 µm | 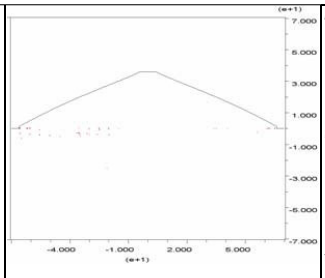 Model 8 (joint dips, -5°, 100°) PW: 35-7 µm | 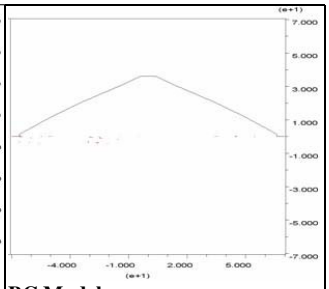 **BC Model** PW: 27-5 µm |
| 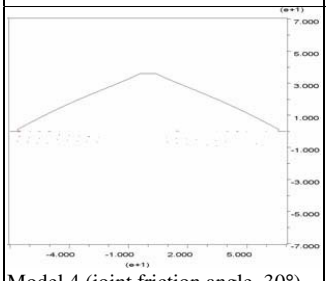 Model 4 (joint friction angle, 30°) PW: 27-5 µm | 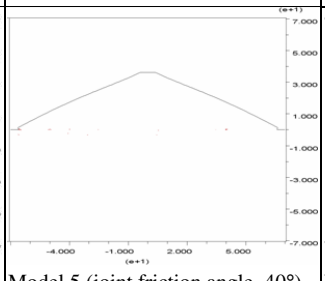 Model 5 (joint friction angle, 40°) PW: 24-5 µm | 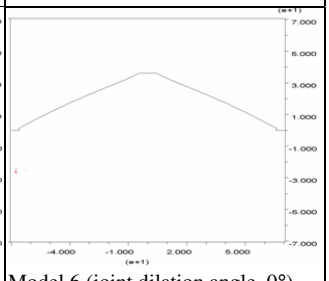 Model 6 (joint dilation angle, 0°) PW: 18-4 µm |
| 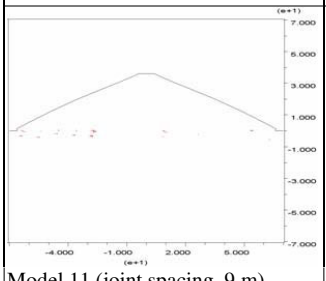 Model 11 (joint spacing, 9 m) PW: 13-3 µm | 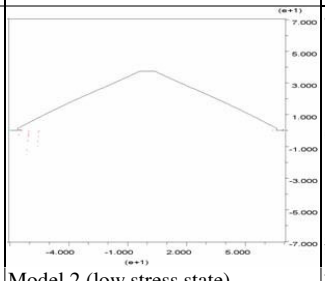 Model 2 (low stress state) PW: 9-2 µm | 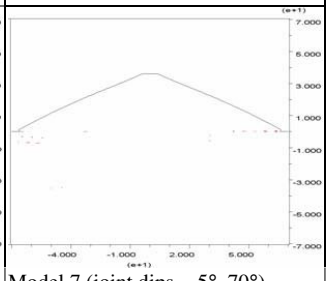 Model 7 (joint dips,, -5°, 70°) PW: 6-1 µm |

Figure 5.11 (continued)

### Stage 2, Shear displacements in the rock mass

The impounding of the reservoir increases the pore pressure along the interface between dam and foundation at the heel of the dam. As mentioned in Section 5.2.1, "*False displacement caused by UDEC simulation*", the combined effects from uplift pressure near the heel of the dam and water pressure on the upstream side of the dam result in lifting up the heel of the dam (Figure 5.2). This phenomenon is an effect of UDEC, and all maximum normal- and shear displacements near this area are considered with caution.

Largest amount of shear deformation is obtained for Model 1, which consist of a stress relationship obtained from overcoring, with large deviatoric stresses (cf. Figure 4.1). Deformation is mainly restricted to a rather consistent zone in a banking joint under the downstream side of the dam below 0 m depth, which is about 30 m long, Some 2/3 m long deformation along subvertical joints is also observed in this area.

Variation to lowest joint friction angle (Model 3) and of joint dips (Model 8) involve larger areas of shearing along banking joints than for Model 1, but the maximum amount of shear displacement is smaller (Figure 5.12). Higher values of joint friction angles (BC Model and Model 4) deform similar areas, but subsequently smaller magnitudes of shear deformation. In a similar way, Model 7 has lower shear magnitudes but involve similar areas of deformation. The higher dip of banking joints in Model 9 result in more stable conditions than Models 8 and 7. In Model 9, shearing is restricted to subvertical joints under the width of the entire dam down to about 10 m depth.

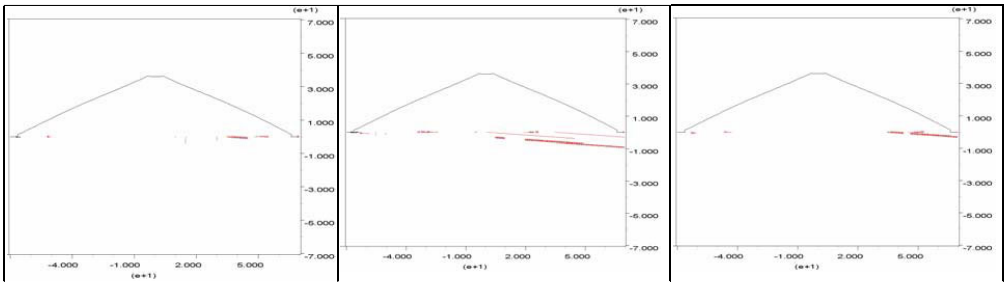

| Model 1 (high stress state) | Model 3 (joint friction angle, 25°) | Model 8 (joint dips, -5°, 100°) |
|---|---|---|
| PW: 3000-600 µm | PW: 2100-420 µm | PW: 2100-420 µm |

Figure 5.12 Shear displacements for the BC Model and Models 1-14 during Stage 2 along Cross-Section A. The scale on both axes is in tens of meters; hence, the width of all models is about 120 m and the height is about 140 m. The red dots show location of shear displacements, with thicker lines indicating higher magnitudes of displacements. Note that the range of displacements varies for each plot window (PW).

| | | |
|---|---|---|
| 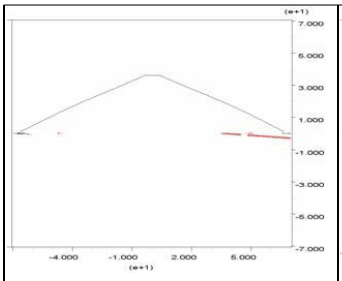 **BC Model** PW: 1800-360 µm | 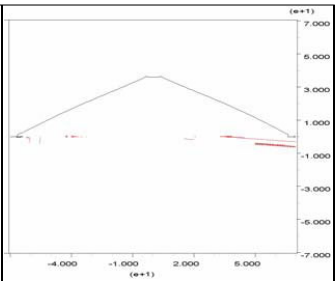 Model 4 (joint friction angle, 30°) PW: 1750-350 µm | 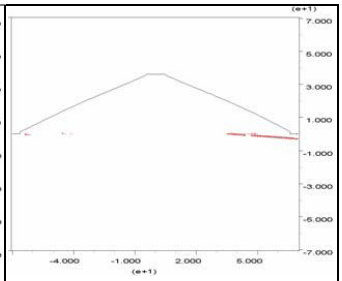 Model 7 (joint dips,, -5°, 70°) PW: 1340-268 µm |
| 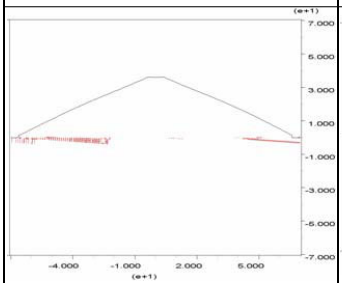 Model 10 (joint spacing, 1 m) PW: 1230-246 µm | 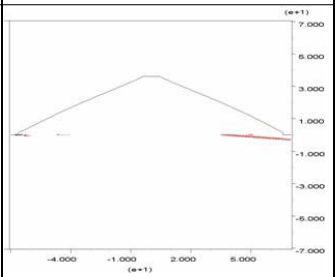 Model 12 (hydraulic aperture, 0.5 mm); PW: 1210-242 µm | 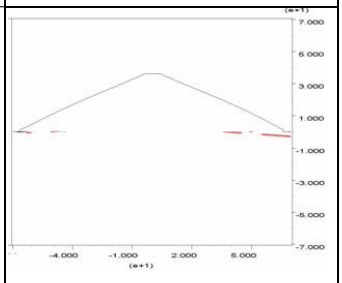 Model 14 (hydraulic aperture, 2.5 mm); PW: 746-149 µm |
| 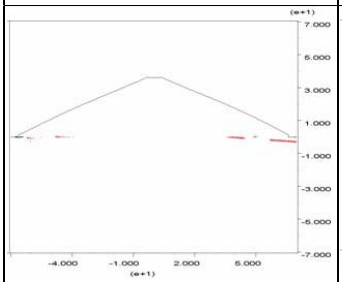 Model 13 (hydraulic aperture, 1 mm); PW: 728-146 µm | 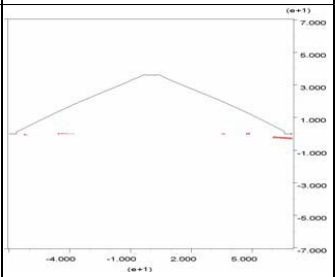 Model 11 (joint spacing, 9 m) PW: 710-142 µm | 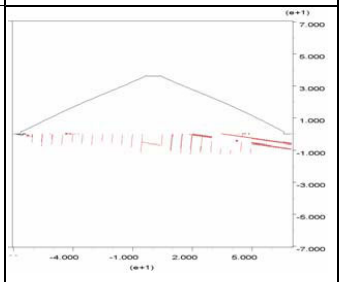 Model 9 (joint dips, -10°, 85°) PW: 641-128 µm |
| 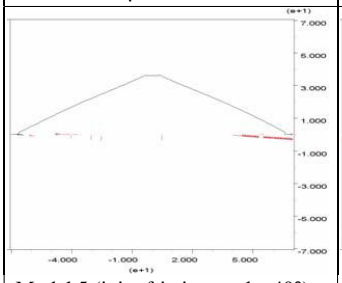 Model 5 (joint friction angle, 40°) PW: 459-92 µm | 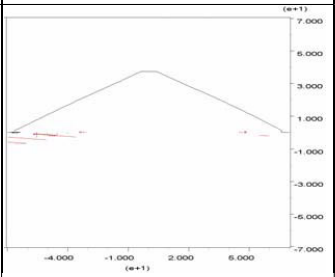 Model 2 (low stress state) PW: 232-48 µm | 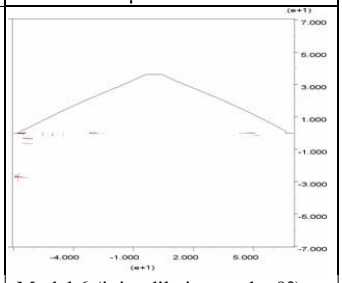 Model 6 (joint dilation angle, 0°) PW: 90-18 µm |

Figure 5.12 (continued)

### Stage 2, Normal displacements in the rock mass

Impounding the reservoir with water results that Model 3 has largest amount of normal deformation. This deformation is observed in the subvertical discontinuity very close to the top of the foundation (Figure 5.13). In the horizontal direction it is located near the middle part of the dam. The slight increase of friction angle to 30 ° in Model 4 results in the dislocation of the opening to the downstream side. However, the area of maximum normal displacement is the same, and it occurs in the subvertical discontinuity close to the top of the foundation as in Model 3.

Reduced spacing between the discontinuities in the Model 10 identifies the almost the same location and area of opening in the subvertical discontinuity, though the maximum amount of normal displacement is twice lower. Increased magnitude of in-situ stresses in Model 1 results in extension of area of maximum normal displacement in subvertical discontinuity, compare to Model 4, though the magnitude is much lower.

The rest of the models reveals opening of the discontinuities along the whole foundation of the dam as in subvertical as in banking discontinuities. Considering the magnitude of these displacements they are not important.

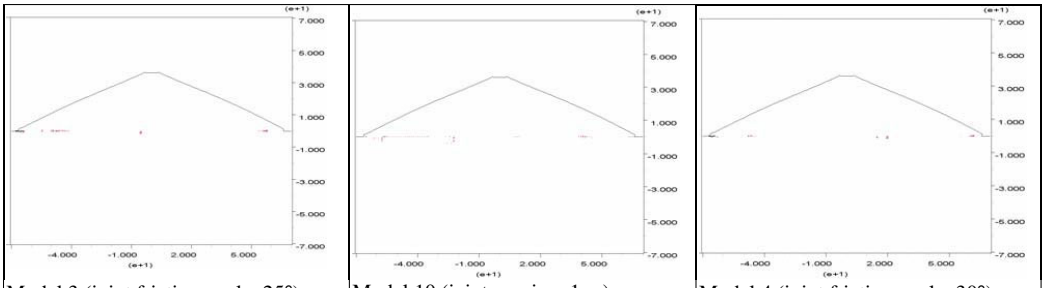

Model 3 (joint friction angle, 25°)
PW: 2170-434 µm

Model 10 (joint spacing, 1 m)
PW: 1420-284 µm

Model 4 (joint friction angle, 30°)
PW: 1030-205 µm

Figure 5.13 Normal displacements for the BC Model and Models 1-14 during Stage 2 along Cross-Section A. The scale on both axes is in tens of meters; hence, the width of all models is about 120 m and the height is about 140 m. The red dots show location of shear displacements, with thicker lines indicating higher magnitudes of displacements. Note that the range of displacements varies for each plot window (PW).

| | | |
|---|---|---|
| 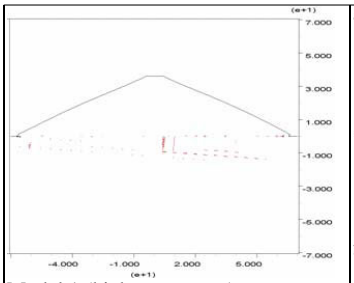 Model 1 (high stress state) PW: 310-62 µm | 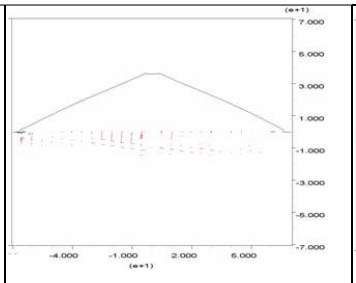 Model 9 (joint dips, -10°, 85°) PW: 162-32 µm | 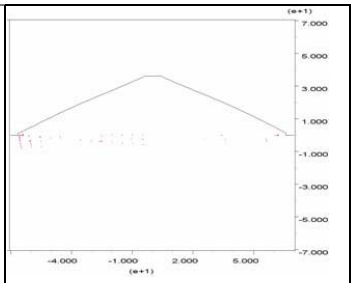 Model 8 (joint dips, -5°, 100°) PW: 160-32 µm |
| 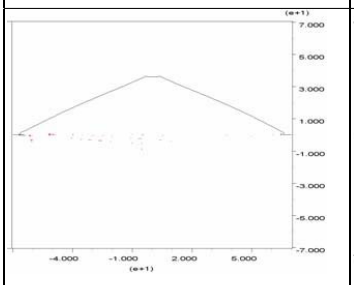 Model 5 (joint friction angle, 40°) PW: 156-31 µm | 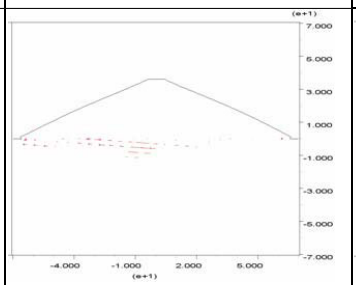 Model 7 (joint dips,, -5°, 70°) PW: 110-22 µm | 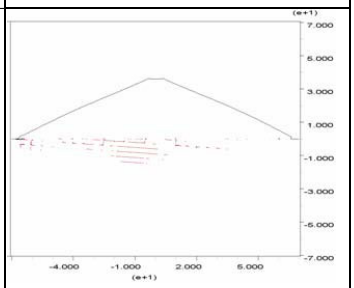 **BC Model** PW: 96-19 µm |
| 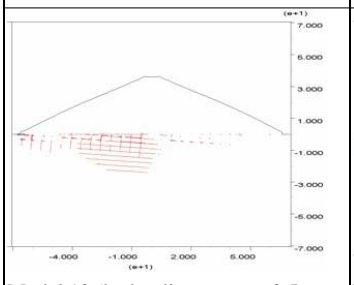 Model 12 (hydraulic aperture, 0.5 mm); PW: 66-13 µm | 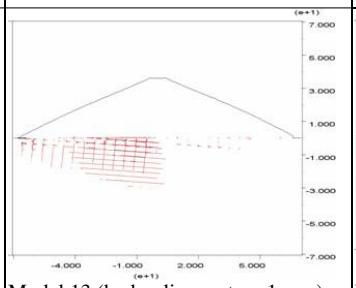 Model 13 (hydraulic aperture,1 mm); PW: 50-10 µm | 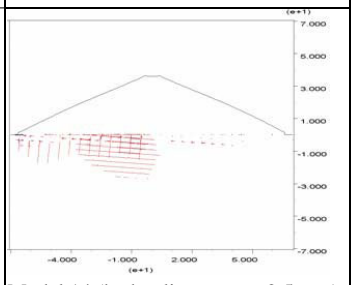 Model 14 (hydraulic aperture,2.5 mm); PW: 41-8 µm |
| 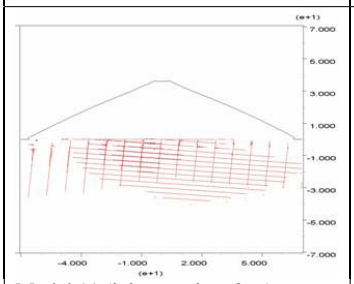 Model 11 (joint spacing, 9 m) PW: 40-8 µm | 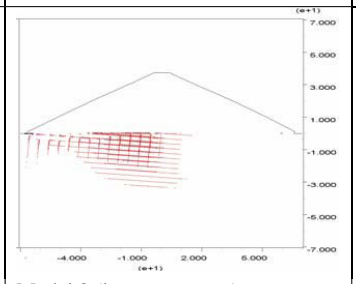 Model 2 (low stress state) PW: 26-5 µm | 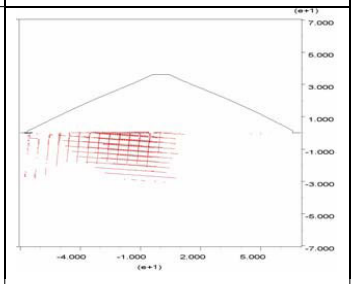 Model 6 (joint dilation angle, 0°) PW: 22-4 µm |

Figure 5.13 (continued)

### Stage 3, Shear displacements in the rock mass

After the reservoir was filled the first time in Stage 2, water level was first reduced to a depth of 10 m, and then increased to 35 m during Stage 3. The maximum amount of shear deformation under such conditions has been observed in the Model 1. This deformation occurs along banking discontinuities at the downstream side of the dame. Some shearing also occur along subvertical discontinuities, located rather close to the middle part of the foundation. Shearing along these subvertical discontinuities propagates up to 10 m below surface (Figure 5.14).

Reduction of the friction angle to 25° in Model 3 results in extensive zone of shearing along banking discontinuities in foundation rock. They propagate across the whole model in horizontal direction and reaches depth up to 10 m. A slight increase of the friction angle in Model 4 results in substantial reduction of the area of shearing, however the maximum shearing along banking discontinuities cover almost the whole foundation

Model 9 identifies the shearing along the same banking discontinuity as in Model 1 plus much shearing in subvertical joints along the whole foundation. However the magnitude of these shearing is much lower than in Model 1.

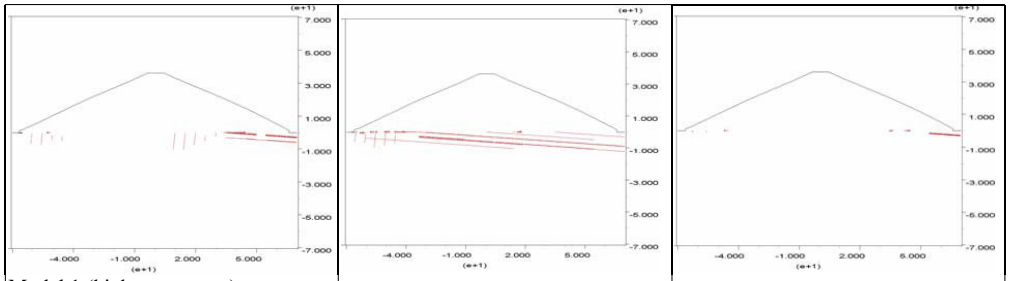

| Model 1 (high stress state) | Model 3 (joint friction angle, 25°) | Model 8 (joint dips, -5°, 100°) |
|---|---|---|
| PW: 6010-1202 µm | PW: 3720-744 µm | PW: 2820-564 µm |

Figure 5.14 Shear displacements for the BC Model and Models 1-14 during Stage 3 along Cross-Section A. The scale on both axes is in tens of meters; hence, the width of all models is about 120 m and the height is about 140 m. The red dots show location of shear displacements, with thicker lines indicating higher magnitudes of displacements. Note that the range of displacements varies for each plot window (PW).

| | | |
|---|---|---|
| 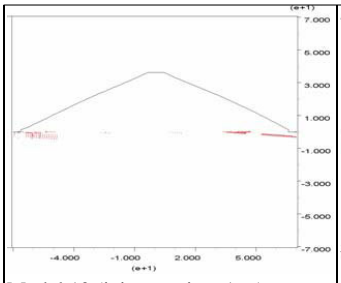 Model 10 (joint spacing, 1 m) PW: 2730-546 µm | 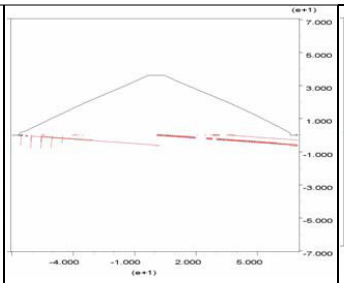 Model 4 (joint friction angle, 30°) PW: 2720-544 µm | 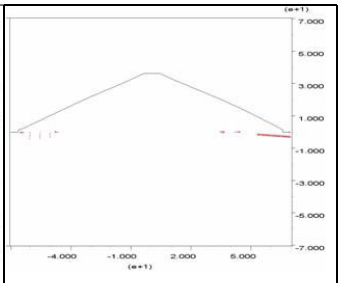 **BC Model** PW: 2570-514 µm |
| 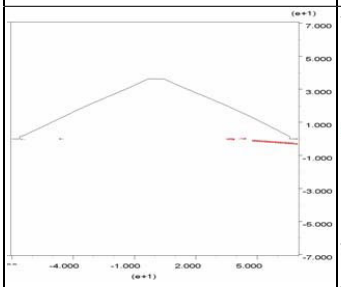 Model 7 (joint dips,, -5°, 70°) PW: 2260-452 µm | 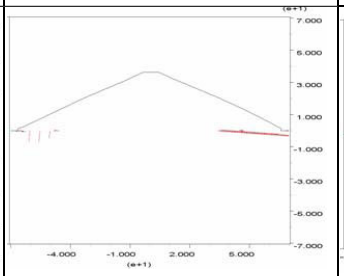 Model 12 (hydraulic aperture, 0.5 mm); PW: 2100-420 µm | 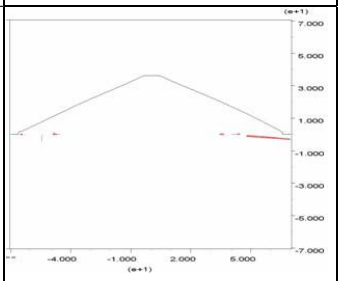 Model 11 (joint spacing, 9 m) PW:1970-394 µm |
| 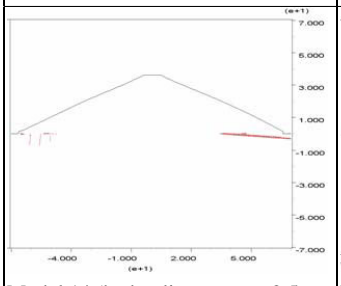 Model 14 (hydraulic aperture, 2.5 mm); PW: 1900-380 µm | 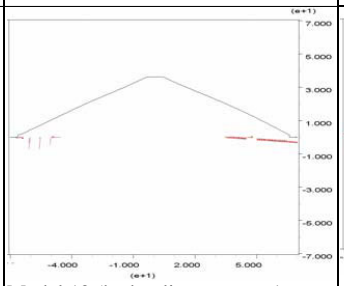 Model 13 (hydraulic aperture, 1 mm)**;** PW: 1840-368 µm | 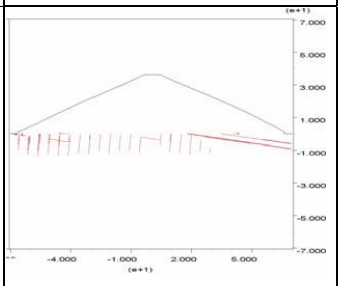 Model 9 (joint dips, -10°, 85°) PW: 1580-316 µm |
| 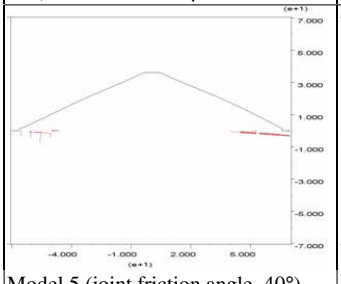 Model 5 (joint friction angle, 40°) PW: 872-174 µm | 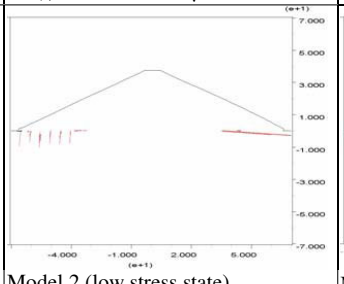 Model 2 (low stress state) PW: 510-102 µm | 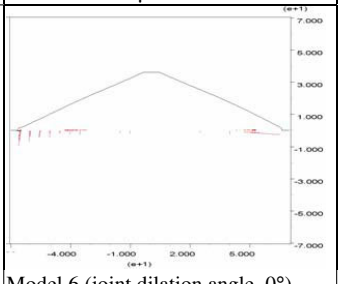 Model 6 (joint dilation angle, 0°) PW: 300-60 µm |

Figure 5.14 (continued)

### Stage 3, Normal displacements in the rock mass

The model with high in-situ stress field Model 1 identifies the most amount of normal motions. This motion is restricted to the subvertical discontinuity, located very close to the middle part of the dam. This opening propagates from top of the foundation up to 10 m into depth. Some small openings have also been observed at the banking discontinuities at the depth around 10 m (Figure 5.15).

Reduced joint spacing of Model 10 results in opening of the subvertical discontinuities in several places along the foundation. These normal displacements are located close to the middle part of the dam on upstream and downstream side. Additionally some opening occurs along banking discontinuities closer to the toe of the dam. However the magnitude of maximum opening is much lower than in Model 1.

The rest of the models reveal normal displacements in different part of foundation rock, however the magnitude of these displacements is considerably lower than in Model 1.

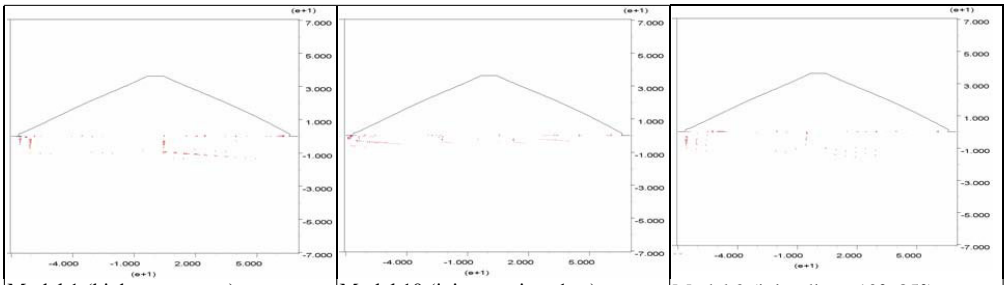

| Model 1 (high stress state) | Model 10 (joint spacing, 1 m) | Model 9 (joint dips, -10°, 85°) |
|---|---|---|
| PW: 1000-200 µm | PW: 485-97 µm | PW: 292-59 µm |

Figure 5.15 Normal displacements for the BC Model and Models 1-14 during Stage 3 along Cross-Section A. The scale on both axes is in tens of meters; hence, the width of all models is about 120 m and the height is about 140 m. The red dots show location of shear displacements, with thicker lines indicating higher magnitudes of displacements. Note that the range of displacements varies for each plot window (PW)

| | | |
|---|---|---|
| 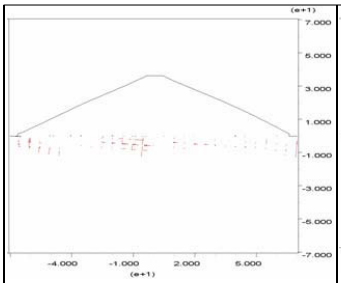 Model 13 (hydraulic aperture, 1 mm); PW: 117-23 µm | 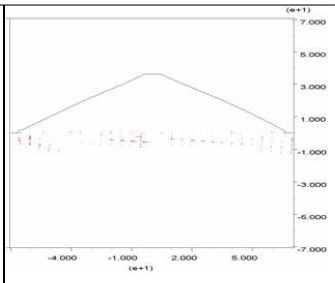 Model 14 (hydraulic aperture,2.5 mm); PW: 112-22 µm | 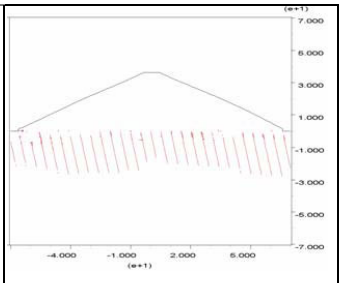 Model 8 (joint dips, -5°, 100°) PW: 110-22 µm |
| 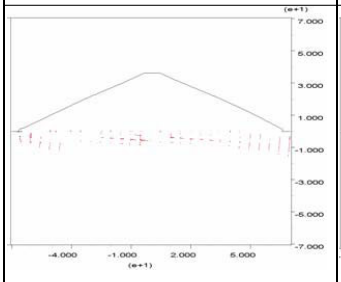 Model 12 (hydraulic aperture, 0.5 mm); PW: 110-22 µm | 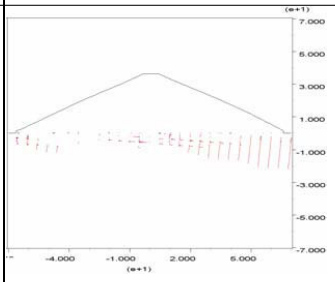 **BC Model** PW: 100-20 µm | 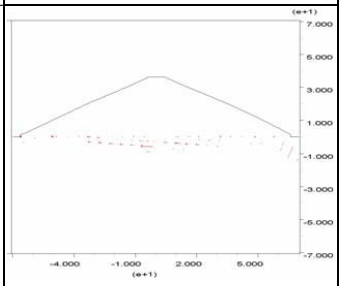 Model 7 (joint dips, -5°, 70°) PW: 100-20 µm |
| 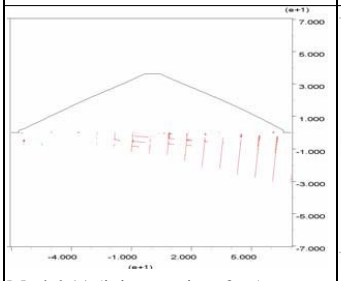 Model 11 (joint spacing, 9 m) PW: 92-18 µm | 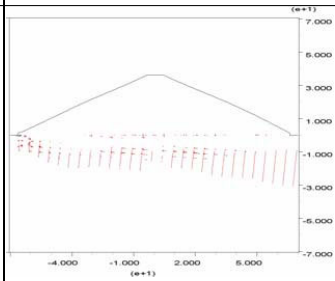 Model 4 (joint friction angle, 30°) PW: 85-17 µm | 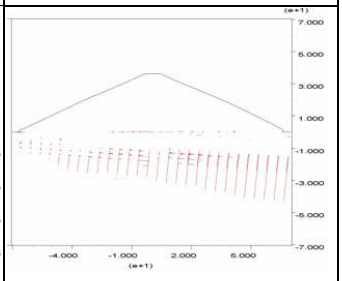 Model 3 (joint friction angle, 25°) PW: 71-14 µm |
| 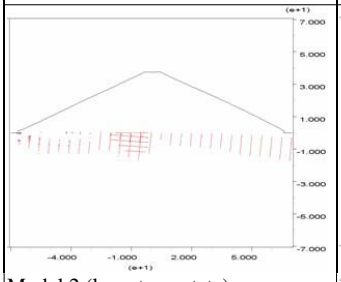 Model 2 (low stress state) PW: 63-13 µm | 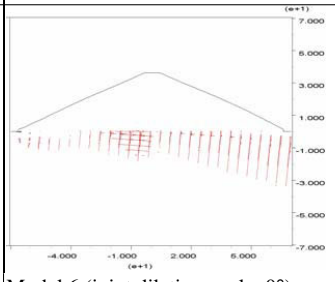 Model 6 (joint dilation angle, 0°) PW: 30-6 µm | 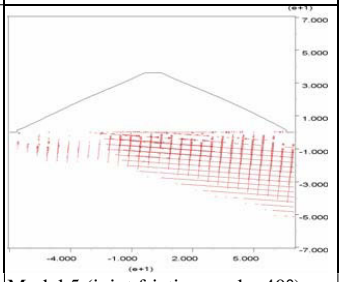 Model 5 (joint friction angle, 40°) PW: 27-5 µm |

Figure 5.15 (continued)

### 5.3.2 Occurrence of displacement along Cross-section B

Stage 2, Shear displacements in the rock mass

Impounding of the reservoir causes extensive shearing in the discontinuities in the banks, at the same time very little amount have been noticed in the rock mass at the bottom. BC Model has highest amount of shearing and it occurs at the bottom rock, close to the left bank. (Figure 5.16) Model 4 has the same magnitude of maximum shearing, however it is located very close to the zone of intersection between bottom and right bank.

Model 5 reveals shearing along the same discontinuity as in BC Model. Reduced spacing between discontinuities in Model 10 results in extensive shearing in the left bank of the reservoir, while increased spacing in Model 11 identifies shearing along subvertical discontinuities in the right bank. The magnitude of maximum shearing in both models are almost the same.

Low in-situ stress results in shearing along subvertical discontinuities along the bottom rock to the depth around 20 m, however the magnitude of this displacement is two times lower than in the BC Model.

The rest of the models reveals quite extensive areas of shearing in banks and bottom of reservoir, however the magnitude of maximum shearing is very small.

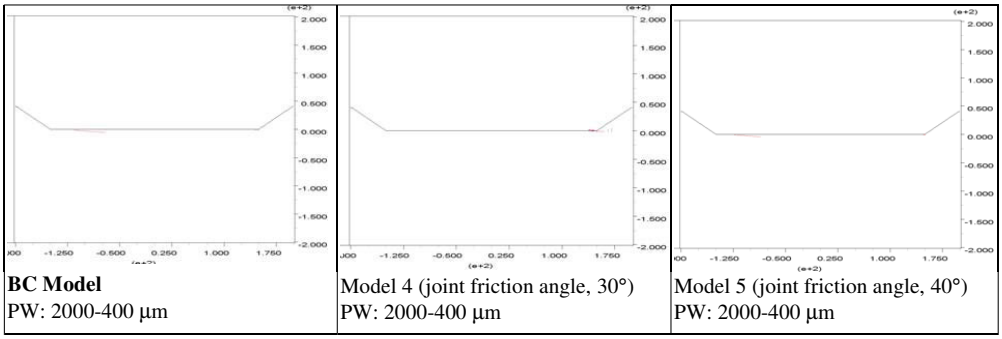

| **BC Model**<br>PW: 2000-400 µm | Model 4 (joint friction angle, 30°)<br>PW: 2000-400 µm | Model 5 (joint friction angle, 40°)<br>PW: 2000-400 µm |
|---|---|---|

Figure 5.16 Shear displacements for the BC Model and Models 1-11 during Stage 2 along Cross-Section B. The scale on both axes is in tens of meters; hence, the width of all models is about 120 m and the height is about 140 m. The red dots show location of shear displacements, with thicker lines indicating higher magnitudes of displacements. Note that the range of displacements varies for each plot window (PW).

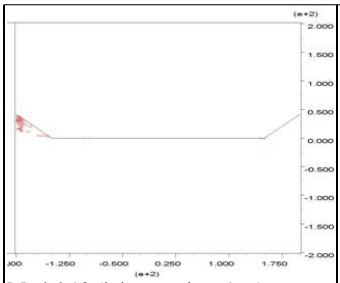

Model 10 (joint spacing, 1 m)
PW: 2000-400 µm

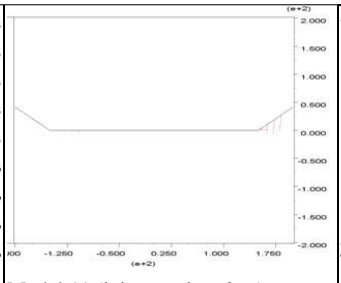

Model 11 (joint spacing, 9 m)
PW: 1420-284 µm

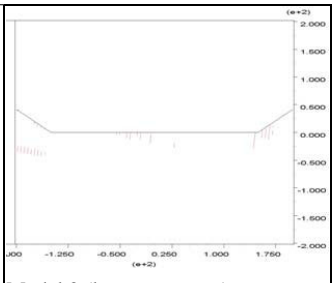

Model 2 (low stress state)
PW: 1000-200 µm

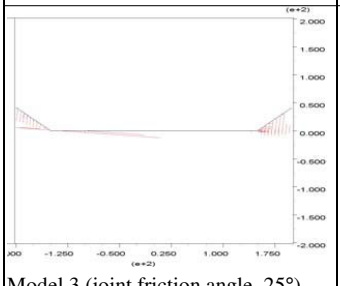

Model 3 (joint friction angle, 25°)
PW: 1000-200 µm

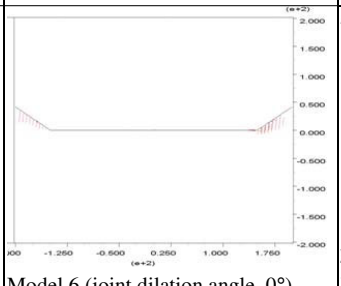

Model 6 (joint dilation angle, 0°)
PW: 1000-200 µm

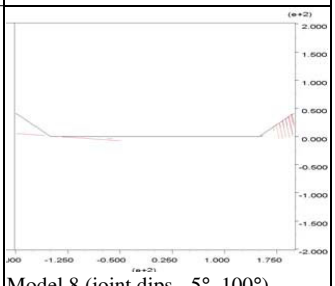

Model 8 (joint dips, -5°, 100°)
PW: 1000-200 µm

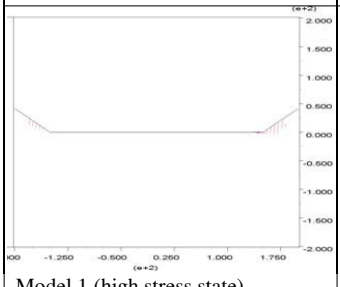

Model 1 (high stress state)
PW: 900-180 µm

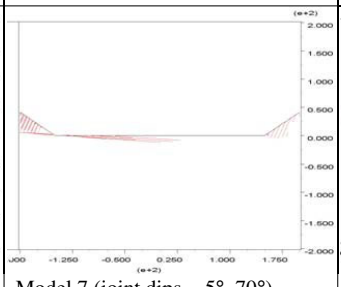

Model 7 (joint dips,, -5°, 70°)
PW: 761-152 µm

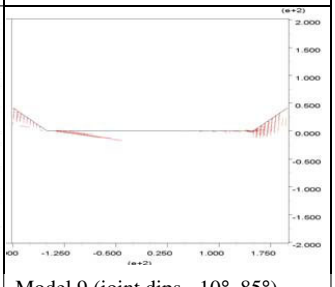

Model 9 (joint dips, -10°, 85°)
PW: 385-77 µm

Figure 5.16 (continued)

### Stage 2, Normal displacements in the rock mass

Model 2 has the highest maximum normal displacement., however it is located very close to the zone of intersection between right bank and bottom. Increased spacing between the discontinuities in the Model 10 reveals the opening at the left bank. Model 5 has the same location of opening of the discontinuities, in the left bank, however the area of opening is much lower (Figure 5.17). The rest of the models have very small maximum normal displacements.

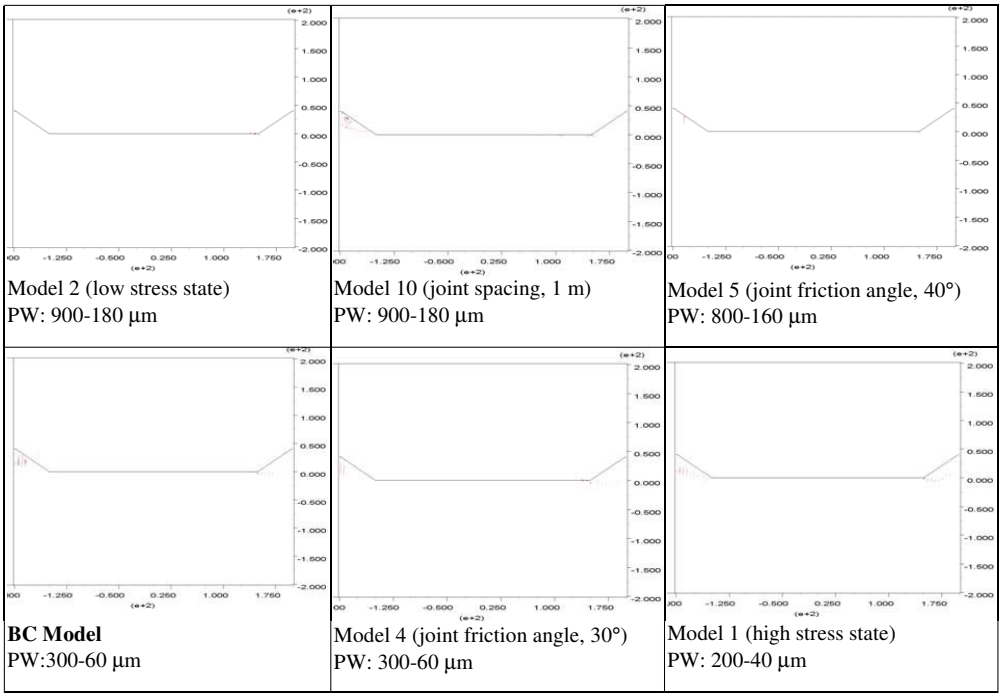

Model 2 (low stress state)
PW: 900-180 µm

Model 10 (joint spacing, 1 m)
PW: 900-180 µm

Model 5 (joint friction angle, 40°)
PW: 800-160 µm

**BC Model**
PW:300-60 µm

Model 4 (joint friction angle, 30°)
PW: 300-60 µm

Model 1 (high stress state)
PW: 200-40 µm

Figure 5.17 Normal displacements for the BC Model and Models 1-11 during Stage 2 along Cross-Section B. The scale on both axes is in tens of meters; hence, the width of all models is about 120 m and the height is about 140 m. The red dots show location of shear displacements, with thicker lines indicating higher magnitudes of displacements. Note that the range of displacements varies for each plot window (PW).

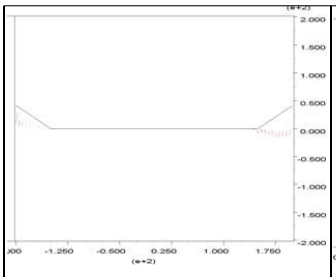

Model 3 (joint friction angle, 25°)
PW: 200-40 µm

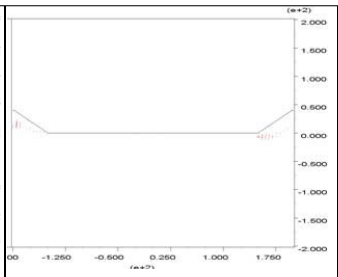

Model 6 (joint dilation angle, 0°)
PW: 200-40 µm

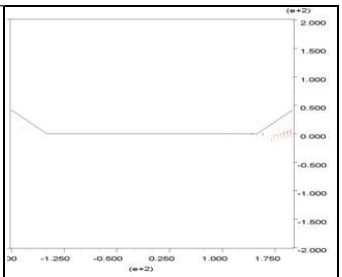

Model 8 (joint dips, -5°; 100°)
PW: 200-40 µm

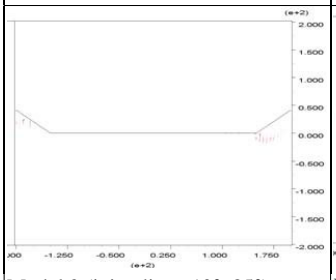

Model 9 (joint dips, -10°, 85°)
PW: 200-40 µm

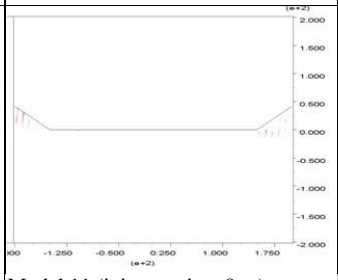

Model 11 (joint spacing, 9 m)
PW: 200-40 µm

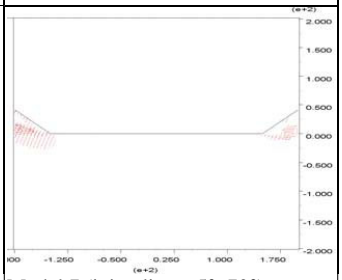

Model 7 (joint dips,, -5°; 70°)
PW: 100-20 µm

Figure 5.17 (continued)

### Stage 3, Shear displacements in the rock mass

Reduced spacing between the discontinuities in Model 10 reveals the shearing at the left bank, as it has been observed in Stage 2. The magnitude of shearing in Stage 3 has been doubled compare to Stage 2. Reduction of in-situ stress in the Model 2 results in shearing of subvertical discontinuities close to the right bank, however this area is very close to the zone of concentration of stresses. Small area of shearing has also been observed at the left bank at the depth around 20 – 30 m. The same area has been registered at the Stage 2 (Figure 5.18).

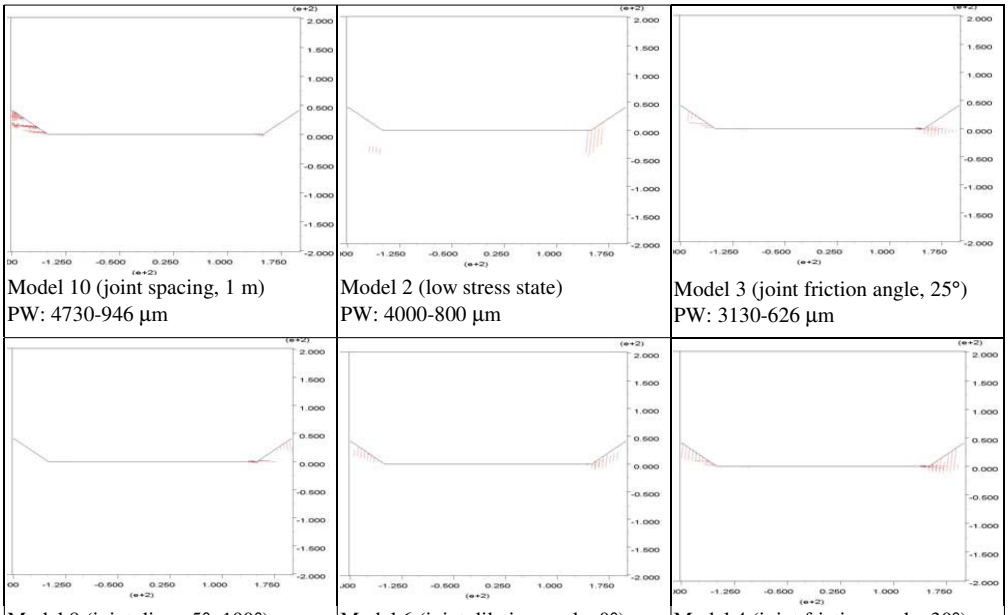

Model 10 (joint spacing, 1 m)
PW: 4730-946 µm

Model 2 (low stress state)
PW: 4000-800 µm

Model 3 (joint friction angle, 25°)
PW: 3130-626 µm

Model 8 (joint dips, -5°, 100°)
PW: 2340-458 µm

Model 6 (joint dilation angle, 0°)
PW: 2000-400 µm

Model 4 (joint friction angle, 30°)
PW: 1960-392 µm

Figure 5.18 Shear displacements for the BC Model and Models 1-11 during Stage 3 along Cross-Section B. The scale on both axes is in tens of meters; hence, the width of all models is about 120 m and the height is about 140 m. The red dots show location of shear displacements, with thicker lines indicating higher magnitudes of displacements. Note that the range of displacements varies for each plot window (PW).

| | | |
|---|---|---|
| 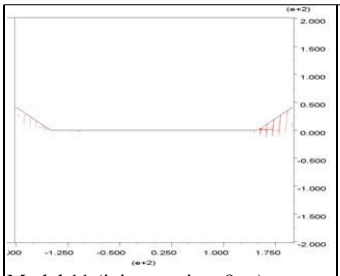 | 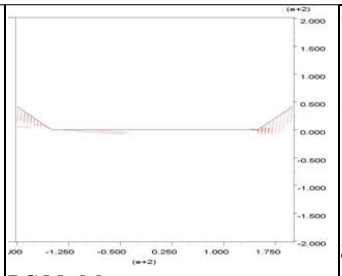 | 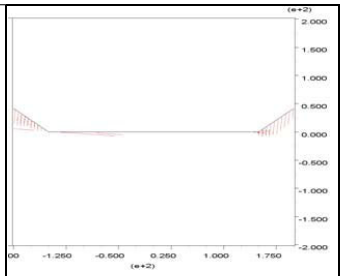 |
| Model 11 (joint spacing, 9 m)<br>PW: 1430-286 µm | **BC Model**<br>PW: 1400-280 µm | Model 5 (joint friction angle, 40°)<br>PW: 1290-258 µm |
| 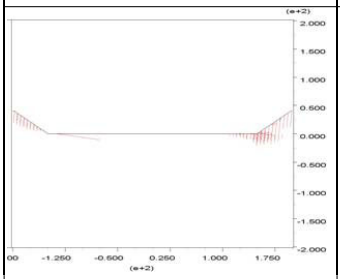 | 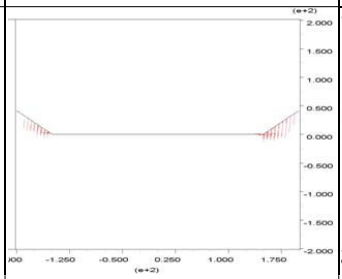 | 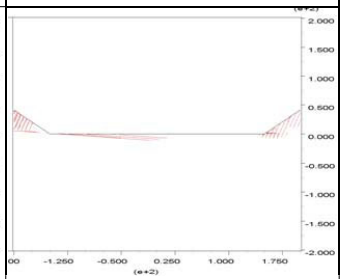 |
| Model 9 (joint dips, -10°, 85°)<br>PW: 1150-230 µm | Model 1 (high stress state)<br>PW: 962-192 µm | Model 7 (joint dips,, -5°, 70°)<br>PW: 945-189 µm |

Figure 5.18 (continued)

### Stage 3, Normal displacements in the rock mass

The largest maximum opening of the discontinuities have been observed in Model 10. The area of opening is located at the left bank, the same area where extensive shearing has been registered. (Figure 5.19) Increased dip angle of the subvertical discontinuities in Model 8 results in opening at the righ bank, the same area where shearing has been identified. However the magnitude of opening in this model is considerably lower compare to the Model 10. The rest of the models identify even smaller magnitude of maximum normal displacements.

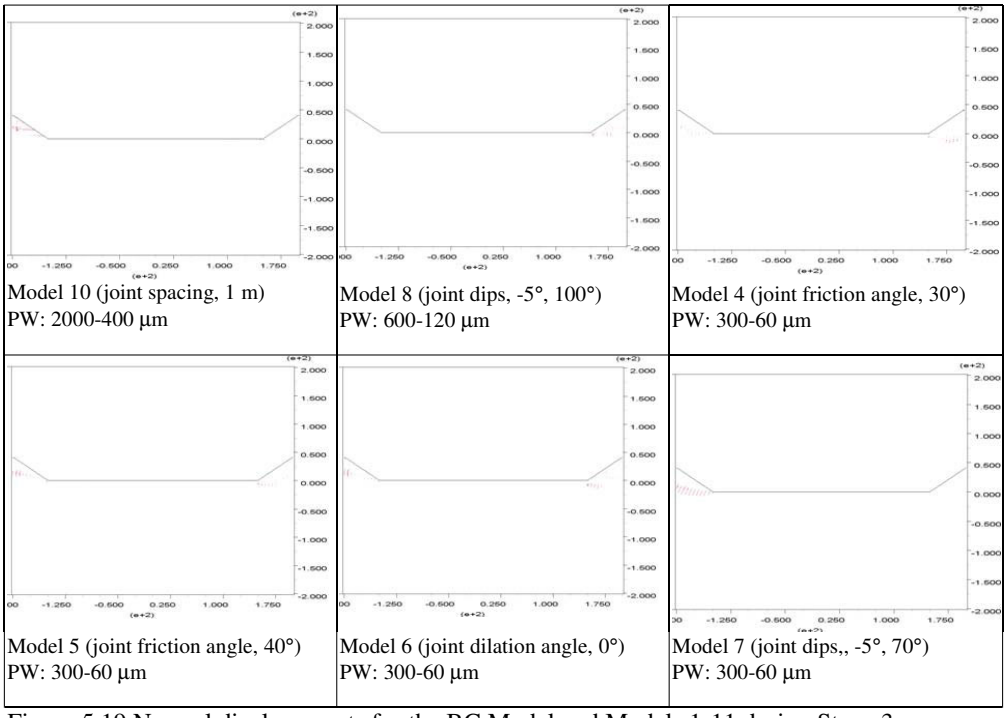

Model 10 (joint spacing, 1 m)
PW: 2000-400 µm

Model 8 (joint dips, -5°, 100°)
PW: 600-120 µm

Model 4 (joint friction angle, 30°)
PW: 300-60 µm

Model 5 (joint friction angle, 40°)
PW: 300-60 µm

Model 6 (joint dilation angle, 0°)
PW: 300-60 µm

Model 7 (joint dips,, -5°, 70°)
PW: 300-60 µm

Figure 5.19 Normal displacements for the BC Model and Models 1-11 during Stage 3 along Cross-Section B. The scale on both axes is in tens of meters; hence, the width of all models is about 120 m and the height is about 140 m. The red dots show location of shear displacements, with thicker lines indicating higher magnitudes of displacements. Note that the range of displacements varies for each plot window (PW).

| | | |
|---|---|---|
| 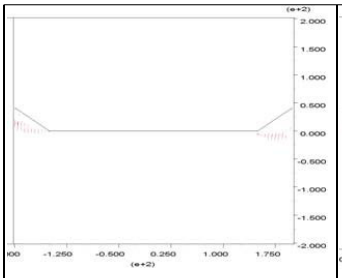 **BC Model** PW: 200-40 µm | 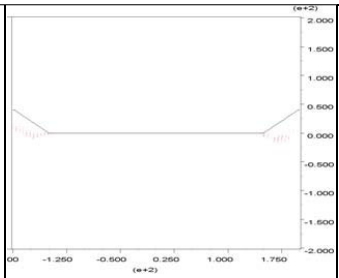 Model 1 (high stress state) PW: 200-40 µm | 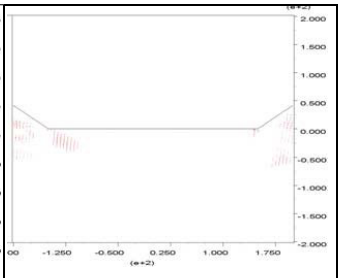 Model 2 (low stress state) PW: 100-20 µm |
| 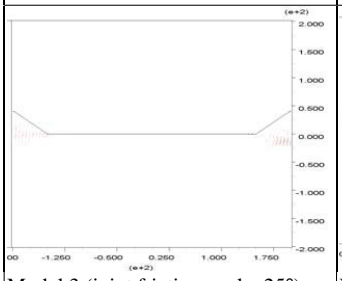 Model 3 (joint friction angle, 25°) PW: 200-40 µm | 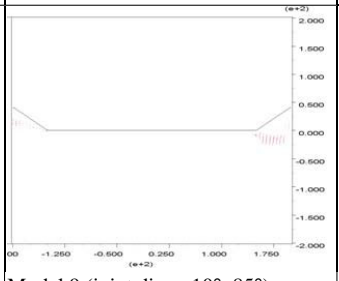 Model 9 (joint dips, -10°, 85°) PW: 200-40 µm | 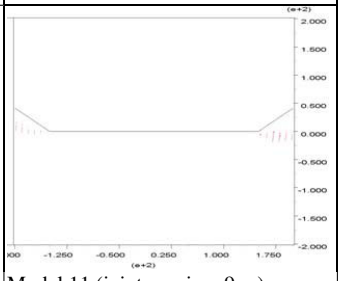 Model 11 (joint spacing, 9 m) PW: 200-40 µm |

Figure 5.19 (continued)

# 6. DISCUSSION

Much research has been done on the mechanic behavior of foundation rock under concrete and masonry dams [e.g. *Barla et al.*, 2004; *Dolezalova,* 2004]. This is the first numerical study that focuses on the mechanic response of a Swedish type of rock mass under embankment dams using UDEC. Different stages of the life time of an embankment dam have been studied.

The first objective of this thesis is to reveal and increase the understanding of the rock mass response to the construction of an embankment dam. The construction of the dam includes static loading of the weight of the dam, and the weight of water in the reservoir. The second objective of this thesis is to investigate how static and cyclic loads of the hydropower dam affect the stability of the dam in terms of foundation rock and the degradation process of the grout curtain.

The numerical code UDEC has been used to simulate the mechanical behavior of a fractured rock mass under different loading conditions. Chapter 4.2, "*Limitations and assumptions*" describes simplifications that have been made. The values of parameters used in the analyses have been chosen to represent typical Swedish rock mass conditions. The rock mass behavior has been studied along two perpendicular cross-sections. Tables 5.1 and 5.2 present values of input parameters for a BC model and 11-14 models along the two cross sections.

This chapter is divided into two main parts that corresponds to the main objectives of this thesis. The results regarding the rock mass response to the construction of the dam is discussed in the first part. Both the rock mass response to the static weight of the dam and the weight of water are considered. Because most dam incidents occur during the first filling of the reservoir [*National Research Council, 1983*], special consideration is given to this stage. The results regarding the rock mass response to static and cyclic loading are discussed in the second part. Discussions on stability of the rock mass and degradation of the grout curtain are included.

## 6.1 Rock mass response to dam construction

### 6.1.1 Effects from static weight of the dam

Stage 1 corresponds to the time of dam construction when the static weight of the dam is applied on the rock mass. The sensitivity analyses of Stage 1 along Cross-section A show that the model with reduced spacing between subvertical discontinuities (Model 10) has the highest magnitude shear and normal displacements (Table 5.4 and Figures 5.10, 5.4, and 5.5). Maximum shearing is occurring along subvertical discontinuities from heel in the direction to the middle part of the dam close to the dam-foundation interface. At the same time, the location of maximum opening is observed at the end of this shear zone and it is very close to the middle part of the dam. The magnitude and location of the shearing does not poses significant threat to the dam, because the outer shell of the dam can handle quite high shearing in the rock foundation [*Singh,* 1995]. However, the occurrence of 0.7 mm large normal displacement close to the middle part of the dam in

Model 10 may pose a threat to dam stability (Table 5.4 and Figure 5.11). *Reinius* [1988] stated that construction of an embankment dam on rock foundation develops tension stresses in rock. He suggest that if tensional stresses result in opening in the order of 1 mm close to the core, this may result in soil transport from the core to the rock foundation. This may lead to the disintegration of the impermeable core.

The results suggest that variation of the remaining parameters poses little, if any interest for rock mass stability (Table 5.4). The sensitivity analyses resulted in small magnitudes of displacement, and/or that the displacements occurred in areas of the foundation that are insensitive to such displacements. For example, the rock mass under the outer shell is designed to handle significant amount of shearing displacement without loosing its functionality [*Singh,* 1995].

### 6.1.2 Effects from static weight of the water in the reservoir

Stage 2 is the time of dam construction when the static weight of the water in the reservoir is applied on the rock mass. Such load conditions result in additional development of shear- and normal displacements in the models. In term of maximum shearing, the BC Model, and Models 1, 3, 4, 8, 9, 10 and 12 reveal the highest amount of shearing. However the BC Model, Models 8 and 12 are considered to be unimportant, because the maximum shear displacement occurs only under the outer shell, which can handle quite high shearing in rock foundation [*Singh,* 1995]. The magnitude of maximum shearing is quite small in Model 9 (Table 5.5), so this model has not been taken into further consideration. The remaining models (number 1, 3, 4 and 10) have sufficiently large magnitudes and /or critical location of shear displacements. Model 1 has a “low” stress state (cf. Figure 4.1), Models 3 and 4 have joint friction angles of 30° and 40°, respectively, and Model 10 has a joint spacing of 1 m.

Evaluation of maximum normal displacements in the Stage 2 reveals that Model 1, 3, 4 and 10 are interested either in term of magnitude or location of the opening, hence the same models that are considered to be most critical with respect to shearing (Figure 5.5). The magnitudes of normal displacements are quite high for Models 3 and 4. Moreover, the opening occurs near the middle part of dam, and just below the interface between dam and foundation. Model 1 has a much lower magnitude of opening (~0.3 mm). However, opening occurs very close to the grout curtain and the core, which would make it important, especially for a zoned embankment dam. Displacement occurs along subvertical discontinuity close to the interface between dam and foundation at the upstream side in Model 10. However, small joint spacing of Model 10 is considered to be important, because the magnitude of normal displacement is rather high (~1.4 mm). Hydraulic apertures of that order may results in transport of soil material from the outer shell of dam into foundation rock [*Reinius*, 1988].

## 6.2 Effects of static and cyclic loading

### 6.2.1 Rock mass stability

The effect of static load on rock mass in Cross-section A is discussed above; the reader is referred to Chapter 6.1.2 "*Effects from static weight of the water in the reservoir*".

#### Rock mass response along Cross-section A

The water table was first reduced to 10 m, and then increased to 35 m during Stage 3, which is designed to study effects of cyclic loading. The magnitudes of shearing are higher during Stage 3, than during Stage 2 (Figure 5.4, and Tables 5.5 and 5.6). The results of the BC Model, and Models 1, 3, 4, and 7-14 propose relatively high values of shearing, over 1 mm. Deformations of this size can be insignificant, but if the location is unfavorable, they may have a negative effect on the stability. Shearing occurs under the outer shell of the embankment dam for the BC Model and Models 7, 8, 10, and 11-14 (Figure 5.14). Because this area can tolerate considerable amount of shearing [e.g. *Singh*, 1995], these models are not further investigated.

Both the change of in-situ stresses in Model 1, and the increase in the dip angle of banking joints in Model 9 result in shear displacement along subvertical discontinuities. The shearing occurs close to the grout curtain, near the middle part of the dam. The reduction of the joint friction angles in Models 3 and 4 result in extensive shearing along banking discontinuities over the entire width of the foundation (Figure 5.14).

The most interesting results with respect to location and magnitude of normal displacements are obtained for Models 1 and 10 (Figures 5.15 and Table 5.6). The change of the in-situ stress field (Model 1) results in opening of a subvertical discontinuity very close to the middle part of the dam, at the top of foundation. A normal displacement of 0.3 mm is observed along the same discontinuity during Stage 2 (Figure 5.13. The magnitude of normal displacement has increased to 1.0 mm in Stage 3.

The reduced spacing of subvertical joints (Model 10) results in about 0.5 mm of normal displacement at several places at the top of the foundation, very close to the middle part of dam, and on the downstream side. Cyclic loading in Stage 3 result in lower magnitudes of normal displacement, compared to Stage 2 (Figure 5.5). Normal displacement occurs a bit far away from middle part in Stage 2. The location of normal displacement makes this parameter critical rather than its magnitude. The observed change in behavior from Stages 2 to 3 implies that the variation in the height of the water table results in shifts in the location and amount of normal deformation.

The other models either have too small magnitudes of maximum normal displacement, or these displacements occur in areas of the models that are insensitive to obtained deformations. Therefore, they are of little interest for further investigation.

### Rock mass response along Cross-section B

The sensitivity analyses along Cross-section B are conducted to identify potential areas with normal displacement of discontinuities near the bottom of the reservoir. These displacements are considered to be important, because deformation along these discontinuities may propagate into sections further under the dam. This may create new pathways for water seepage, transport of soil material from the dam into the foundation rock, and be a reason of degradation of grout curtain. The results show that most normal displacements are restricted to the banks of the reservoir (Figure 5.19). These displacements have been analyzed because they can result in opening of discontinuities in the abutments of the dam.

Extensive shear- and normal displacements have been observed close to the intersection between banks and bottom of the reservoir. It is related to the concentration of the stresses in this area due to corner effect (see Chapter 5.2.1, "*False displacement caused by UDEC simulation"*). This phenomenon is especially apparent in the right bank, where extensive displacement of a banking discontinuity occurs (Figure 5.17).

Shear displacements along Cross-section B are insignificant in terms of magnitude (Figure 5.6). Even if Cross-section B would be located closer to the dam, and in contact with the outer shell, it can handle rather high shear displacements in the foundation [e.g. *Singh*, 1995]. At the same time, the distance between the heel of the dam and the core is relatively large. It is assumed that the actual value of shearing is unimportant, especially at the scale of the models. Therefore only short description of the shear displacement is done below.

The highest values of maximum shear displacements along Cross-section B are obtained for Models 10, 2, and 3 (Table 5.7 and Figure 5.8). Model 10 has a joint spacing of 1 m, whereas Model 2 has an altered stress state obtained from overcoring data. Model 3 has a joint friction angle of 25°. The amounts of shear displacement are significantly lower for three parameters after Stage 2; no critical parameters are found (Figure 5.8). Shearing displacements in Models 2 and 3 occur very close to the inflection points between the banks and bottom of the reservoir where the stress concentrations are high (Figure 5.18), which may imply that these results are false.

Model 10 reveal a zone with extensive shearing in the left bank (Figure 5.18). This zone is occurring in the same area in Stage 3 as in Stage 2 (Table 5.7 and 5.8). The only difference is that the magnitude is higher in Stage 3. A reduced distance between the subvertical discontinuities reduces the size of intact blocks, which result in lower stress on the discontinuities. Further reduction in effective stress magnitudes are offered by the water pressure from the reservoir [e.g. *Terzhagi*, 1943].

Evaluation of maximum normal displacement after Stage 2 along Cross-section B propose that a reduced joint spacing (Model 10) reduced the stability (Table 5.7). The magnitude of normal displacement is quite high (0.9 mm), and it found in the left bank, where shearing has been observed (Figure 5.17). The other models have small

magnitudes of maximum normal displacement, or deformation is occurring near the inflection points with high stress concentrations.

Results from Stage 3 reveal the same pattern as after Stage 2: The joint spacing of 1 m in Model 10 is critical for stability (Figure 5.19). Displacements along discontinuities develop further, from 0.9 to 2 mm in Stages 2 and 3, respectively. Most other models have rather small magnitudes of normal displacements (Table 5.8). An exception is Model 8, which has a normal displacement of 0.6 mm. However, normal displacement is occurring adjacent to the area with high stress concentrations, so this value may be false.

#### Total water flow through rock mass

Evaluation of the influence of different parameters on total flow through the rock mass in Stage 2 identifies that increase of the hydraulic aperture has the highest influence (Table 5.5). In addition to hydraulic aperture, the joint spacing of 1 m in Model 10, and the change of in-situ stresses in Model 1, results in increased water flow through the rock mass. It seems logical that the increase in number of discontinuities results in an increased number of possible path ways for water to flow through the rock mass.

Stage 3 identifies the same important factors as by Stage 2: The altered in-situ stress field (Model 1), reduced spacing between subvertical discontinuities (Model 10), and variation of the hydraulic aperture (Models 12-14). Stage 3 result in a higher amount of water flow than Stage 2 (Tables 5.5 and 5.6). Hydraulic aperture is the most important parameter for affecting the water flow. Consequently, variation of this parameter results in distinctly different water flow.

The increase of water flow through the rock when compare Stage 2 and Stage 3 in the case of high stress is related probably to the fact that when water released from reservoir, the rock mass is relieved from compressive stress and extensive shearing/opening occurs. When the reservoir is filled again the opened discontinuities are partially closed, so this causes higher conductivity through rock.

Model 10 that has a joint spacing of 1 m has a water flow of 1.77 l/s in Stage 2 (Table 5.5). The water flow has increased to 2.45 l/s in Stage 3. The corresponding values of total water flow are is 1.05 l/s for Stage 2 and 1.16 l/s in Stage 3 as the result of changing the stress state in Model 1. A probable explanation to these increases is that more discontinuities opens when the reservoir is emptied.

### 6.2.2 Degradation of the grout curtain

According to recommendations by the *Grouting Manual* [1980], the grout curtain is usually grouted before the body of the dam is constructed on the foundation rock. The reason for such an early emplacement of the grout curtain is because the access to the area after construction of dam is limited. This approach is not ideal, because the additional weight of the dam body on the grout curtain may lead to the development of displacements of grouted joints. *Swedenborg* [2001] argues that the integrity of the dam is reduced when water is flowing though the grout curtain. Even though these results

cannot directly be translated to the numerical models, it is proposed that the displacements mentioned above may jeopardize the effectives of the grout curtain.

The results of Stage 1 identifies that reduced spacing between the discontinuities (Model 10) of Cross-section A is important for shear and normal displacements. Figures 5.6 and 5.7 show that this value result in larger displacement that any other values in the other models. Note that the actual value of displacement it is not considered from practical point of view. Other factors which may be considered significant are the stress field of Model 1, the reduced dip angle of subvertical discontinuities of Model 8, and the increases dip angle of banking discontinuities of Model 9. Nevertheless, Figures 5.6 and 5.7 show that the three parameters have much smaller influence on the magnitude of displacement than the joint spacing of Model 10. Remaining models have even smaller magnitude of maximum shear- and normal displacements in grout curtain (Table 5.3).

Impounding of the reservoir with water in Cross-section A (Stage 2) causes quite high shearing of grouted discontinuities. The highest value (~2 mm) is obtained Model 3 that has a joint friction angle of 25° (Figure 5.6 and Table 5.4). The other models identify rather small magnitudes of shearing, so they are not further considered. The highest normal displacement has been observed in Model 10, which has a 1 m spacing of subvertical discontinuities. However, the actual value of this maximum normal displacement is small, only 64 μm. Even smaller magnitudes are obtained for the other models (Figure 5.7 and Table 5.4). The variation of individual parameters in the sensitivity analyses show that the chosen parameters generally have little influence on normal displacement of discontinuities in the grout curtain.

The strengths of discontinuities in Stage 3 are reduced by decreases in joint friction angles (Model 3 and 4). The result is an extensive shearing in the grout curtain. The maximum shear displacement is almost 3 mm (Table 5.8), however, the reduction of the friction angle has not resulted in any significant amount of normal displacements in the models (Tables 5.8). The greatest influence on the amount of normal displacement is obtained in Models 12 – 14, in which the hydraulic aperture is increased from 0.5, 1.0 and 2.5 mm, respectively. A reduced spacing between discontinuities to 1 m in Model 10 also results in increases of normal displacements of discontinuities.

# 7. CONCLUSIONS

Results from this study identify the rock mass behavior after construction of the embankment dam and first impounding of the reservoir. The study also includes investigation of the rock mass response to static and cyclic loading with respect to the stability of the rock mass and degradation of the grout curtain.

The conclusions regarding the rock mass response to dam construction are:

- Construction of the dam generally induces limited shear- and normal displacements in the rock mass. These displacements are considered to be insignificant. In the next stage, when water is impounded in the reservoir, more significant displacements are generated.
- Occurrence of high density of discontinuities (i.e. a small joint spacing) result in normal opening of discontinuities after the construction of the dam. This magnitude increases after the reservoir is filled with water.
- Application of high in-situ stresses (i.e. a high maximum horizontal stress, and a lower minimum horizontal stress) apparently has no influence on the rock mass behavior after construction embankment dam. On the other hand, this stress state introduces shear- and normal displacements along the discontinuities after the reservoir is filled.
- Variation of the joint friction angle influence the shear strength of the joint. Construction of the dam does not result in reduced shear strength. However, the water in the reservoir alters the effective stresses and reduces the shear strength. Consequently, considerable amount of shearing and opening of discontinuities occurs after the reservoir is filled with water.

The conclusions regarding the rock mass response to static and cyclic loading are:

- Variations of the water table in the reservoir results in further deformation of the rock mass, either under the dam or in the reservoir. In general, deformations of all parameters included in the sensitivity analyses increase after one period of cyclic loading, though at different scale.
- The combined effect of high in-situ stresses and cyclic loading of water result in extensive shearing of discontinuities, followed by opening, with the change in shearing magnitude being more significant than that of normal opening.
- A small joint friction angles facilitates opening of discontinuities after the reservoir was filled with water the first time. The first period of cyclic loading of water has only resulted in small differences in shearing.
- Increase in frequency of subvertical discontinuities result in considerable opening of the discontinuities after the first impounding of the reservoir. The later variation of the water table have not resulted in further development, so this factor is critical for the first filling of the reservoir.

– Increased hydraulic aperture have not resulted in significant changes in shear and normal displacements in the rock mass, however significant influence on the conductivity of rock has been identified. In terms of amount of water passing through rock mass the increased hydraulic aperture is a critical parameter.

# 8. RECOMMENDATIONS FOR FUTURE RESEARCH

The development of this project gave ideas regarding how this type of investigation can be improved.

First of all further investigation of different parameters of rock mass in simple 2D models e.g. weathering effect of rock mass, presence of layers, presence of zones with different properties, and existence of faults should be implemented.

Secondly, numerical analyses should be implemented for the investigation of the real case. That way the model may be tuned and the validity of the model could be proved. Based on developed code, further, more detailed investigation can be carried out with high confidence in the results.

Another factor that should be considered if high confidence is required from the analyses. If yes, the model should be a 3D. Implementation of a 3D approach will help to consider the influence of the parameters, which had to be disregarded in 2D approach. That way the result could achieve better accuracy and validity.

A lot of analysis are carried out with implementation of the Mouh-Coulomb failure criteria. The reason behind that it is easier to obtain data for this criteria, however sometimes implementation of another failure criteria would guarantee better results.

Further investigation is required to understand the best way to simulate the grout curtain. Should it be permeable or impermeable. In reality it is impossible to fill all discontinuities to guarantee the full sealing.

# 9. REFERENCES

Amadei, B., O. Stephansson (1997). Rock stress and its measurement, Chapman & Hall, London.

Bandara, W.L.H.M.T., K.A.U.S. Imbulana (1996). Hydrological safety of dams, 2nd International Conference on Dam Safety Evaluation, Central Board of Irrigation and Power, India, pp. 171-183.

Barla, G., Bonini, M., Cammarata, G. (2004). Stress and seepage analyses for a gravity dam on a jointed granitic rock mass, Numerical modeling of Discrete Materials, pp. 263-268.

Barton, N. (1973). Review of a new shear strength criterion for rock joints. Engineering Geology, 8: 287-332.

Barton, N. (1974). A review of the shear strength of filled discontinuities in rock, Norwegian Geotechnical Institute, 105:1-38.

Barton, N. R., V. Choubey (1977). The shear strength of rock joints in theory and practice, Rock. Mech. 10 (1-2): 1-54.

Bieniawski Z. T (1976). Rock mass classification in rock engineering. In: Bieniawski ZT, editor. Exploration for rock engineering, Proceedings of the Symposium, vol. 1. Rotterdam: Balkema, pp.97-106.

Brown, E.T., B.H. Brady (1985). Rock mechanics for underground mining, George Allen & Unwin London.

Bérubé, A.P. (2004). Investigating the Streaming Potential Phenomenon Using Electric Measurements and Numerical Modelling with Special Reference to Seepage Monitoring in Embankment Dams. Luleå University of Technology, Doctoral Thesis, 2004:59.

Cai M., Kaiser P.K. Uno H. etc. (2004). Estimation of rock mass deformation modulus and strength of jointed hard rock masses using the GSI system. International Journal of Rock Mech and Mining Science, 41: 3-19.

Cheng, S-T. (1993). Statistics on dam failures, Reliability and Uncertainty Analyses in Hydraulic Design, p 97-105.

Dolezalova, M. (2004). Numerical analysis of an old masontry dam using UDEC, Numerical modeling of Discrete Materials, pp. 269-277.

Duncan C.W. (1999). Foundation on Rock. Second Edition, E & FN Spon.

Edelbro, C. (2004). Evaluation of rock mass strength criteria. Luleå University of Technology. Licentiate thesis, 2004-72. 153 pp.

Eriksson, M., H. Stille, J. Andersson (2000). Numerical calculations for prediction of grout spread with account for filtration and varying aperture, Tunnelling and Underground Space Technology, 15 (4): 353-364.

Eriksson, M. (2002). Grouting field experiment at the Äspö Hard Rock Laboratory Tunnelling and Underground Space Technology, 17(3): 287-293.

Fell, R., MacGregor, P., Stapledon, D., and Bell, G. (2005). Geotechnical engineering of dams, Leiden A.A. Balkema.

Foster M., Fell R., Spannagle M., (2000). The statistics of embankment dam failures and accidents. Can. Geotech. J.37: 1000-1024.

Goldin A.L., Rasskazov L.N. (1992). Design of Earth Dams, Rotterdam : Balkema, 1992.

Goodman R. E. (1980). Introduction to Rock Mechanics, John Wiley and Sons.

Grouting Manual (1980). Water Resources Commission of NSW. 3rd edition.

Hakami. E. (1995). Aperture distribution of rock fractures, *Ph.D.*, Royal Institute of Technology, Stockholm, Sweden.

Hudson, J.A., Cooling, C.M. (1988). In situ rock stresses and their measurement in the UK—Part I. The current state of knowledge. International Journal of Rock Mechanics and Mining Sciences & Geomechanics, 25 (6): 363–370.

Hoek. E., E. T. Brown (1978). Trends in relationships between measured in situ stresses and depth, International Journal of Rock Mechanics and Mining Sciences & Geomechanics, 15: 211 -215.

Hoek. E., J. W. Bray (1981). Rock slope engineering, London, Instn Min. & Metall.

Hoek, E., P. K. Kaiser, W.F. Bawden (1997). Support of underground excavations in hard rock. Rotterdam: Balkema.

Hoek. E., E. T. Brown (1997). Practical estimates of rock mass strength, Int. Journal Rock Mechanics & Mining Science, 34 (8): 1165 - 1186.

Hoek E., Marinos P., Benissi M. (1998). Applicability of the geological strength index (GSI) classification for very weak and sheared rock masses. The case of Athens Schist Formation. Bull Eng Geol Env; 57:151-60.

Hoek, E., Carranza-Torres, C., Corkum, B. (2002). Hoek–Brown failure criterion – 2002 ed. In: Proceedings of the 5th North American Rock Mechanics Symposium and 17th Tunnelling Association of Canada Conference: NARMS-TAC 2002, July 7–10, University of Toronto, pp. 267–271. Updated version (October 2, 2002). Available from: <www.rocscience.com>.

Hwang, N.H.C., R.J. Houghtalen (1996). Fundamentals of hydraulic engineering systems, 3rd edition, Prentice Hall, New Jersey.

ICOLD (1974). Lessons from Dam Incidents.

ICOLD (1983). Deterioration of Dams and Reservoirs.

ICOLD (1987). Dam safety guidelines, Bulletin 59, ISNN 0534-8239, 185 pp.

ICOLD (1995). Dam failures statistical analysis. Bulletin 99. Published by The International Commission on Large Dams.

ICOLD (2002). Risk Assessment in Dam Safety Management: A Reconnaissance of

Benefits, Methods and Current Applications ICOLD Bulletin, Draft, International Commission on Large Dams, August.

Idel, K. H. (1980). Seepage through jointed rock Sealing and drainage measures for earthfill and masonry dams, Symposium on Problems and Practice of Dam Engineering, pp. 225 – 232.

ISRM (1975). Suggested methods for determining shear strength: ISRM 9F, 1T ISRM Commission on Standard. Lab. Field Tests. Committee on Field Tests, Document, N1, FEB. 1974, 23P. International Journal of Rock Mechanics and Mining Science & Geomechanics Abstracts, 12(3): A3.5.

ISRM (1978). Suggested methods for quantitative description of discontinuities in rock masses, International Journal of Rock Mechanics and Mining Sciences & Geomechanics, 15: 319 – 368

ISRM (1981). International Society for Rock Mechanics (ISRM), Commission on classification of rocks and rock masses, Int. J. Rock Mech. Min., 18: 85–110.

ISRM (1983). Suggested methods for determining the strength of rock materials in triaxial compression: revised version.

Itasca (2005). *UDEC* version 4.0. Manual. Minneapolis, ICG.

Ivars, D. M. (2004). Inflow into excavations – a coupled hydro-mechanical three-dimensional numerical study, *Ph.D*., Royal Institute of Technology, Stockholm, Sweden.

Johansson, S. (1997). Seepage monitoring in embankment dams, *Ph.D*., Royal Institute of Technology, Stockholm, Sweden.

Johansson, F. (2005). Stability analyses of large structures founded on rock – an introductory study, Licentiate Thesis, Royal Institute of Technology, Stockholm, Sweden.

Korsfelts, T., Z. Lublin, M. Lagerquist, A. Persson, A. Andersson, C. Lindberg, , D.G. Andersson, D. Waluszewski, E. Veibäck, J. Cato, K. Petersson (2007). Energiläget 2007, Svensk energimyndigeten. Available from: < www.energimyndigheten.se>

Leijon, B. A. (1989). Relevance of point wise rocks stress measurements – analysis of overcoring data, Int. Journal Rock Mech. Min. Science & Geomech., 26: 61-68.

Matsuoka H., L. Sihong, S. De'an, U. Nishikata (2001). Development of a new in-situ direct shear test. ASTM geotechnical testing journal, 24 (1): 92-102.

McGrath, S. (2000). Study international practice and use of risk assessment in dam management, *Report*, Churchill Trust, Canberra, ACT, Australia.

Müller, B., M.L. Zoback, K. Fuchs, L.G. Mastin, S. Gregersen, N. Pavoni, O. Stephansson, C. Ljunggren, (1992). Regional patterns of tectonic stress in Europe. Journal of Geophysical Research 97 (B8): 11783-11803.

National Research Council (1983). Safety of Existing Dams, Evaluation and Improvement. National Academy Press.

Nordlund, E., G. Rådberg, J. Sjöberg (1997). Bergmekanikens grunder, Upplaga 1.4, Luleå, Sweden.

Patton, F. D. (1966). Multiple modes of shear failure in rock and related material, *Ph.D.* Thesis, University of Illinois.

Reinius (1988). Stresses and cracks in the rock foundation of an earthfill dam, *Water Power & Dam Construction*, 40: 33 – 38.

Reinecker, J., Heidbach, O., Tingay, M., Sperner, B. and Müller, B. (2005). The release 2005 of the World Stress Map (available online at www.world-stress-map.org).

RIDAS (2002). Hydropower industry dam safety guidelines, Svensk Energi.

RIDAS (2007). Gruvindustrins riktlinjer för dammsäkerhet, SweMin.

Rocscience (2007). RocLab, Ver. 1.031. Freeware available at http://www.rocscience.com/products/RocLab.asp on 30 November 2007.

Samad, A.M., Bare, W.D., Taggart W.C., Pflaum J.M. (1987). Statistical analysis of embankment dam failures, Hydraulic Engineering, Proceedings of the 1987 National Conference, Williamsburg, VA, USA, p 582-587.

Singh, B. (1995). Engineering for embankment dams, Rotterdam : Balkema.

Stephansson O. (1993). Rock stress in the Fennoscandian shield, Comprehensive Rock Engineering –Principles, Practice and Projects, vol. 3, chapter 17, pp. 445-459. Oxford: Pergman Press.

Sjöberg, J., U. Lindfors, F. Perman, D. Ask, (2005). Evaluation of the state of stress at the Forsmark site. Preliminary site investigation Forsmark area - version 1.2. SKB R-05-35.

Sjöberg, J., F. Perman (2007). Initiala bergspänningar i Stockholmsområdet – Underlag för projektering av Citybanan, Vattenfall.

Swedish Energy Agency, 2006

Swedenborg, S. (2001). Rock mechanical effects of cement grouting in hard rock. Doctoral thesis, Chalmers tekniska högskola. ISSN 0346-718X.

Terzaghi, K. (1943). Theoretical soil mechanics, John Wiley & Sons, pp. 510.

Thorpe, R., Watkins, D.J., Ralph, W.E., Hsu, R., Flexser, S. (1980). Strength and permeability tests on ultra-large Stripa granite core. Technical information report No. 31. Lawrence Berkeley Laboratory, University of California, Berkeley.

Thiel, K. (1989). Rock Mechanics in hydroengineering, Elsevier, Amsterdam.

Töyrä, J. (2006). Behaviour and stability of shallow underground constructions. Licentiate thesis, LTU, 2006:76.

Varshney R.S. (1995). Engineering for Embankment Dams.

U.S. Army Corps of Engineers (1984). Grouting technology, Engineering Manual No. 1110-2-3501.

U.S, Army Corps of Engineers (2004). General design and construction considerations for earth and rock-fill dams, Engineering manual No. 1110-2-2300.

Vattenfalls handbook (1988). Jord- och stenfyllningsdammar.Vattenfall (Stockholm). ISBN: 91-7186-271-4.

Wahlström E. (1974). Dams, dam foundations, and reservoir sites, Elsevier Scientific Publishing Company, New York.

Weaver, K. D, A.B. Bruce (2007). Dam foundation grouting. American Society of Civil Engineers (New York, N.Y.): 471pp.

Windelhed, K. (2001). Dammsäkerhet, Jetinjektering, en intressant reparationsmetod för jorddammar – förstudie, Elforsk rapport 01:10, Elforsk AB, Stockholm, Sweden.

Wyllie, D. C., C. W. Mah (2004). Rock Slope Engineering, Civil and Mining, Spon Press, London & New York.